Available online at www.sciencedirect.com
SCIENCE DIRECT®
Physics Reports 425 (2006) 1 – 78
PHYSICS REPORTS
www.elsevier.com/locate/physrep

High-accuracy mass spectrometry with stored ions

Klaus Blaum[a, b, *]

[a] *Institut für Physik, Johannes Gutenberg-Universität, 55099 Mainz, Germany*
[b] *GSI-Darmstadt, Planckstraße 1, 64291 Darmstadt, Germany*

Accepted 27 October 2005
Available online 18 January 2006
editor: J. Eichler

Abstract

Like few other parameters, the mass of an atom, and its inherent connection with the atomic and nuclear binding energy is a fundamental property, a unique fingerprint of the atomic nucleus. Each nuclide comes with its own mass value different from all others. For short-lived exotic atomic nuclei the importance of its mass ranges from the verification of nuclear models to a test of the Standard Model, in particular with regard to the weak interaction and the unitarity of the Cabibbo–Kobayashi–Maskawa quark mixing matrix. In addition, accurate mass values are important for a variety of applications that extend beyond nuclear physics. Mass measurements on stable atoms now reach a relative uncertainty of about 10^{-11}. This extreme accuracy contributes, among other things, to metrology, for example the determination of fundamental constants and a new definition of the kilogram, and to tests of quantum electrodynamics and fundamental charge, parity, and time reversal symmetry. The introduction of Penning traps and storage rings into the field of mass spectrometry has made this method a prime choice for high-accuracy measurements on short-lived and stable nuclides. This is reflected in the large number of traps in operation, under construction, or planned world-wide. With the development and application of proper cooling and detection methods the trapping technique has the potential to provide the highest sensitivity and accuracy, even for very short-lived nuclides far from stability. This review describes the basics and recent progress made in ion trapping, cooling, and detection for high-accuracy mass measurements with emphasis on Penning traps. Special attention is devoted to the applications of accurate mass values in different fields of physics.

PACS: 07.75.+h; 21.10.Dr; 29.20.Dh; 32.10.Bi

Keywords: Atomic masses; Binding energy; Ion cooling techniques; Ion detection techniques; Nuclear masses; Paul trap; Penning trap; Storage ring

Contents

1. Introduction 2
2. History of atomic and nuclear mass measurements 6
3. Principles of storage devices for charged particles 8
   3.1. Generation of the electric trapping potential 8
   3.2. Radiofrequency quadrupole and Paul traps 9
   3.3. Penning traps 12
      3.3.1. Ideal Penning trap 12

* Corresponding author at: Institut für Physik, Johannes Gutenberg-Universität, 55099 Mainz, Germany.
E-mail address: blaumk@uni-mainz.de.

0370-1573/$ - see front matter © 2005 Elsevier B.V. All rights reserved.
doi:10.1016/j.physrep.2005.10.011

3.3.2. Real Penning trap . . . 15
3.4. Storage rings . . . 18
4. Ion manipulation and mass measurement techniques . . . 19
4.1. Ion motion excitation in Penning traps . . . 20
4.1.1. Dipole excitation . . . 20
4.1.2. Quadrupole excitation . . . 21
4.2. Frequency measurement techniques . . . 24
4.2.1. Time-of-flight detection . . . 25
4.2.2. Detection by image charges . . . 26
4.3. Cooling and accumulation techniques . . . 27
4.3.1. Buffer gas cooling . . . 28
4.3.2. Resistive cooling . . . 29
4.3.3. Evaporative cooling . . . 31
4.3.4. Electron cooling . . . 31
4.4. Mass determination and calibration issues . . . 33
4.5. Resolving power and accuracy . . . 37
5. Production and separation techniques for exotic nuclides . . . 40
5.1. Isotope separation on-line . . . 41
5.2. In-flight separation . . . 41
6. Production and storage of highly charged ions . . . 42
7. Challenges in high-accuracy mass spectrometry with ion traps . . . 44
8. Ion trap mass spectrometers worldwide . . . 45
9. Mass spectrometry on radioactive ions . . . 48
9.1. Nuclear structure studies . . . 49
9.2. Test of nuclear mass models and mass formulas . . . 51
9.3. Nuclear astrophysics studies . . . 55
9.4. Fundamental interactions and Standard-Model tests . . . 57
10. Mass spectrometry on stable ions . . . 59
10.1. Double-beta decay and input data for neutrino mass . . . 60
10.2. Test of CPT . . . 61
10.3. Test of quantum electrodynamics in strong fields . . . 62
10.4. New definition of the kilogram . . . 64
10.5. Fundamental constants . . . 64
11. Future projects . . . 66
12. Concluding remarks . . . 67
Acknowledgements . . . 68
References . . . 68

1. Introduction

High-accuracy mass values for atoms give us access to atomic and nuclear binding energies that represent the sum of all the atomic and nucleonic interactions [1]. Thus, accurate mass values, together with other information, provide stringent tests of the weak interaction, quantum-electrodynamics, and the Standard Model (see Table 1). Accuracy required for the mass depends on the physics being investigated and ranges from $\delta m/m = 10^{-5}$ to better than 10^{-8} for radionuclides which often have half-lives considerably less than a second [2–4], and even down to $\delta m/m = 10^{-11}$ for stable nuclides [5–7].

Presently the masses of about 3200 nuclides are known or estimated, as listed in the recent Atomic-Mass Evaluation AME2003 [8,9] and summarized in Fig. 1. They are obtained by different methods in mass spectrometry. The highest mass accuracy on stable and radioactive atomic ions to date is achieved with ion traps. Not only in mass spectrometry but also in many other areas of science ion traps play an increasingly important role. They are employed for example for studies in atomic, nuclear, and particle physics such as g-factor measurements [11–13], quantum optics and computing [14,15], realization of frequency standards [14,16], laser spectroscopy [14,16,17], as well as for tailoring and improving the properties of radioactive ion beams [18,19].

The reasons for the high accuracy obtained and this broad usage of trapping devices are the manifold advantages of a three-dimensional ion confinement in well controlled fields [18]: First, an extended time of observation is available,

Table 1
Fields of application and the generally required relative uncertainty on the measured mass $\delta m/m$ to probe the associated physics

Field	Mass uncertainty
Chemistry: identification of molecules	10^{-5}–10^{-6}
Nuclear physics: shells, sub-shells, pairing	10^{-6}
Nuclear fine structure: deformation, halos	10^{-7}–10^{-8}
Astrophysics: r-process, rp-process, waiting points	10^{-7}
Nuclear models and formulas: IMME	10^{-7}–10^{-8}
Weak interaction studies: CVC hypothesis, CKM unitarity	10^{-8}
Atomic physics: binding energies, QED	10^{-9}–10^{-11}
Metrology: fundamental constants, CPT	$\leqslant 10^{-10}$

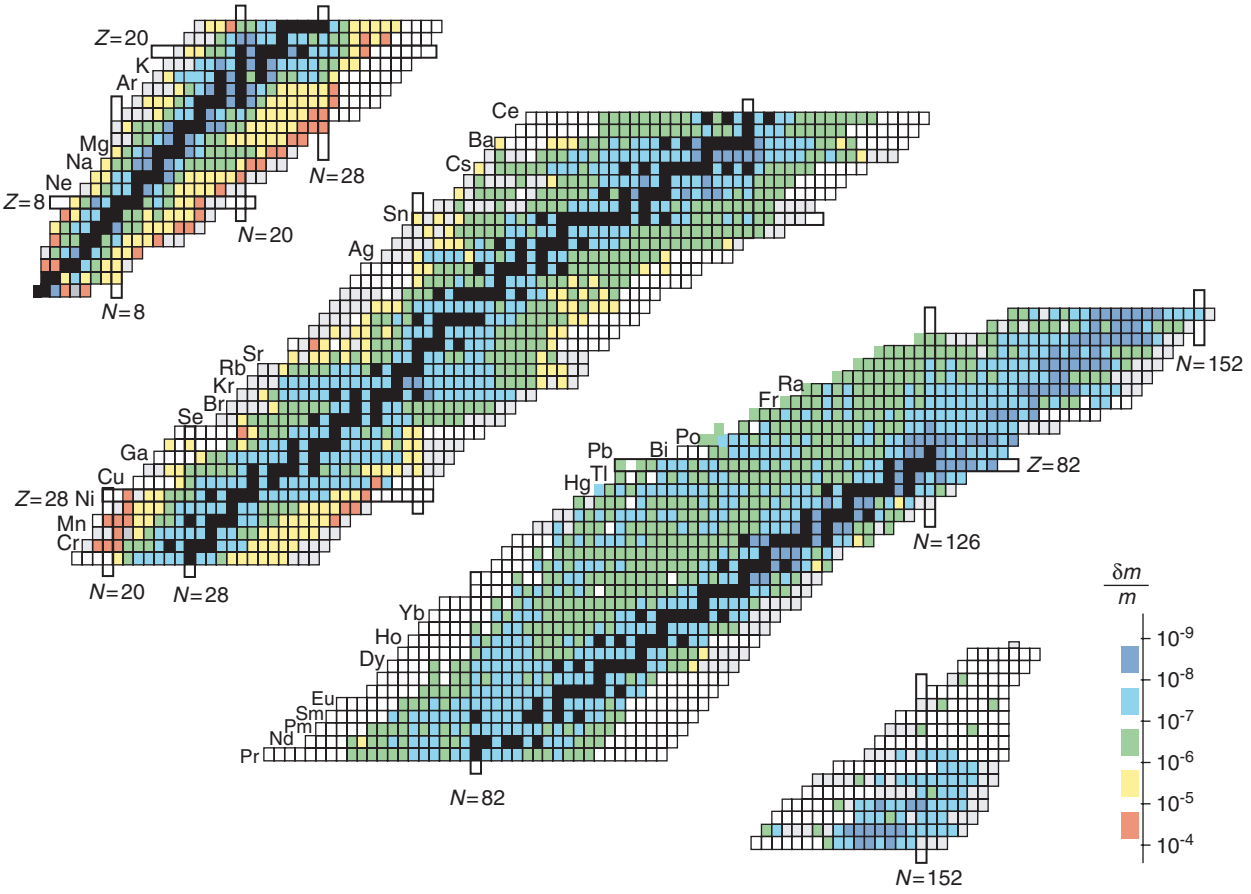

Fig. 1. (Color) Nuclear chart with the relative mass uncertainties $\delta m/m$ of all known nuclides shown in a color code (see scale bottom right of the nuclear chart, stable nuclides are marked in black). Masses of gray-shaded nuclides are estimated from systematic trends [9]. Some isotopes of the named elements have been studied with the Penning trap mass spectrometer ISOLTRAP at ISOLDE/CERN [10].

in principle for radionuclides only limited by the half-life. Second, single-ion sensitivity can be reached and third, ions can be stored in an ideal controlled environment. Apart from their use for direct mass determination, ion traps serve as tools to improve the performance of other methods and techniques: By accumulation and cooling of ions from sources outside the trap, ion beams of high brilliance can be obtained, which in particular enables effective use of rare species. Charge breeding inside traps allows the investigation of highly charged ions, and polarized ion bunches can be effectively produced [19].

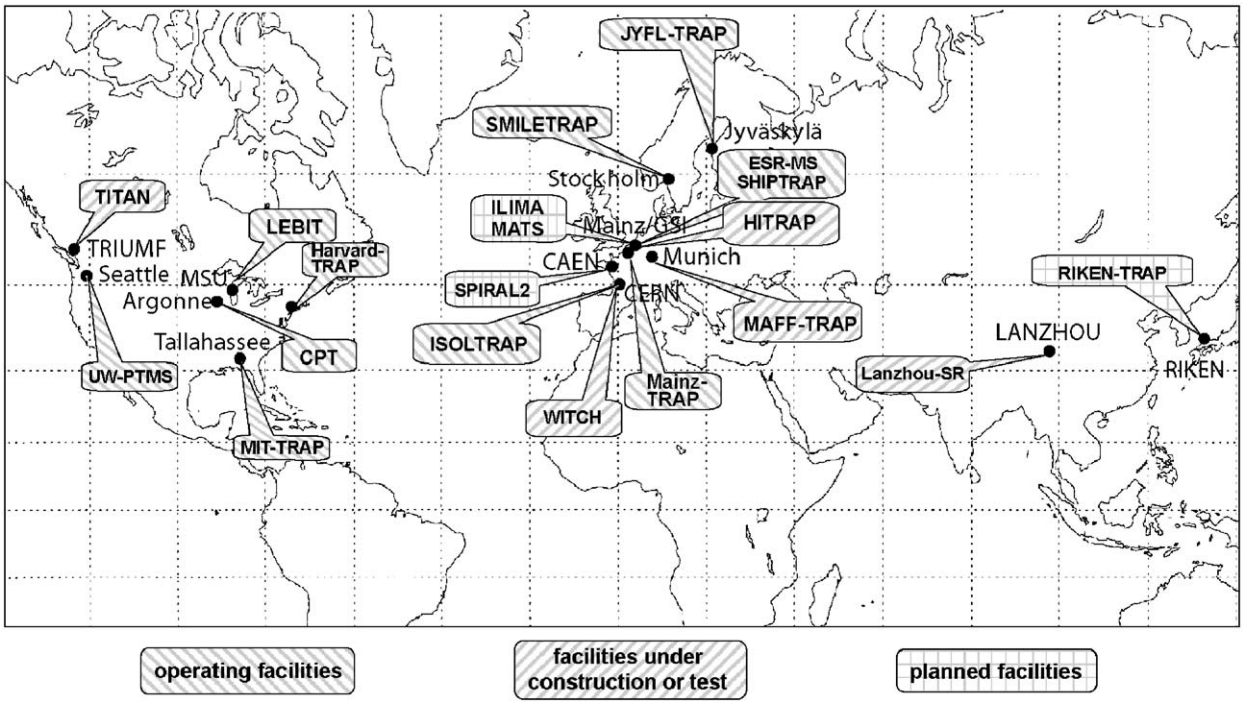

Fig. 2. Storage rings and Penning trap facilities for high-accuracy mass measurements on stable and short-lived nuclides which are in operation, under construction or planned. The names of the experiments are either taken from original publications or invented by the author as an acronym for this review.

As will be outlined in detail below, aside from storage rings two types of traps are generally used for mass determination: dynamical Paul (radiofrequency) traps and static Penning traps. The first type is widely used in analytical chemistry. A number of textbooks and reviews are available which deal with the techniques and results obtained with these devices [20,21]. Penning traps find applications where extremely high mass resolution and accuracy are required. Some recent articles [1,2,18,19,22] give overviews and details of its application. A general summary of the use of ion traps especially for mass spectrometry can be obtained by the proceedings of the following conferences: “Trapped Charged Particles and Fundamental Physics”, Asilomar, 1998 [23], “Atomic Physics at Accelerators: Mass Spectrometry (APAC 2000)”, Cargèse, 2000 [24], “14th International Conference on Electromagnetic Isotope Separation and Techniques Related to their Application (EMIS-14)”, Victoria, 2002 [25], “Trapped Charged Particles and Fundamental Physics”, Wildbad Kreuth, 2002 [26], and “The Fourth International Conference on Exotic Nuclei and Atomic Masses (ENAM2004)”, Pine Mountain/Georgia, 2004 [27].

In this review particular emphasis is given to the application of Penning traps and storage rings for high-accuracy mass determination of short-lived and stable nuclides. This is justified by the strong efforts in recent years to construct new storage rings and Penning trap mass spectrometers at accelerators. These devices will add new results to the exciting ones that have been obtained at existing facilities. In Fig. 2 these world-wide facilities are displayed (more details are available from Table 2). All existing and planned trap facilities will be briefly described in Chapter 8. Other high-accuracy mass spectrometry devices for short-lived radionuclides like radiofrequency spectrometers, as for example the Smith-type rf-spectrometer MISTRAL [28,29] installed at ISOLDE/CERN, or time-of-flight mass spectrometers like the magnetic-rigidity spectrometer SPEG at GANIL [30,31] and the coupled-cyclotron complex at GANIL [32,33], are described in [1,34] and will not be discussed in the following.

In the first part of this review a brief history of mass spectrometry will be given, starting with the determination of the charge-to-mass ratio of an electron and ending with high-accuracy Penning trap mass spectrometry.

The second part deals with the basics and challenges of ion trapping, cooling, and detection. Three major types of storage devices and their underlying principles will be discussed: radiofrequency quadrupole (Paul) traps [35] where

Table 2
Present and future ion storage and trapping devices for high-accuracy mass spectrometry on stable and exotic nuclides

Name	Institute	Kind of trap	Chg.	Stat.	Ref.
CPT	ANL/Chicago	GC/RFQ/PT	sci	op	[46,47]
ESR-MS	GSI/Darmstadt	SR	hci	op	[48]
Harvard-TRAP	CERN-Boston/USA	PT	sci	cp	[49]
HITRAP	GSI/Darmstadt	PT	hci	uc	[50,51]
ILIMA	GSI-FAIR/Darmstadt	SR	hci	pl	[52]
ISOLTRAP	ISOLDE/CERN	RFQ/PT	sci	op	[10,53]
JYFLTRAP	Jyväskylä	RFQ/PT	sci	op	[54]
Lanzhou-SR	Lanzhou	SR	hci	uc	[55,56]
LEBIT	MSU/East Lansing	GC/RFQ/PT	sci	op	[57]
Mainz-TRAP	Mainz	PT	hci	cp	[58]
MIT-TRAP	Cambridge–Tallahassee	PT	sci	op	[59]
MAFF-TRAP	Munich	GC/RFQ/EBIS/PT	hci	uc	[60]
MATS	GSI-FAIR/Darmstadt	GC/RFQ/EBIT/PT	hci	pl	[61]
RIKEN-TRAP	RIKEN/Tokyo	GC/RFQ/PT	sci	pl	[62]
SHIPTRAP	GSI/Darmstadt	GC/RFQ/PT	sci	op	[63]
SMILETRAP	MSL/Stockholm	EBIS/PT	hci	op	[64]
SPIRAL2-TRAP	GANIL/Caen	RFQ/PT	sci	pl	[43]
TITAN	TRIUMF/Vancouver	RFQ/EBIT/PT	hci	uc	[65]
UW-PTMS	Seattle	PT	sci	op	[66,67]
WITCH	ISOLDE/CERN	PT	sci	uc	[68]

Many of them serve also for other experiments such as decay and laser spectroscopy studies. In addition to the name of the experiment and the place of installation the table also includes the trapping devices involved in the experiment (GC = gas cell, RFQ = gas-filled segmented radiofrequency quadrupole (Paul) trap, EBIS = electron beam ion source, EBIT=Electron beam ion trap, PT = Penning trap, SR = storage ring), the use of singly (sci) or highly charged ions (hci), and the status of the experiment (cp = completed, op = in operation, uc = under construction or test, pl = planned).

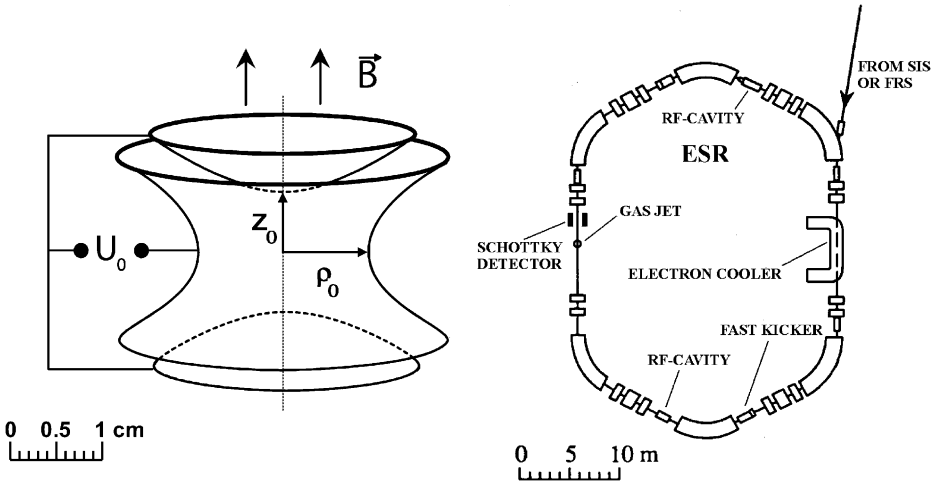

Fig. 3. A sketch of the two main devices for direct high-accuracy mass measurements: on the left a hyperbolical Penning trap and on the right an about 1000-fold larger (see scale) storage ring.

a time-varying quadrupole electric field is applied to the electrodes for confinement, Penning traps [36] which use a combination of a homogeneous magnetic field with a static electric quadrupole field, and storage rings [37] consisting of dipole magnets and magnetic lenses. For comparison, Fig. 3 shows a sketch of both kind of traps: a "little" Penning trap with about 3 cm in diameter and a "large" storage ring with a diameter of 20 m. Since ion cooling and efficient ion detection is essential for many applications of these devices the most important cooling and detection techniques will be presented. Meanwhile many experiments take advantage of the use of highly charged ions, or deal with radionuclides. Thus, the major production mechanisms of highly charged ions and radionuclides will be addressed as well.

In the third part fundamental applications and major achievements of high-accuracy mass measurements on short-lived and stable nuclides in different fields of physics (see also Table 1) are summarized. With the accuracy that is reached, a number of new domains could be accessed beside nuclear physics, in which the determination of atomic or nuclear masses is of importance. These are particle physics, nuclear astrophysics, stellar nucleosynthesis, neutrino physics, and metrology. One example is the study of super-allowed β-decays which enables a determination of the weak vector coupling constant and in this way to test the unitarity of the Cabibbo–Kobayashi–Maskawa (CKM) quark mixing matrix [38,39]. Beside accurate branching ratios and half-lives, very accurate Q-values, i.e. mass differences of mother and daughter nuclei, are required. In metrology, mass measurements on stable nuclides contribute to a new definition of the kilogram, the last SI unit that is still based on a prototype, and to accurate determinations of fundamental constants such as the fine-structure constant α. Since some of the applications require mass accuracies for specific nuclides or high production yields that are not yet available but will become available in the near future at new radioactive ion beam facilities such as GSI-FAIR (Germany) [40], RIA (USA) [41], RIKEN (Japan) [42], and SPIRAL2 (France) [43], a number of Penning trap and storage ring experiments are under construction or planned (see Table 2). Therefore an overview on new trap experiments and technical challenges associated with them will be given as well.

2. History of atomic and nuclear mass measurements

The mass spectrometry branch of science goes back to the year 1897, when Joseph John Thomson (1856–1940) demonstrated the existence of the electron as an electrically charged particle, and measured the ratio of its mass to its charge [44,45]. This is exactly the kind of measurement used in modern mass determinations, where what is actually measured is the charge-to-mass ratio q/m of individual atomic or molecular ions. For his studies, Thomson was awarded the Nobel Prize for physics in 1906.

However, the first breakthrough in mass spectrometry was at the border between physics and chemistry. It was again Thomson who discovered and investigated the existence of the isotopes of the elements by passing ion beams through crossed electric and magnetic fields [69]. In 1912 he found that Ne atoms existed with masses 20 and 22 [70]. His student Francis William Aston (1877–1945) contributed greatly to the investigation of the occurrence and abundances of isotopes and received for his work the Nobel Prize for chemistry in 1922. The citation for the award included "for his discovery, by means of his mass spectrograph, of isotopes, in a large number of non-radioactive elements, ...". Aston had developed a velocity-focussing mass spectrograph by using a magnetic field that produced a deflection in the opposite direction to that caused by the electric field and doubly as large. As a result, the position of the focal lines did not vary with the velocity of the ions [71].

Using this technique it was found, in 1920, that the atomic masses of isotopes did not differ exactly by simple multiples of the mass of a neutron [72]. These mass deficits (also called *mass defects*) were the first hint of the binding force that keeps the atomic nucleus stable [73]. According to Einstein's energy-mass relation [74], $E = mc^2$, the energy E caused by this binding force corresponds to a change in mass m. Eddington (1920, 1926) correctly interpreted the mass defect as the binding energy of the nucleus and solved the puzzle of the source of solar energy over the time-scale necessary for evolution: the nuclear transmutation of hydrogen into helium. As it will be shown later (see Section 9.3) there is still a close relationship between high-accuracy mass measurements and nuclear astrophysics. Aston's mass spectrograph had a resolving power of about $\Re = 1000$ and he performed systematic measurements on more than 200 nuclides [75]. The relative mass accuracy he reached was of the order of 10^{-4}, sufficient to establish the near constancy of the binding energy of about 8 MeV per nucleon for most nuclides, with a weak maximum at ^{56}Fe. This was in agreement with the concept of the nuclear forces being saturable, which led to the liquid-drop model of the nucleus, proposed at that time by Gamow (1930) [76], von Weizsäcker (1935) [77], and Bethe and Bacher (1936) [78].

Since then new mass spectrometry techniques have been developed that have brought a great increase in precision, about one order of magnitude per decade, and a significant expansion of the fields of physics that can be addressed (see Table 1). Fig. 4 demonstrates the impressive progress in uncertainty of atomic mass measurements on ^{28}Si during the last 70 years.

Double-focusing instruments with high mass-resolution, in which ions are focused for both direction and velocity at the same time, were developed around 1936 for the purpose of accurately determining the atomic weights of the elements and their isotopes by Dempster [79], Bainbridge and Jordan [80], and Mattauch and Herzog [81,82]. Measurements with these instruments reached a resolution of about 1 in 20 000.

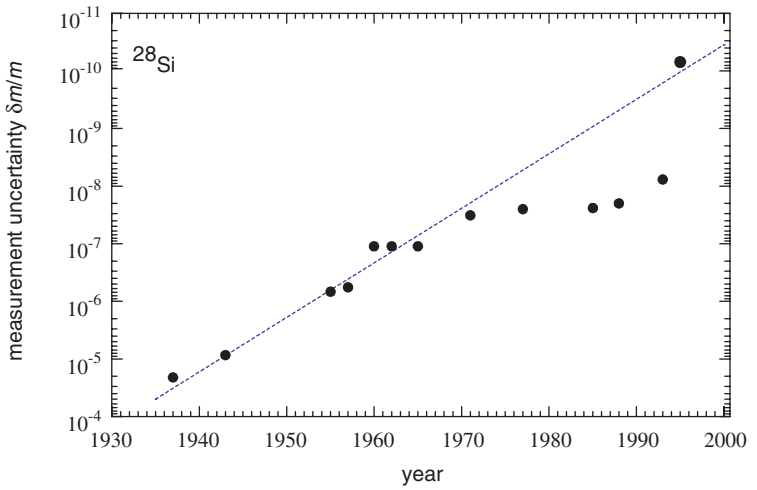

Fig. 4. Progress in mass uncertainty for ^{28}Si. Major steps have been achieved by developing new mass spectrometers or new techniques. The average progress is one order of magnitude in mass uncertainty every 10 years, as indicated by the solid line. The big improvement at around 1993 came about by the use of single-ion Penning trap mass spectrometry (courtesy of Audi).

A further improvement was obtained in mass spectrometers with higher order (directional) focussing, by Johnson and Nier [83], and by Barber and Duckworth [84,85] for isotope analysis during the Second World War. These devices enabled mass measurements with an accuracy of 10^{-7}, which later was improved even further. In nuclear physics these measurements played an important role in establishing the concept of shell structure in atomic nuclei, which was proposed by Jensen and Mayer et al., in their independent-particle model [86–93]. Magic nuclear numbers of neutrons and protons, N_0 and $Z_0 = 8$, 20, 28, 50, 82, and $N_0 = 126$, have played a decisive role in describing the nuclear system since nuclei with these proton and/or neutron numbers show exceptional stability, i.e. extra binding beyond what was expected from the smooth trend of the liquid-drop model. About a quarter century later, the discovery of strongly deformed intruder ground states of, for example, ^{30}Ne, ^{31}Na, and ^{32}Mg by mass spectrometry [94] and other accurate nuclear experiments suggested that the magic shell structure can be weakened or broken, even if protons or neutrons form a closed shell ($N = 20$ in this case).

Parallel to the improvements of the classical mass spectrometers a new method for mass spectrometry was investigated by Paul and coworkers [95,96]: the use of multipole electric and magnetic fields to focus and mass separate charged particles. One product of that research is the linear radiofrequency quadrupole mass filter, nowadays routinely used for example for residual gas analysis, environmental studies, gas chromatography, and for molecular studies in chemistry and biochemistry. A few years later this two-dimensional storage device was extended to a storage tool that enabled the confinement of charged particles with a specific charge-to-mass ratio q/m in all three dimensions [97,98]. Today this device is known as the *Paul trap*. However, in the field of high-accuracy mass spectrometry Paul traps are mostly used for ion beam preparation, since the achievable resolution in mass measurements is limited by the stability of the electric field. It is therefore the second type of trap that is now used routinely for high-accuracy mass measurements, i.e., the *Penning trap*.

The fundamental idea of the Penning trap dates back to the late 1930s when F.M. Penning published his work on increasing the sensitivity of ionization vacuum gauges by using an axial magnetic field perpendicular to the momentum of the charged particles [99]. However, his device had no electrodes perpendicular to the magnetic field for a three-dimensional confinement. This addition is credited to Pierce [100] who added *end hats* in the axial direction. It was also he who described in detail an electron trap using a field geometry consisting of a pure quadrupole electric field produced with hyperboloidal electrodes and a superposed uniform axial magnetic field. These are the ingredients for a high-accuracy Penning trap mass spectrometer as used in many setups of today. The name *Penning trap* was proposed by Hans G. Dehmelt who performed outstanding experiments with isolated electrons at rest. For the development of the ion trap techniques Hans G. Dehmelt and Wolfgang Paul received the Nobel Prize for physics in 1989 [11,35]. The prize was shared with Norman F. Ramsey for the invention of the separated oscillatory fields method and its use in the hydrogen maser and other atomic clocks [101].

Today, the highest accuracy in measurements of any quantity in any field of science is obtained when the measurand can be converted into frequency. For mass spectrometry this was first demonstrated by Smith [102,103] who developed a *mass synchrometer* which enabled the measurement of the cyclotron frequency of ions confined in a magnetic field. After more than one decade of a plateau in precision and sensitivity (see Fig. 4), in the 1990s the new Penning trap technique based on frequency measurements revolutionized the field of high-accuracy mass spectrometry [104–106]. These developments were based on the earlier work by Gräff et al., who, in 1980 [107], performed the very earliest high-accuracy Penning trap measurements; that of the proton-electron mass ratio.

A third type of trap is the storage ring, which is about three orders of magnitude larger than the Paul and Penning traps. At the experimental storage ring ESR at GSI Darmstadt [37], two complementary mass spectrometry techniques have been developed, Schottky mass spectrometry (SMS) [108] and isochronous mass spectrometry (IMS) [109]. Both techniques are based on the measurement of the revolution frequency of stored high energetic ions. ESR–SMS and ESR–IMS were used in several experimental runs for mapping large areas of the nuclidic mass surface.

However, the relative mass accuracy of storage ring mass spectrometry is so far limited to about 2×10^{-7} [110], whereas with Penning traps an accuracy can be reached of 10^{-8} and better for short-lived nuclides with half-lives well below 100 ms [111,112], and of 10^{-11} for stable ions [5–7]. With storage rings and Penning traps, single-ion sensitivity and a resolving power of more than one million were demonstrated for short-lived radionuclides, enough to resolve even excited nuclear states, the nuclear isomers [113–116]. Most recently the possibility has been demonstrated of using Penning trap mass spectrometry to determine ion-molecule reaction pathways, kinetics, and equilibria in the gas phase [5].

None of these mass spectrometry methods based on ion trapping would have been so successful without the development of appropriate detection and cooling techniques of the stored ions (see Sections 4.2 and 4.3, respectively). In storage rings the cooling is generally achieved by collinear beams of electrons which force the ions to travel at the same speed as the electrons [117]. In addition, stochastic cooling and laser cooling are applied. In Penning traps the most often used techniques are mass-selective buffer gas cooling [118] and resistive cooling [119]. The basics of the different types of ion traps will be discussed in the following.

3. Principles of storage devices for charged particles

To obtain full spatial confinement requires a potential minimum in all three dimensions. Moreover, the most desirable confining force is one that causes simple harmonic motion of the confined particle, i.e., one that is proportional to the distance of the particle from the center of confinement. Since no simultaneous trapping in three dimensions is possible by purely electrostatic potentials, three-dimensional confinement is achieved in a Penning trap by the superposition of a homogeneous magnetic field providing radial confinement and an axially symmetric electrostatic quadrupole field providing axial confinement. For Paul traps, a radiofrequency quadrupole (RFQ) field is employed for the confinement of ions. The principles of ion traps have been summarized in several textbooks and further detail can be obtained in [20,120,121].

3.1. Generation of the electric trapping potential

Fig. 5 shows the electrode configurations used in Paul and Penning traps for the generation of the electric trapping field. The traps consist of three electrodes; two end electrodes and a ring electrode, which in the ideal case are hyperboloids of revolution. Appropriate potentials are applied so as to generate an axially symmetric electric quadrupole potential

$$\Phi = \frac{\Phi_0}{4d^2}(\rho^2 - 2z^2) \tag{1}$$

with Φ_0 being the potential difference between adjacent electrodes, $\rho^2 - 2z^2 = \rho_0^2$ defines the geometry of the ring electrode, $\rho^2 - 2z^2 = -2z_0^2$ defines the geometry of the end electrodes, and $2d^2 = z_0^2 + \rho_0^2/2$ is a measure for the characteristic trap dimension. Cylindrical electrodes can also be employed to generate the electric trapping potential with the advantage of a larger storage volume and an easier machining and alignment (see Fig. 5c), but with the disadvantage of introducing higher-order electric multipoles into the trapping region.

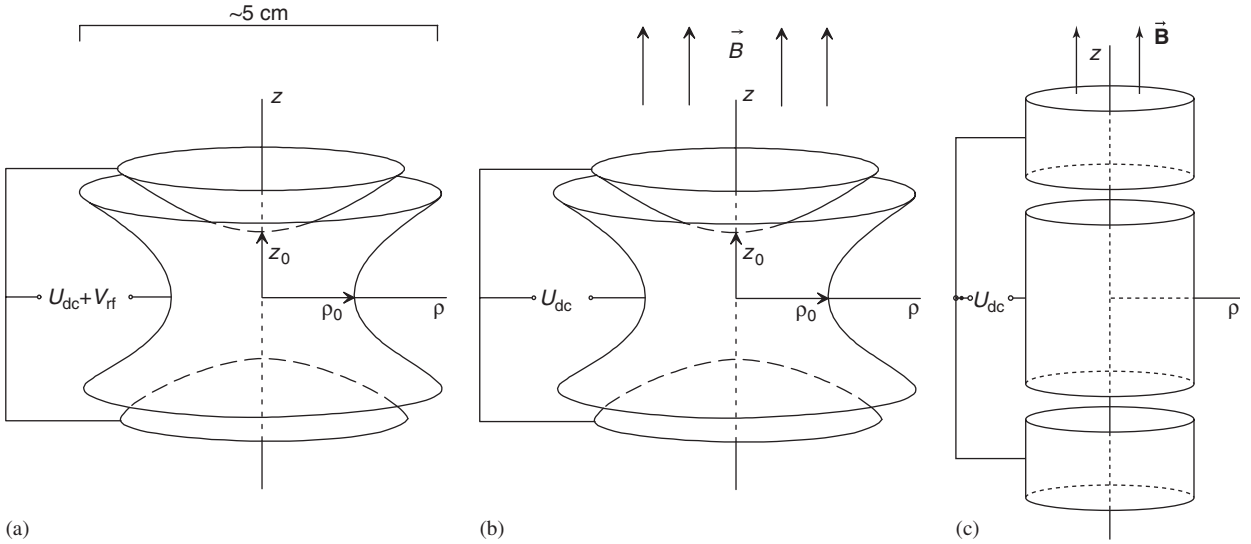

Fig. 5. Electrode configurations of a Paul (a) and Penning trap (b, c), consisting of two end electrodes and a ring electrode with hyperboloidal (a, b) or cylindrical shape (c). For charged particle storage a trap voltage with proper polarity is applied between the ring electrode and the end electrodes.

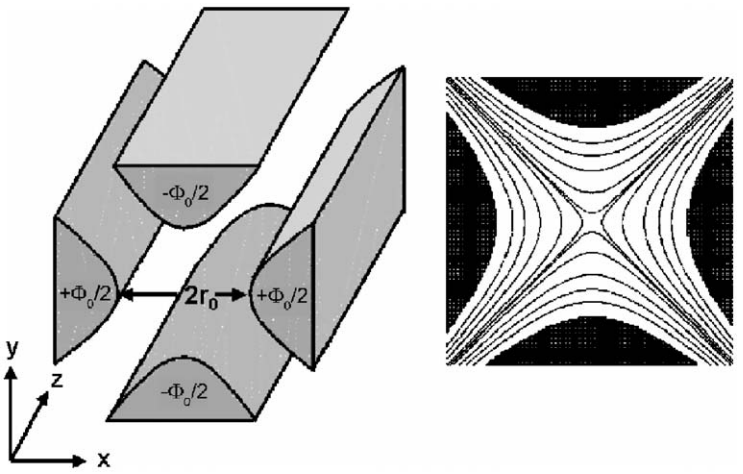

Fig. 6. Left: Radiofrequency quadrupole mass filter electrodes having hyperbolic cross-section. Right: Equipotential lines for a quadrupole field generated with the electrode structure shown left.

3.2. Radiofrequency quadrupole and Paul traps

Paul and Steinwedel first described the linear radiofrequency quadrupole mass spectrometer (QMS), also named the radiofrequency quadrupole mass filter (QMF) or ion guide, in 1953 [95,97]. This device provides two-dimensional ion confinement and mass separation by oscillating electric fields. It was continuously improved and extended to three dimensions [98,122] in the now-called Paul trap. Both are widely used in various branches of science. The principles and applications of a quadrupole mass spectrometer are summarized in the textbook by Dawson [20].

An ideal quadrupolar geometry (see Fig. 6) is formed by four hyperbolic electrodes of infinite length with two perpendicular zero-potential planes that lie between the electrodes and intersect along the center-line z-axis. For mass analysis both a static electric (dc) potential and an alternating (ac) potential in the rf range are applied to the electrodes of the linear Paul mass filter which is used, for example, in rest gas analysis or analytical chemistry [123]. The relative

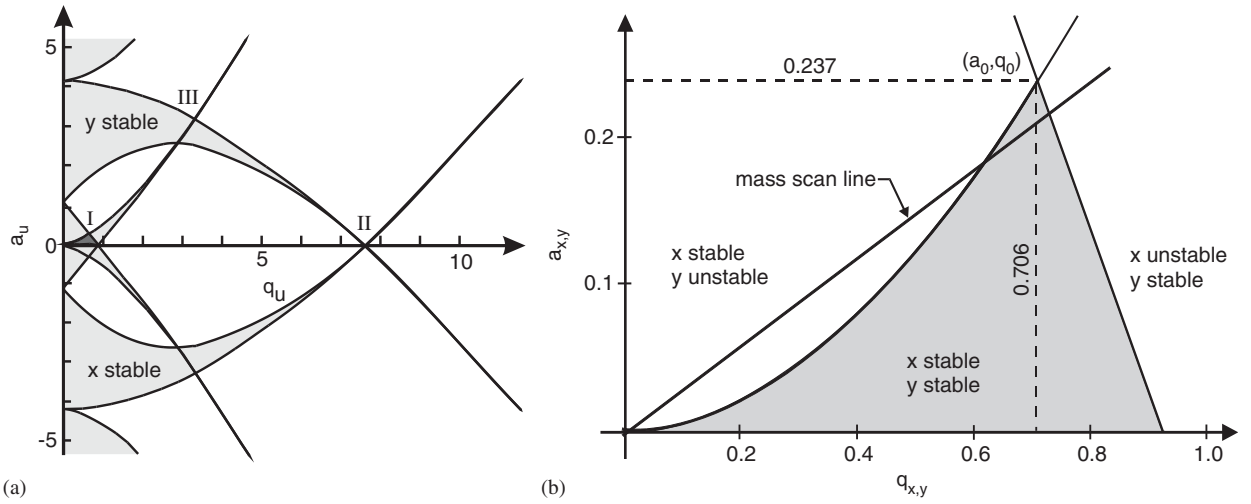

Fig. 7. (a) Stability regions (gray shaded) of the linear Paul trap and the quadrupole mass filter. (b) Stability region I from (a) in more detail. It is the first region of simultaneous stability in x- and y-direction.

amplitudes of the dc and ac potentials control the ability of the system to mass filter a low energy beam of ions travelling along the z-axis. Assuming idealized field conditions within the structure, with vanishing component in the z-direction, the potential distribution $\Phi(\vec{r}, t)$ is given by

$$\Phi(\vec{r}, t) = \frac{\Phi_0(t)}{2} \frac{(x^2 - y^2)}{r_0^2} \tag{2}$$

and

$$\Phi_0(t) = \tfrac{1}{2}(U_{\mathrm{dc}} + V_{\mathrm{rf}} \cos \omega_{\mathrm{rf}} t) \ , \tag{3}$$

where r_0 is the radius defined by the circle tangential to the four hyperbolic electrodes, U_{dc} is the dc potential and V_{rf} is the amplitude of the rf potential between adjacent electrodes. V oscillates with angular frequency $\omega_{\mathrm{rf}} = 2\pi\nu_{\mathrm{rf}}$. Thus, relative to the trap center the potentials of adjacent electrodes oscillate at an amplitude that is half that of the applied potential difference and 180° out of phase with each other. Satisfying the Laplace equation $\nabla^2\Phi = 0$ the potential (2) is invariant in the z-direction. The force of the trapping field on the trapped ion leads to an equation of motion which is of Mathieu type [124]:

$$\frac{\mathrm{d}^2 u}{\mathrm{d}\xi^2} + (a_u - 2q_u \cos 2\xi)\, u = 0 \ , \tag{4}$$

where $\xi = \omega t/2$ and u represents the x or y displacement of the ion independent in both directions. The parameters a_u and q_u are related to the potentials U_{dc} and V_{rf} by

$$a_u = a_x = -a_y = \frac{4qU_{\mathrm{dc}}}{mr_0^2\omega^2} \ , \tag{5}$$

$$q_u = q_x = -q_y = \frac{2qV_{\mathrm{rf}}}{mr_0^2\omega^2} \ , \tag{6}$$

where q/m is the charge-to-mass ratio of the ion. The solution of Mathieu's equations for motion in the x–y-plane contains either a growing exponential factor or an oscillatory term of finite radial extent, depending on the parameters a_u and q_u. Fig. 7 shows the Mathieu stability diagram in the (a_u, q_u)-plane for the linear quadrupole. The shaded areas denote the stable solutions in x- or y-direction. Overlap of the stable areas for both directions lead to two-dimensional

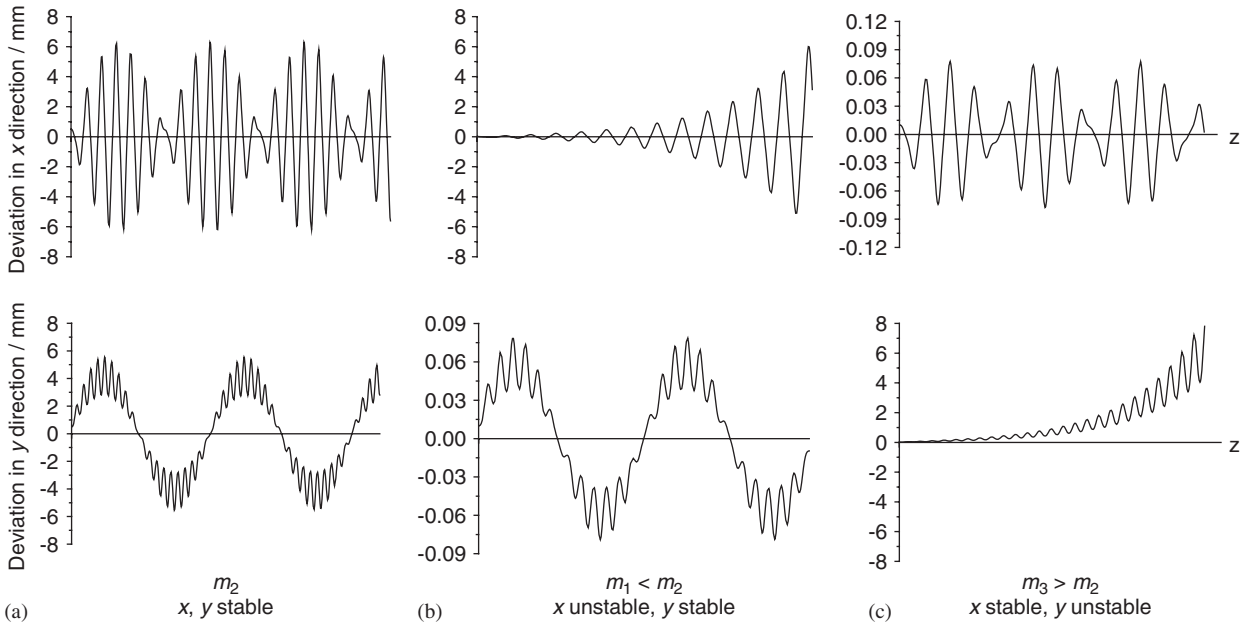

Fig. 8. Projection of three-dimensional ion trajectory simulations onto the x- and y-coordinate for a mass m_2 with stable trajectories (a), an light ion with mass $m_1 < m_2$ and unstable motion in the x-direction (b), and an heavy ion with mass $m_3 > m_2$ and y-unstable trajectory (c). The masses are according to the ones indicated in the stability diagram in Fig. 7. The macro- and the micro-oscillations in the ion motion are clearly visible.

stability. For practical purpose, only the first stability region near the origin of the Mathieu diagram (see Fig. 7b) is usable for mass spectrometry. Discussion of the other regions of stability can be found in [125,126].

From Mathieu's stability region it becomes obvious that with proper choice of a_u and q_u, or U_{dc} and V_{rf}, respectively, all linear radiofrequency traps and ion guides can be used as mass filters. Since both a_u in Eq. (5) and q_u in Eq. (6) are mass dependent there is only a certain range of masses that can be stored for given trap parameters. When the stability conditions are fulfilled, the ion is radially confined and the motional spectrum contains the frequencies

$$\omega_{u,n} = (\beta_u + 2n)\omega t/2, \quad u = x, y, \quad 0 \leqslant \beta_u \leqslant 1, \quad n = 0, \pm 1, \pm 2, \ldots , \tag{7}$$

where β_u is the stability parameter [20]. The fundamental frequencies are given by $n = 0$, thus

$$\omega_{u,0} = \tfrac{1}{2}\,\beta_u \omega \tag{8}$$

and the ion motion can be described by a fast micromotion and a slow macromotion (see Fig. 8). They oscillate around the z-axis with finite amplitude. For (a_u, q_u)-values outside this stable region, and thus for ions with lower or higher masses, the ion motion is unstable, either in the x-direction, in the y-direction, or in both. As shown by the ion trajectory simulations [123] in Fig. 8, ions with unstable trajectories steadily move away from the z-axis during oscillations and ultimately strike the electrodes and are removed. For ions with stable trajectories the oscillation amplitudes stay limited. This mass filter feature finds a very common application in rest gas mass analyzers where linear radiofrequency quadrupoles are generally used. Simultaneously scanning the amplitudes of U_{dc} and V_{rf} along a "mass scan line" of fixed ratio of $U_{\mathrm{dc}}/V_{\mathrm{rf}} = a_u/(2q_u)$, as indicated in Fig. 7, gives the mass spectrum. Only ions with (a_u, q_u)-values in the range where the working line is inside the stability region will have stable motion. The closer the line is to the apex of this area the higher the resolving power of the mass filter. Alternatively to the (U, V)-variation, the mass spectrum could also be obtained by scanning the radiofrequency ν_{rf} with fixed amplitudes of both rf and dc voltages. However, this is very uncommon in practise. Under optimized conditions a neighboring mass suppression of up to 10^8 can be demonstrated [127] which is important in respect to, for example, the application of resonance laser ionization quadrupole mass spectrometry for ultratrace analysis [128–130].

Three-dimensional confinement of ions can be achieved in such a linear structure by longitudinally segmenting the four rods and applying the appropriate dc potentials $U_{\mathrm{dc}}(z)$ to the segments [131–133]. Fig. 9 shows the segmented

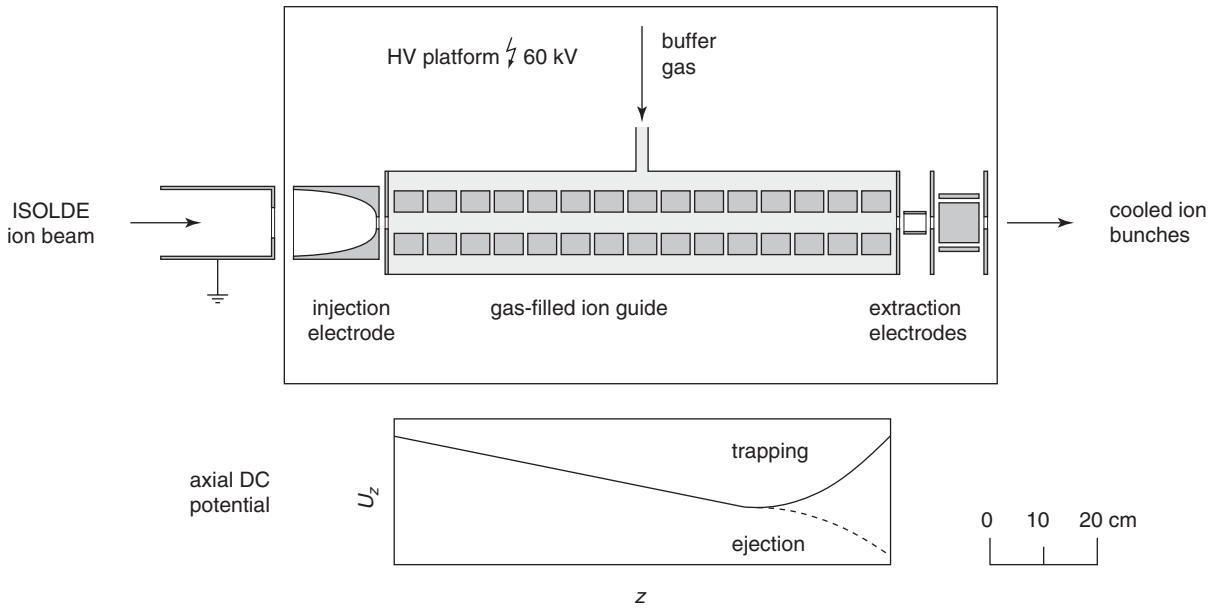

Fig. 9. Detailed sketch of the segmented linear Paul filter as used at ISOLTRAP [132]. The 60-keV ions delivered by the on-line isotope separator ISOLDE [134] are decelerated by placing the whole setup close to 60 keV. The ions are radially confined by a radiofrequency quadrupole field and cooled within some milliseconds in buffer gas collisions to nearly the temperature of the buffer gas. The axial potential is varied by application of different dc voltages to the segmented rods. The ions are accumulated in a linear-Paul-trap region near the end of the radiofrequency structure and after ejection reaccelerated to the transport energy of about 2.8 keV.

Paul filter used as a beam conditioning trap at ISOLTRAP at ISOLDE/CERN [132,133]. The potential on the axis that results when the appropriate voltages are applied to the rod segments is indicated in the lower part of Fig. 9. In the buffer-gas-filled ion guide, whose total length is about 1 m, the ions are radially confined and both radially and longitudinally cooled by buffer gas collisions (see also Section 4.3.1) until they accumulate in a trap region near the end of the ion guide. Typically these buffer-gas-filled beam preparation RFQ traps are operated at gas pressures of about 10^{-2}–10^{-3} mbar, at a radiofrequency of about 1 MHz, and at rf amplitudes of up to 125 V, depending on the ion mass. The overall efficiency that is reached by such an ion beam cooler and buncher in transmission mode is more than 90% and in bunching mode is more than 50% for 60-keV beams. This enables easy and efficient transport of the ion beam to the next experiment or trap setup [131].

The further development from linear to ideal three-dimensional hyperboloidal quadrupole traps (see Fig. 5a) is reviewed, for example, by March et al. [135]. Since Paul traps with hyperboloidal electrodes are in general not used for high-accuracy mass spectrometry but for a variety of analytical applications in chemistry and biochemistry [136–138], and to perform high-accuracy laser spectroscopy with stored ions [17,139], these trap configurations are not considered in more detail here. Instead, the second type of a three-dimensional ion confinement, the Penning trap, will be discussed.

3.3. Penning traps

3.3.1. Ideal Penning trap

For the storage of charged particles in a Penning trap a strong homogeneous magnetic field $\vec{B}$ for radial confinement and a weak static electric field for axial trapping are superposed. The latter is created by a voltage U_{dc} applied between the ring electrode and the two end electrodes. Fig. 5(b) presents a sketch of an ideal Penning trap configuration with hyperboloidal electrodes. A detailed description of charged-particle storage in a Penning trap is given in the review article by Brown and Gabrielse [36].

An ion with a charge-to-mass ratio q/m stored in a pure magnetic field $\vec{B} = \vec{B}(z)$ in the z-direction and with a velocity component v perpendicular to the direction of the magnetic field will experience a Lorentz force $\vec{F}_L = q\vec{v} \times \vec{B}$. This

force confines the charged particle in the radial direction and the ion performs a circular motion with angular frequency

$$\omega_c = \frac{q}{m} B \ . \tag{9}$$

Since there is no binding in the direction of the magnetic field lines, i.e. in the axial direction, a three-dimensional confinement is obtained in the Penning trap by superposing a weak static electric quadrupole potential

$$\Phi(z, r) = \frac{U_{dc}}{2d^2}\left(z^2 - \frac{1}{2}r^2\right) \ , \tag{10}$$

given in cylindrical coordinates.

Such a potential can be obtained by a geometry with three electrodes of hyperboloidal shapes, where the surfaces are identical to the equipotential surfaces (see Fig. 5b). U_{dc} is the applied trapping voltage (with proper polarity) between the ring electrode and the two end electrodes and, again,

$$d^2 = \frac{1}{2}\left(z_0^2 + \frac{r_0^2}{2}\right) \tag{11}$$

describes the dimension of the trap (where $2r_0$ and $2z_0$ are the inner ring diameter and the closest distance between the end electrodes, respectively, see Fig. 5).

Solving the equation of motions for all three coordinates,

$$m\ddot{z} = qE_z \tag{12}$$

and

$$m\ddot{\vec{\rho}} = q(\vec{E}_\rho + \dot{\vec{\rho}} \times \vec{B}) \ , \tag{13}$$

with the electric field strengths

$$E_z = -\frac{U_{dc}}{d^2} z \tag{14}$$

and

$$\vec{E}_\rho = \left(\frac{U_{dc}}{2d^2}\right)\vec{\rho} \ , \tag{15}$$

results in three independent motional modes as shown in Fig. 10: (i) the harmonic trapping motion along the trap axis at the axial oscillation frequency ω_z, (ii) the circular cyclotron motion at the reduced cyclotron frequency ω_+, and (iii) the circular magnetron or drift motion at the magnetron frequency ω_-. The latter two are radial motions, i.e. perpendicular to the trap axis. The slow magnetron motion is centered at the trap axis and provides the "guiding center" of the cyclotron motion (see projection in Fig. 10).

For an ideal electric quadrupole field the three eigenfrequencies are

$$\omega_z = \sqrt{\frac{qU_{dc}}{md^2}} \ , \tag{16}$$

$$\omega_+ = \frac{\omega_c}{2} + \sqrt{\frac{\omega_c^2}{4} - \frac{\omega_z^2}{2}} \ , \tag{17}$$

$$\omega_- = \frac{\omega_c}{2} - \sqrt{\frac{\omega_c^2}{4} - \frac{\omega_z^2}{2}} \ , \tag{18}$$

where $\omega = 2\pi\nu$. In order that the motion be bounded, the roots of Eqs. (17) and (18) must be real, leading to the trapping condition

$$\omega_c^2 - 2\omega_z^2 > 0 \ . \tag{19}$$

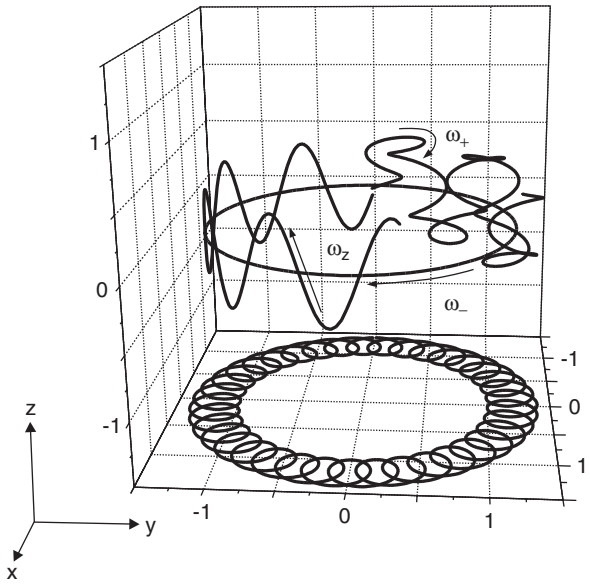

Fig. 10. Schematic trajectory (three-dimensional and projection onto the x–y-plane) with ideally three independent eigenmotions of an ion in a Penning trap: a harmonic oscillation in the axial direction (axial motion with frequency ω_z), and a radial motion that is a superposition of the modified cyclotron motion with frequency ω_+ and the magnetron motion with frequency ω_-.

Combining this condition with Eqs. (9) and (16), the conditions for stable confinement of charged particles in the ideal Penning trap can be expressed in terms of the applied fields as follows:

$$\frac{|q|}{m} B^2 > \frac{2|U_{\mathrm{dc}}|}{d^2}, \quad qU_{\mathrm{dc}} > 0 \ . \tag{20}$$

This determines the minimum magnetic field required to balance the radial component of the applied electric field.

The amplitudes and phases of the harmonic and circular motional modes depend on the initial conditions, i.e. the position and velocity of the ion in the moment of creation in the trap volume or the circumstances of its injection from an external source. The superposition of the independent motional modes can yield different kinds of ion trajectories. The ion motion can be manipulated by the application of additional time-varying electric fields. This will be discussed in detail in Section 4.

The eigenfrequencies of the ion motion are uniquely determined by the trap parameters, i.e. the magnetic field magnitude B, the trapping potential U_{dc}, and the trap dimension d (see Eq. (11)). A serial expansion of the radial eigenfrequencies results in

$$\omega_- \approx \frac{U_{\mathrm{dc}}}{2d^2 B} \tag{21}$$

and

$$\omega_+ \approx \omega_{\mathrm{c}} - \frac{U_{\mathrm{dc}}}{2d^2 B} \ . \tag{22}$$

The magnetron frequency (18) is, in the first order approximation, independent of the mass of the stored charged particles. Table 3 gives eigenfrequency values for ions with different masses in a 7-T strong magnetic field and typical trap parameters. The magnitudes of the eigenfrequencies follow the order

$$\omega_- < \omega_z < \omega_+ \ . \tag{23}$$

Table 3
Eigenfrequencies $\nu_i = \omega_i/2\pi$ of singly charged ions with different masses in a hyperbolic Penning trap with operation parameters $r_0 = 6.38$ mm, $z_0 = 5.5$ mm, $U_{dc} = 10$ V, and $B = 7$ T

	A/u					
	1	39	85	133	197	250
ν_+	107.5 MHz	2.752 MHz	1.260 MHz	803.7 kHz	541.1 kHz	425.4 kHz
ν_z	982.8 kHz	157.4 kHz	106.6 kHz	85.22 kHz	70.02 kHz	62.16 kHz
ν_-	4.493 kHz	4.501 kHz	4.509 kHz	4.518 kHz	4.531 kHz	4.541 kHz

Important relations between the eigenfrequencies in respect to mass spectrometry are

$$\omega_c = \omega_+ + \omega_- \ , \tag{24}$$

$$\omega_c^2 = \omega_+^2 + \omega_-^2 + \omega_z^2 \ , \tag{25}$$

$$2\omega_+\omega_- = \omega_z^2 \ . \tag{26}$$

Thus, for the mass determination of the stored charged particle two main options are available: (i) a direct measurement of the cyclotron frequency sideband ω_c (see Section 4.2.1) or (ii) a measurement of the individual frequencies, either only the two radial or all three eigenfrequencies (see Section 4.2.2). Both techniques will be discussed in more detail later. Eq. (25) is independent of imperfections to first order and is called the *Brown-Gabrielse Invariance Theorem* [140].

The total energy of an ion stored in a Penning trap is given by the sum of the kinetic and potential energies of each eigenmotion [36]:

$$E = E_+ + E_z + E_- = \frac{m}{2} r_+^2(\omega_+^2 - \omega_+\omega_-) + \frac{m}{2} r_z^2\omega_z^2 + \frac{m}{2} r_-^2(\omega_-^2 - \omega_+\omega_-) \ . \tag{27}$$

The potential energies $-e\left(U/d^2\right) r_\pm^2 = -mr_\pm^2\omega_z^2 = -\frac{m}{2} r_\pm^2(\omega_+\omega_-)$ of the two radial motions are negative due to the potential hill which the ions experience in the radial direction. Since $\omega_+ > \omega_-$, the total energy of the modified cyclotron motion is positive while that of the magnetron motion is always negative (see also Section 4.1). The importance of the negative magnetron energy with respect to buffer gas cooling of the stored particles will be discussed later.

3.3.2. Real Penning trap

In reality one has deviations from the ideal Penning trap with pure quadrupole electric field and uniform magnetic field [36,121]: field inhomogeneities, trap imperfections, misalignment of the trap axis with respect to the magnetic field axis, etc. lead to a dependence of the motional frequencies on the motional amplitudes and thus to shifts in the eigenfrequencies and broadenings of the observed resonances. This results in limitations for the resolving power and systematic uncertainties in the mass determination. An accurate knowledge on these imperfections and their influences is therefore essential for the design of a Penning trap mass spectrometer. The most important trap imperfections will be briefly discussed.

Electric field imperfections. Deviations from the pure quadrupolar field as defined in Eq. (10) are caused by electric field imperfections. They occur due to the geometrical imperfections of the trap construction itself such as the holes in the end electrodes for injection and ejection of the ions or from the unavoidable truncation of the electrodes. Deviations from the ideal quadrupolar field are generally expressed in terms of a multipole expansion of the trapping potential. Frequency shifts caused by the octupole and dodecapole contributions have been calculated [36,141]. For the sum frequency $\omega_c = \omega_+ + \omega_-$, the frequency shift $\Delta\omega_c^{elec}$ depends on the amplitudes of the individual eigenmotions and is given by

$$\Delta\omega_c^{elec} = \Omega_c^{elec}\left[\frac{3}{2}\frac{C_4}{d^2}(\rho_-^2 - \rho_+^2) + \frac{15}{4}\frac{C_6}{d^4}(\rho_z^2(\rho_-^2 - \rho_+^2) - (\rho_-^4 - \rho_+^4))\right] \tag{28}$$

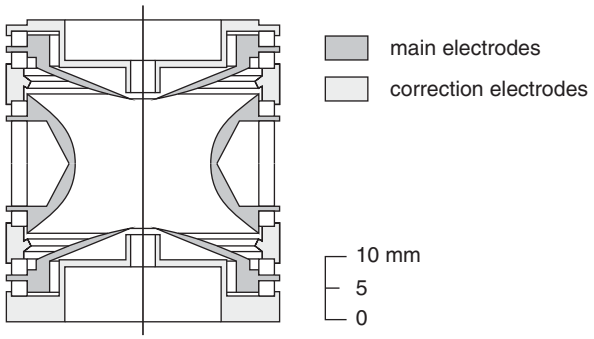

Fig. 11. Detailed sketch of a real hyperboloidal precision Penning trap. The correction electrodes are designed such as to reduce deviations from the ideal quadrupole field [53].

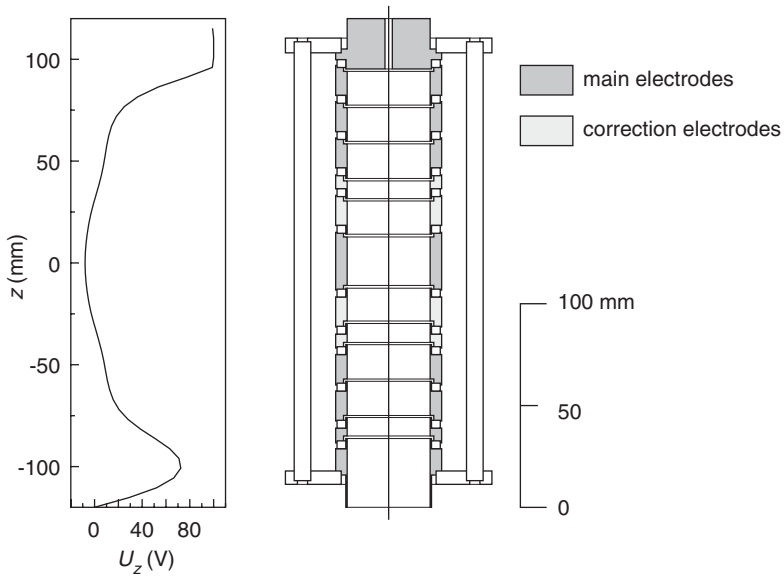

Fig. 12. Detailed sketch of a real cylindrical Penning trap. The graph on the left shows the potential on the axis which results from the appropriate voltages applied to the cylinder segments. A harmonic potential is created around $z = 0$ whereas the extended potential well is used for efficient capture of injected ions [142].

with

$$\Omega_c^{\mathrm{elec}} = \frac{\omega_-}{1 - \omega_-/\omega_+} \approx \omega_- \approx \frac{U_0}{2d^2 B} \,. \tag{29}$$

C_4 and C_6 are the coefficients of the octupole and dodecapole components of the electric field.

In order to minimize the deviations from the ideal quadrupole field and the resulting frequency shifts, correction electrodes are added to the Penning trap configuration. Figs. 11 and 12 show examples of real hyperboloidal and cylindrical Penning traps.

The frequency shifts can furthermore be minimized by use of a trap with a large characteristic dimension d and a small trap potential U_{dc} and by having small motional amplitudes of the stored ions. The frequency shift $\Delta\omega_c^{\mathrm{elec}}$ is practically mass independent because of the mass independence of Ω_c^{elec}. It leads always to a systematic uncertainty in the mass determination due to the use of a reference mass m_{ref} for the magnetic field calibration (for the discussion of the mass determination procedure and calibration issues see Section 4.4). The relative mass uncertainty of an ion of

mass m and cyclotron frequency ω_c is

$$\frac{\Delta m}{m} = \frac{\Delta\omega(m_{\mathrm{ref}} - m)}{m}(\omega_c + \Delta\omega) \propto m - m_{\mathrm{ref}} \ . \tag{30}$$

Therefore it is desired to have mass references as close as possible. Mass doublets, i.e., reference ion and ion of interest having the same atomic mass number, are the foremost choice but in most cases they are not available or not well enough known.

Electric-field imperfections can also lead to frequency shifts via the induced image charge of the ions on the trap electrodes. This shift ($\Delta\omega_+ = -\Delta\omega_-$) scales inversely to the cube of the trap dimension and hence the effect is more pronounced for a small trap [143].

A deviation of the electrostatic-field axis relative to the magnetic-field axis also causes systematic uncertainties in mass determination since it shifts all eigenfrequencies [36]. For the sum frequency $\omega_- + \omega_+$ the resulting shift $\Delta\omega_c^{\mathrm{tilt}}$ can be calculated [141] and is found to be mass independent. For small tilting angles $\Theta \ll 1$ the shift is given by

$$\Delta\omega_c^{\mathrm{tilt}} \approx \tfrac{9}{4}\,\omega_-(\sin^2\Theta) \ . \tag{31}$$

Magnetic field instabilities and imperfections. Some of the greatest limitations in high-accuracy Penning trap mass spectrometry are magnetic-field inhomogeneities and fluctuations. Several mechanisms for a change in the magnetic-field amplitude of a superconducting magnet exist:

1. The current in the superconducting coils of the magnet decreases steadily due to the *flux creep* phenomenon [144,145]. It occurs when flux lines, which are pinned to inhomogeneities of the superconducting material, jump from one pinning site to another. With modern superconducting solenoids this logarithmic decay can be approximated, for time intervals up to years, by a linear decrease.
2. When objects containing ferromagnetic or paramagnetic materials are brought within a short distance of a few meters or less of the magnet, they are magnetized. This magnetization distorts the field of the magnet.
3. Temperature and pressure fluctuations in the helium and nitrogen reservoir of the superconducting magnets. These cause changes in the magnetic permeability of the materials surrounding the Penning trap, such as the vacuum chamber, and the trap material itself, usually oxygen-free high-conductivity copper, and thus in the magnetic-field homogeneity and strength [146].

Nowadays homogeneities of $\Delta B/B < 10^{-8}$ over a volume of $1\,\mathrm{cm}^3$ and relative field stabilities of $(\delta B/\delta t)(1/B) < 10^{-8}/\mathrm{h}$ can be reached, for example, by stabilizing both the temperature in the warm bore and the pressure in the Dewar vessel of the experimental setup, as demonstrated at SMILETRAP [64].

Frequency shifts occur if the magnetic field is a function of the even powers of the distance from the trap center [36]. In that case the ion experiences average magnetic fields that depend on the amplitude of its motion. The lowest multipole term of interest is a magnetic hexapole component β_2. It creates a frequency shift of

$$\Delta\omega_c^{\mathrm{magn}} \approx \beta_2\omega_c(\rho_z^2 - \rho_-^2) \ . \tag{32}$$

In contrast to the frequency shifts discussed for the electric field imperfections, this shift is proportional to the cyclotron frequency of the stored ion and does not give rise to calibration errors, provided the motional amplitudes are the same for both ion species. Since this can only be achieved within certain limits, it is still important to construct the trap such that magnetic inhomogeneities are minimized.

Ion–ion interactions. In high-accuracy trap experiments the ideal case is to have only one ion stored in the trap at any one time. This is because Coulomb interaction with another ion will affect the ion motion and thus the cyclotron frequency. This has been observed and investigated for both Paul traps [147] and Penning traps [113,148,149]. Only the later case is addressed here.

If the simultaneously stored ions are of the same species, i.e., having identical mass, the driving frequency acts on the q/m center of the stored ion cloud and no frequency shift is observed [119]. The effect of the presence of contaminant ions having different masses expresses itself by the appearance of two or even more separate resonances (assuming sufficient resolving power). As the ion number in the trap increases, these resonances successively approach each other. At the same time, the centroids are shifted to lower frequencies. The size of the shift of one species is found to be

proportional to the number of stored ions of the other species and vice versa. When the unperturbed resonances cannot be resolved, only a single resonance is observed, which is narrower than expected from a simple superposition of the individual resonances.

A quantitative description of the observed frequency shifts must take into account the coupling of all eigenmotions by Coulomb interaction. Until now no general analytical solution has been found for the equation of motion, neither for the Paul trap nor for the Penning trap. Nevertheless, it is possible to confirm the observations qualitatively by a three-dimensional simulation of the motion of simultaneously stored ions [113,150].

In practice, it is therefore essential to have a pure ion sample stored in the trap. If that is not possible, the cyclotron frequency can be extrapolated to a single stored ion in the trap, by analyzing the cyclotron frequencies for different numbers of stored ions [111].

Image charges. An oscillating ion induces image charges in the trap electrodes, that create an electric field which in turn reacts on the stored ion and shifts its motional frequencies. This effect was investigated in detail by Van Dyck [143] and Porto [151]. Using a simple model in which the trap is replaced by a conducting spherical shell of radius a, the image charge creates an electric field given by

$$\vec{E} = \frac{1}{4\pi\epsilon_0}\frac{qa}{(a^2 - r^2)^2}\vec{r}\ . \tag{33}$$

This field has to be added to the trapping field and thus it causes a shift in the axial frequency amounting to

$$\Delta\omega_z = -\frac{1}{4\pi\epsilon_0}\frac{q^2}{2ma^3\omega_z}\ . \tag{34}$$

This shift becomes significant for small traps and a large number of stored ions but since it is of purely electrostatic origin, the electric field-independent sideband frequency $\omega_c = \omega_+ + \omega_-$ is not affected.

3.4. Storage rings

While the dimensions of Paul and Penning traps are typically only of the order of a few centimeters, storage rings, that are also widely used as large ion traps, have diameters of a few tens of meters. The basic components of ion storage-cooler rings are a set of bending and focusing magnetic multipole fields, a so-called lattice, as shown in Fig. 13, which is a sketch of the experimental storage ring (ESR) at GSI Darmstadt (Germany) [37].

The ion trajectory is a closed orbit where the ions oscillate with an energy E_P and momentum p_P, which are dependent on the magnetic field amplitudes and the bending radii of the magnets. In reality, due to the finite emittance of the ion beam and to the unavoidable imperfections of the fields, the ions perform quasi-periodic betatron (sinusoidal like) oscillations around the ideal trajectory (see Fig. 13) [152]. The oscillations are solutions of the basic "Hill equation" that describes the ion orbit as a function of the bending radius, the momentum spread, and of the focusing strength. The amplitude $A(s)$ of this betatron oscillation is given by the emittance of the beam ϵ_y and the amplitude function $\beta_y(s)$. The latter itself is given by magnetic guiding fields. The symbol y represents the transversal coordinate and s the longitudinal coordinate, respectively. The number of oscillations per turn is given by

$$Q_y = \frac{1}{2\pi}\oint_c \frac{1}{\beta(s)}\,\mathrm{d}s\ . \tag{35}$$

In order to avoid the coherent amplification of smallest perturbations that would cause an immediate loss of the stored ions, the ratio of orbit length and betatron wavelength should not be an integer or a simple algebraic number, i.e., 1/2, 1/3, etc.

Also important is the relation between the momentum of the circulating particles p_P and their revolving frequency v. Deviations Δp_P from the ideal momentum result in a change of the ion trajectory and thus of the revolving frequency. There is a linear relation between the relative momentum change $\Delta p_P/p_P$ and the relative frequency change $\Delta v/v$:

$$\frac{\Delta v}{v} = \left(\frac{1}{\gamma^2} - \frac{1}{\gamma_t^2}\right)\frac{\Delta p_P}{p_P}\ . \tag{36}$$

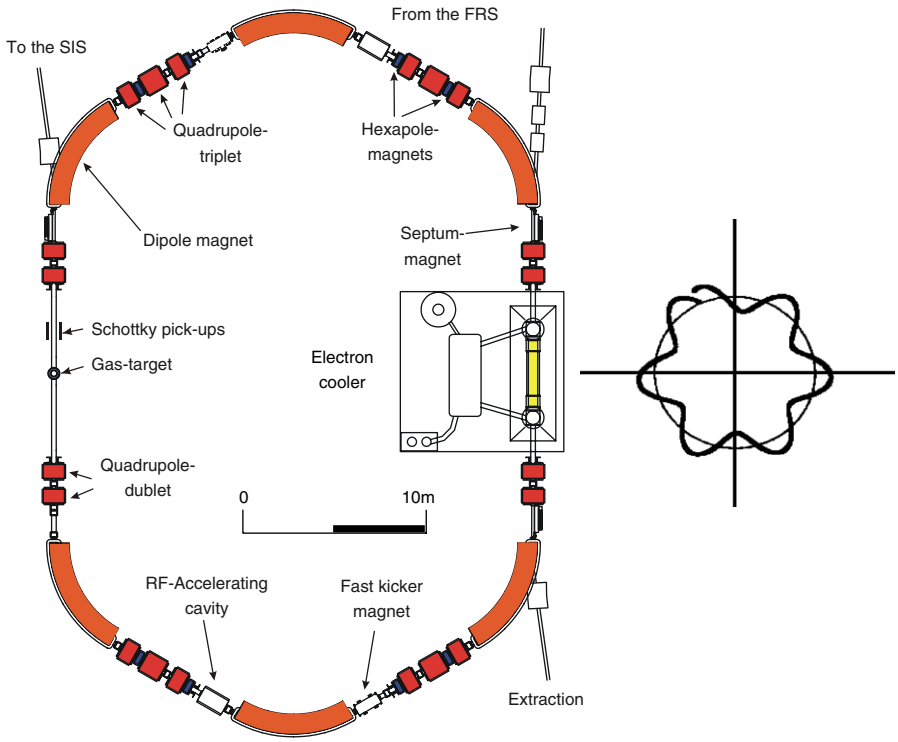

Fig. 13. (Color) (left) Schematic view of the experimental storage ring ESR at GSI-Darmstadt. Highly charged ions are injected into the ESR directly from the heavy-ion synchrotron (SIS) or after fragmentation and separation in the fragment separator (FRS). The ring consists of six 60° dipole magnets and six quadrupole triplets and doublets, respectively, to keep the ions on their ideal trajectory. Also shown are the basic components along with the diagnostic and experimental elements. On the right is an inset showing the Betatron oscillation superposed on the ideal trajectory ("Sollbahn").

The proportional factor includes the relativistic relation between the momentum and velocity of a particle ($1/\gamma^2$ with $\gamma = 1/\sqrt{1-\beta^2}$ the relativistic Lorentz factor and c the velocity of light), and the relation between momentum and trajectory change ($1/\gamma_t^2$) [153]. γ_t is referred to as the *transition-*γ and defined by $\mathrm{d}f/\mathrm{d}p_P|_{\gamma=\gamma_t} = 0$. That is to say, for $\gamma = \gamma_t$ a change in energy or momentum does not cause a change in frequency. For $\gamma < \gamma_t$ an increasing momentum causes a frequency increase. The principles of mass measurements in a storage ring will be described in Section 4.4. The longitudinal momentum spread $\Delta p_P/p_P$ is determined by the equilibrium between the cooling force of the applied cooling technique (see Section 4.3) on the one hand and counteracting heating effects such as intra-beam scattering on the other hand. By means of electron cooling, momentum spreads $\Delta p_P/p_P \leqslant 1 \times 10^{-6}$ are routinely achieved at the ESR for low intensity ion beams [154].

The acceptance of storage-cooler rings is, for a typical energy of 300 MeV/u, restricted to about 10 to 30π-mm-mrad for both the horizontal and vertical emittance. Since a mass-to-charge band m/q of typically $\pm 1\%$ can be stored, heavier ions with the same mass m, but different charge states q, can circulate simultaneously in a storage ring.

4. Ion manipulation and mass measurement techniques

Accumulation, storing, and cooling techniques play an increasingly important role in many areas of science. This is reflected by the awards of Nobel prizes within the last two decades to more than ten pioneers of particle, ion, or atom cooling. In this chapter the main ion manipulation, cooling, and frequency determination techniques in ion traps for mass measurements will be discussed.

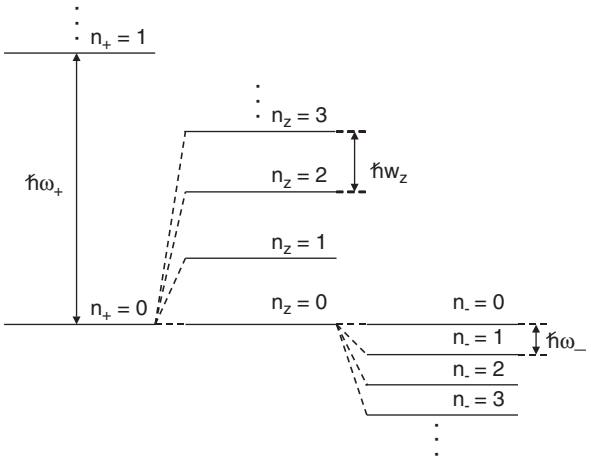

Fig. 14. Energy levels of a spin-less charged particle in an ideal Penning trap (see Fig. 5b). The total energy is given by the sum of the energies of the three independent harmonic oscillations with the modified cyclotron frequency ω_+, the axial frequency ω_z, and the magnetron frequency ω_-. In the center of the trap the potential energy is set to zero.

4.1. Ion motion excitation in Penning traps

The simplest picture of the excitation of ion motion in a Penning trap is the quantum mechanically one: Each of the ideally independent eigenmotions of a stored ion in a Penning trap represents a harmonic oscillator with a fixed eigenfrequency. The Hamilton operator for the radial and axial motion can be written as [155]:

$$H_{xy} = \frac{1}{2m}(p_x^2 + p_y^2) + \frac{1}{8}m\omega_1^2 r^2 - \frac{1}{2}\omega_0 L_z \ , \tag{37}$$

$$H_z = \frac{p_z^2}{2m} + \frac{m\omega_z^2 z^2}{2} \ , \tag{38}$$

where $L_z = xp_y - yp_x$ is the axial component of the angular momentum operator, $r = \sqrt{x^2 + y^2}$, $\omega_1 = \sqrt{\omega_c^2 - 2\omega_z^2}$, and $\omega_c = |\omega_0|$. The frequencies ω_c, ω_z, ω_+, and ω_- are as defined above. The analytical solution of the Schrödinger equation for the Hamiltonian has been obtained by Fock [156] and Darwin [157] and their explicit applications to the Penning trap have been presented for example in [158,159].

By a resonant excitation with an external radiofrequency field the energy of the system can be increased. Fig. 14 shows the energy levels of each eigenmotion that sum to the total energy of the stored spin-less ion:

$$E = \hbar\omega_+(n_+ + \tfrac{1}{2}) + \hbar\omega_z(n_z + \tfrac{1}{2}) - \hbar\omega_-(n_- + \tfrac{1}{2}) \ . \tag{39}$$

The magnetron motion is of special importance since the negative sign in Eq. (39) reveals the inverse energy of the magnetron oscillator, i.e. it contributes negatively to the total energy. That is to say, an increase of the quantum number n_- and thus of the magnetron radius results in a loss of energy of the ion. Applying a dipole electric field changes the quantum number in one of the ladders of the so-called Landau levels. When a Penning trap is operated with an additional azimuthal quadrupole driving field with a frequency that equals a suitable combination (sum or difference $\nu_i \pm \nu_j$) of the frequencies of the fundamental modes of motion, then a periodic conversion of the participating modes into each other is observed, i.e. a coupling of the Landau levels of two different ladders i and j. A detailed description of the ion motion in a Penning trap in a classic and quantum mechanical frame work is given in [160,161].

4.1.1. Dipole excitation

A resonant excitation by a dipole rf field at one of the eigenfrequencies can be used to manipulate the corresponding eigenmotion of one ion species. The increase of the amplitude of the motion can be used to determine the eigenfrequency of the motion, or to remove unwanted ion species, i.e. contaminations, from the trap. A dipole field created by an rf

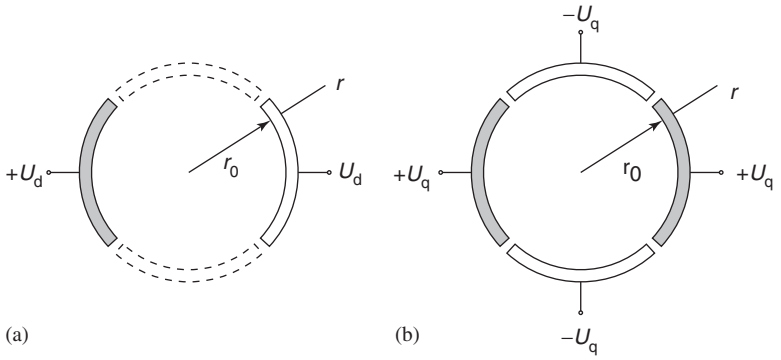

Fig. 15. Radial segmentation of the ring electrode to apply an electromagnetic radiofrequency field. (a) Application of a radiofrequency to opposite ring segments results in first-order approximation in a dipole field. (b) An approximated quadrupole field can be generated by applying a radiofrequency between each opposite pairs of the four-fold segmented ring.

voltage with amplitude U_d and with frequency ω_d applied with 180° phase shifts between two opposite segments of the ring electrode (see Fig. 15) drives one of the radial motions if the corresponding frequency is used, for example, for the radial x-component:

$$\vec{E}_x = \frac{U_d}{a} \cos(\omega_d t - \phi_d)\hat{x} \ . \tag{40}$$

Thus, the magnetron and the cyclotron motion can be addressed independently: For the isolation of specific ions from an ensemble of several species, the unwanted ions are radially ejected by an excitation field covering the appropriate ω_+ ranges. Similarly the axial motion can be excited by an dipole field generated by applying an rf voltage with frequency ω_z between the two end electrodes.

For excitation of the magnetron oscillation the phase difference between the initial ion magnetron motion ϕ_- and the exciting dipolar field ϕ_d, $\Delta\phi_- = \phi_d - \phi_-$, has a strong effect on the magnetron radius ρ_-, as shown in Fig. 16 [112]. The calculated final magnetron radius as a function of the dipolar-excitation duration T_d is shown in Fig. 16(a) for three different phase differences. In Fig. 16(b), the calculated final magnetron radius ρ_- is plotted against the phase difference $\Delta\phi_-$ for different values of the dipolar-excitation durations T_d.

4.1.2. Quadrupole excitation

A quadrupole excitation at the sum of individual eigenfrequencies can be used to couple eigenmotions and to determine frequencies. The most direct approach for mass spectrometry is the measurement of the sum frequency $\nu_c = \nu_+ + \nu_-$ (Eq. (24)) which corresponds to a coupling of the modified cyclotron and magnetron oscillation. Later we will see (Section 4.3.1) that it is also important in buffer gas cooling in Penning traps. The coupling of the two radial motions can be achieved by an azimuthal quadrupolar rf field with the frequency ω_{rf} applied with 180° phase shifts on sets of ring-electrode segments perpendicular to each other (see Fig. 15b):

$$\vec{E}_x = \frac{2U_q}{a^2} \cos(\omega_{rf} t - \phi_{rf}) y\hat{x} \ , \tag{41}$$

$$\vec{E}_y = \frac{2U_q}{a^2} \cos(\omega_{rf} t - \phi_{rf}) x\hat{y} \ . \tag{42}$$

When in resonance, $\omega_{rf} = \omega_c$, a full periodic conversion between the two motional radii ρ_+ and ρ_- is obtained [162]. Fig. 17 shows the calculated effect of quadrupole excitation at ν_c. Initially there is only magnetron motion. Because of the excitation the amplitude of the cyclotron motion increases while the amplitude of the magnetron motion decreases. After a certain time (depending on the amplitude U_q of the excitation) a full conversion is obtained, i.e. the magnetron motion has disappeared while the amplitude of the cyclotron motion is equal to that of the initial magnetron motion [141]. For non-resonant excitation ($\omega_{rf} \neq \omega_c$) the conversion is not complete [162].

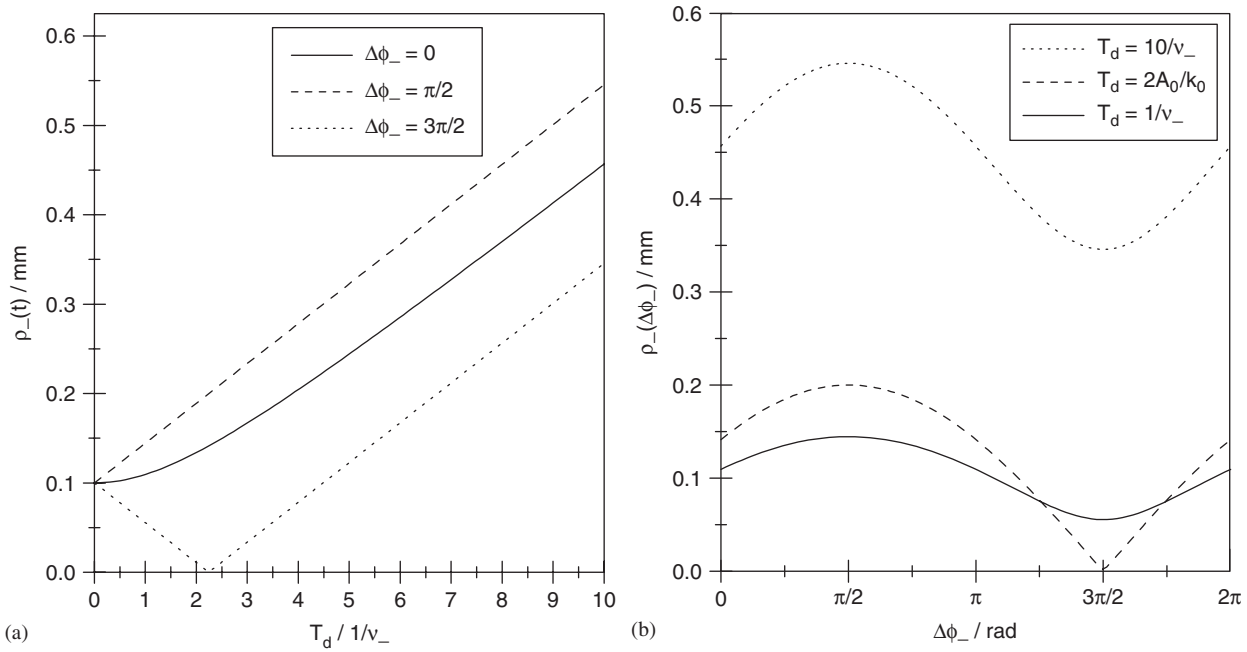

Fig. 16. (a) Calculated final magnetron radius as a function of the duration of the dipolar excitation for three values of the phase difference between the excitation and the final magnetron motion; (b) calculated final magnetron radius as a function of the phase difference between the excitation and the initial magnetron motion for three different excitation durations [112].

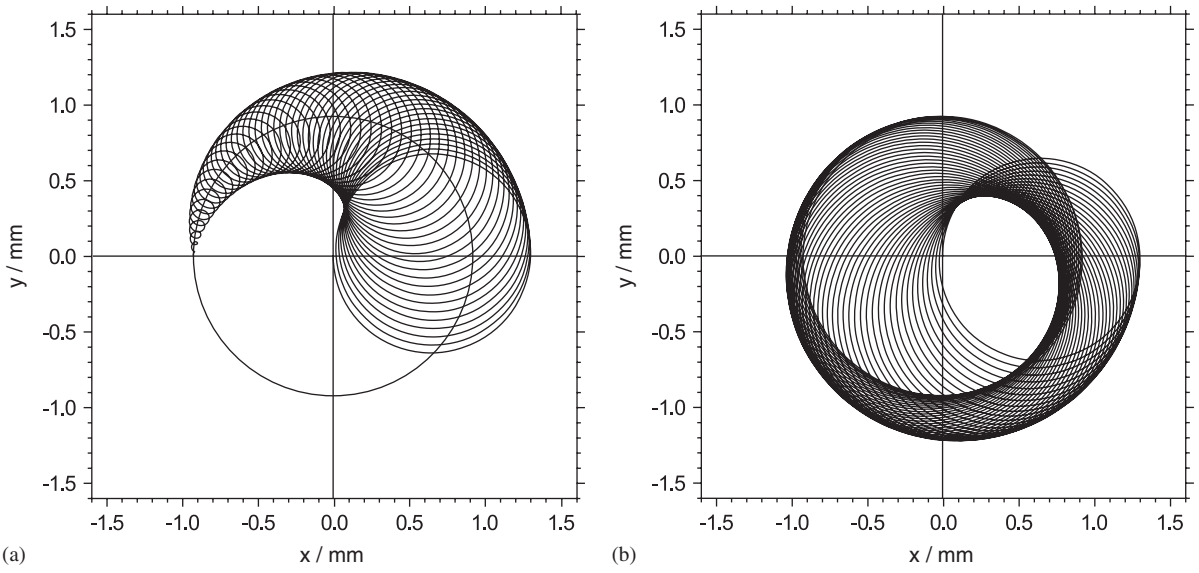

Fig. 17. Conversion of a pure magnetron motion in a pure cyclotron motion in the case of azimuthal quadrupole excitation at $\nu_{rf} = \nu_c$. The motion starts with pure magnetron motion, indicated by the solid circle. Parts (a) and (b) show the first and second half of the conversion.

Since the radial kinetic energy E_r is proportional to the revolving frequency of the trapped ion [36]:

$$E_r(t) \propto \omega_+^2 \rho^+(t)^2 - \omega_-^2 \rho^-(t)^2 \approx \omega_+^2 \rho^+(t)^2 \ , \tag{43}$$

with ρ^+ and ρ^- being the amplitude of the modified cyclotron and magnetron motion, respectively, the resonant coupling of these two motions results in an increase of the radial kinetic energy ($\omega_+ \gg \omega_-$; see Table 3) and thus of

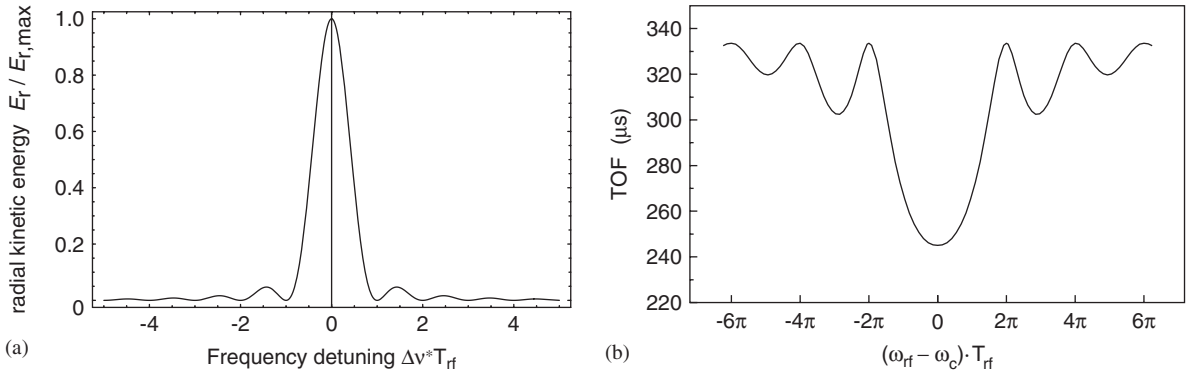

Fig. 18. (a) Radial energy gain of the ion motion in the case of a quadrupole excitation near ω_c and (b) theoretical line shape of the ions' mean time of flight from the trap to the detector both as a function of the frequency detuning $\Delta\omega$ [162]. The energy is normalized to the maximum and the detuning to the reciprocal of the excitation time T_{rf}. The center frequency ($\Delta\omega = 0$) is the true cyclotron frequency ω_c for a given ion mass m.

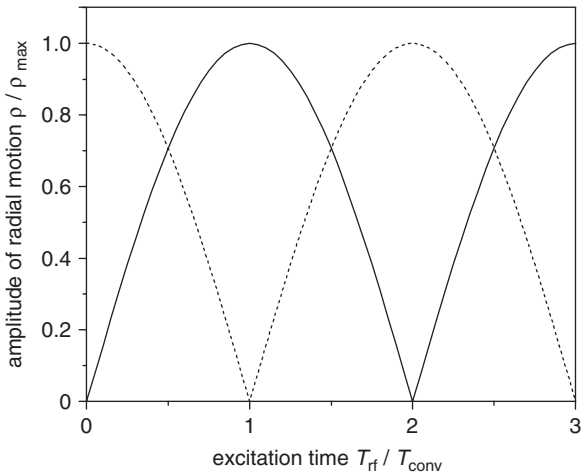

Fig. 19. Magnetron (dashed line) and cyclotron (solid line) amplitudes as a function of the ratio T_{rf}/T_{conv} of excitation time to conversion time.

the associated magnetic moment. The exact functional relation of the energy gain depends on the overall shape of the excitation signal. For a rectangular profile, i.e., the quadrupole excitation is applied at constant amplitude only during the interval T_{rf}, the resulting energy gain (shown in Fig. 18(a) [162]) results in

$$E_r = \frac{\sin^2(\omega_b T_{rf})}{\omega_b^2} \ , \tag{44}$$

with

$$\omega_b = \frac{1}{2}\sqrt{(\omega_{rf} - \omega_c)^2 + (\omega_{conv}/2)^2} \ . \tag{45}$$

The overall effect of the resonant coupling of magnetron and modified cyclotron motions is a harmonic beating between these two radial motions as depicted in Fig. 19 [19]. For $\omega_{rf} = \omega_c$ the beating frequency Ω_0 is proportional to the amplitude V_{rf} of the radiofrequency field. For $\omega_+ \gg \omega_-$ it is

$$\Omega_0 = \frac{V_{rf}}{a^2}\frac{1}{4B} \ , \tag{46}$$

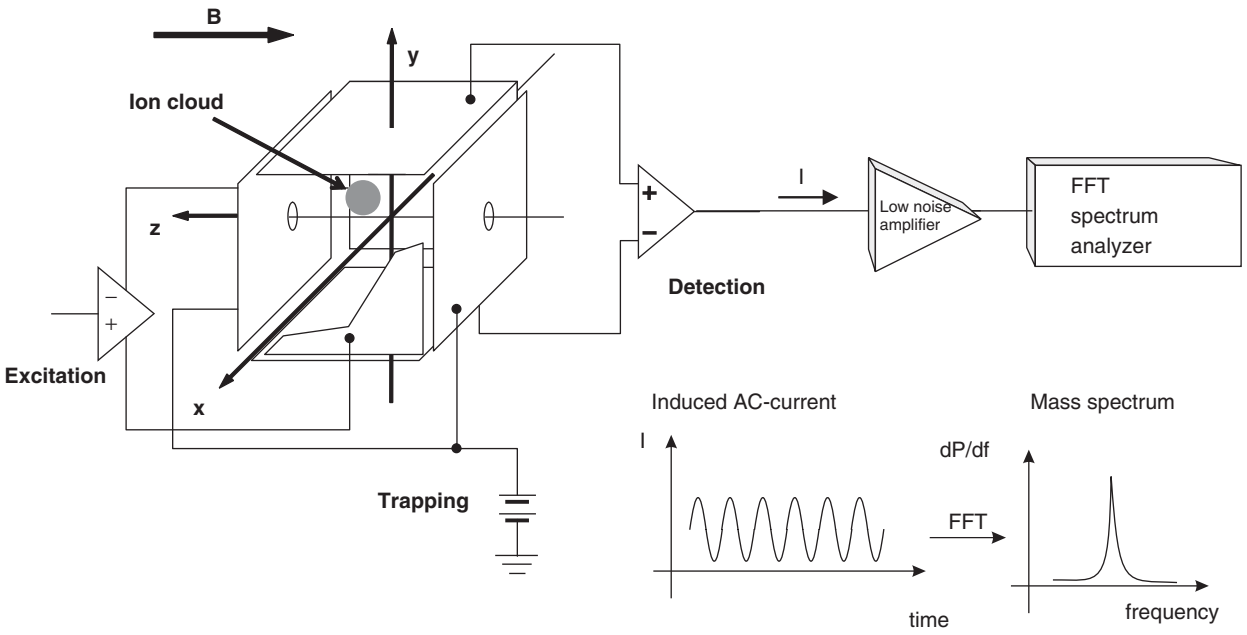

Fig. 20. Sketch of a typical electrode configuration and electronic circuitry for a broad-band non-destructive Fourier-transform mass spectrometer using induced cyclotron resonance detection of the eigenfrequencies. For positive ions the two end plates are at positive potential relative to the four plates parallel to the magnetic field used for ion resonance excitation and detection. The radial or axial oscillations of a collection of stored ions are excited to coherent motion of a specific radius by a radiofrequency signal. The frequency spectrum is obtained by a Fourier transformation of the amplified induced image currents in the electrodes.

where V_{rf} corresponds to the maximum potential of the quadrupole rf field measured on a circle with radius a. The beating frequency is mass independent. A conversion from a pure magnetron to a pure cyclotron motion is obtained after a time T_{conv} which is half the beating period

$$T_{\mathrm{conv}} = \frac{\pi}{\Omega_0} = \frac{4\pi a^2 B}{V_{\mathrm{rf}}} \,. \tag{47}$$

4.2. Frequency measurement techniques

For the frequency measurement of the stored ions one has to distinguish between *destructive* and *non-destructive* techniques. While in the first case the ions are lost after the detection and a new loading of the trapping device is required, in the second case the ions stay in the trap and can be used for another measurement or for further experiments. For mass spectrometry on very short-lived radionuclides (half-lives of seconds or below) the destructive method is not a drawback since the nuclei decay anyhow in a short time period. However, for long-lived radionuclides with low production rates or stable ions a non-destructive frequency measurement technique is favorable.

Currently only two methods are used for measuring cyclotron frequencies in high-accuracy mass spectrometry with ion traps: (1) manipulation of the ion motion by radiofrequency fields and measurement of the *time of flight* (TOF) of the ions from the ion trap after ejection to an ion detector placed outside the magnetic field and (2) *broad-/narrow-band observation* of the oscillating image currents induced by the motion of the ion in the trap electrodes.

The broad-band detection of image charges is also called *Fourier-transform ion–cyclotron resonance* (FT-ICR) mass spectrometry and is, since its inception by Comisarow and Marshall in 1974 [163], widely practiced in chemistry and cluster studies when a large number of ions are stored simultaneously and when the ion cloud is excited to large cyclotron orbits [138,164]. The frequency-domain spectrum and thus the mass spectrum is obtained by Fourier transformation of the digitized time-resolved recorded ICR signal. A typical FT-ICR Penning trap configuration and its electronic circuitry is shown schematically in Fig. 20. The cubic container has the advantage of ease of accurate construction but the disadvantage of electric fields which cannot be described by simple analytical functions. In the following only the

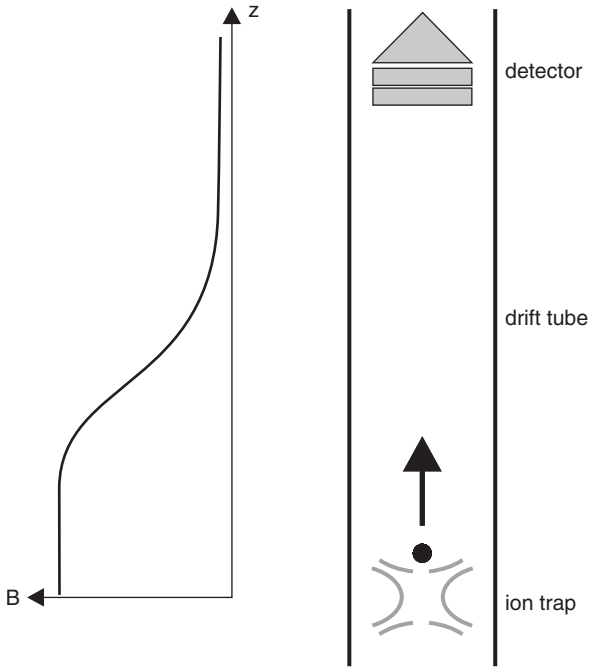

Fig. 21. Principle of the time-of-flight cyclotron resonance detection technique [107].

time-of-flight detection and narrow-band image charge observation methods will be described since they are the only detection techniques used in high-accuracy mass spectrometry on a single or very few stored ions.

4.2.1. Time-of-flight detection

In the time-of-flight ion–cyclotron resonance (TOF-ICR) detection technique [107] the ions are first prepared at a well-defined radius of the magnetron motion. Here, the orbital frequency and, therefore, the orbital magnetic moment $\vec{\mu}$ as well as the associated energy $E = \vec{\mu}\vec{B}$, are small. By application of a resonant quadrupolar excitation, with an appropriate choice of amplitude and excitation time, the magnetron motion is completely converted into the (modified) cyclotron motion (see Section 4.1.2) while the radial radius remains constant [141].

When the ions are ejected from the trap after one full conversion (by lowering the trapping potential of the downstream end electrode) at initially low axial velocity they drift along the axis out of the magnetic field, as shown in Fig. 21. In passing through the magnetic field gradient the ions get accelerated due to the gradient force and thus the axial velocity of the ions increases. The force is proportional to the magnetic moment and hence to the radial energy E_r,

$$\vec{F} = -\vec{\mu}(\vec{\nabla}\vec{B}) = -\frac{E_\mathrm{r}}{B}\frac{\partial B}{\partial z}\hat{z}\ . \tag{48}$$

In each of several experimental cycles, different excitation frequencies are applied. Since the magnetic moment and the radial energy of the ions are larger in resonance due to the higher frequency of the cyclotron motion as compared to the magnetron frequency, the resonantly excited ions arrive earlier at the detector than those ions that have been excited non-resonantly. For the determination of the time of flight the ejection from the trap is the start signal and the ions' arrival at the detector the stop signal. The change in the time of flight from the trap center ($z = 0$) to the detector ($z = z_1$) for a given radial energy E_r can be calculated by

$$T_\mathrm{tot}(\omega_\mathrm{q}) = \int_0^{z_1} \sqrt{\frac{m}{2(E_0 - qU(z) - \mu(\omega_\mathrm{q})B(z))}}\,\mathrm{d}z\ , \tag{49}$$

where E_0 denotes the initial axial energy of the ion and $U(z)$ and $B(z)$ the electric and magnetic potential difference, respectively. A variation of the quadrupole frequency ω_rf results in a characteristic time-of-flight cyclotron resonance

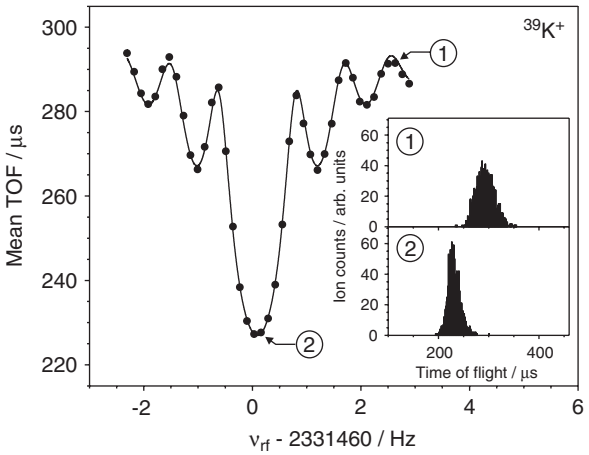

Fig. 22. Cyclotron resonance curve of $^{39}K^+$ for an excitation duration of $T_{rf} = 900$ ms. The solid line is a fit of the theoretically expected line shape to the data [162]. The inset shows two time-of-flight spectra off and in resonance, labeled with (1) and (2), respectively.

curve. The theoretically expected line shape for such a resonance (see Fig. 18b) is mainly determined by the Fourier transformation of the rectangular time excitation profile and is similar to the absolute value of the so called sinc(x)-function $f(x) = \sin(\alpha x)/\alpha x$ [162]. This line profile can be fitted to the experimental data. Such a fit is included in Fig. 22 for the stable nuclide ^{39}K, which shows excellent agreement. The effect of resonant and off-resonant excitation on the time of flight is shown in the inset of Fig. 22. The resonantly excited ions (2) are clearly shifted to lower time-of-flight times compared to the non-resonant case (1). The width of such a TOF-ICR signal, and thus the resolving power, is Fourier limited by the duration of the quadrupolar excitation.

In the isochronous mass spectrometry (IMS) mode of the storage ring the revolution times of each individual stored ion are also measured by a destructive time-of-flight technique. To this end the ions cross a very thin, metallized carbon foil, being typically a few µg cm^{-2} thick, mounted in the ring aperture, and eject at each passage δ-electrons which are guided by electric and magnetic fields to a suitable detector. In this way, every ion produces periodically at each passage a time-stamp. With a proper data analysis software the fast-sampled sum signal can be assigned to individual ions and their mass can be determined via the measured time of flight. Due to energy loses in the foil only a few hundred to a few thousand turns can be observed for one and the same ion.

4.2.2. Detection by image charges

The main advantage of a non-destructive ion detection technique is the possibility to repeat the experiment with the identical trap content, i.e., a reloading of the trap is not required. With the detection of the image charges a full resonance spectrum after one experimental cycle can be obtained instead of repeated probing of the expected cyclotron frequency. This is a huge time saver. However, in high-accuracy mass measurements usually one works with only a single (or only very few) ions in the trap at any given time, in order to avoid any frequency shifts due to space charge effects (see Section 3.3.2). In addition, the amplitudes of the ion motion are kept rather small to avoid the influence of inhomogeneities of the trapping fields. Thus, the image-charge methods have to be very sensitive and highly tuned circuits of high quality factor Q have to be used, as shown in Fig. 23.

The signal-to-noise ratio of a narrow-band image charge detection is given as

$$\frac{S}{N} = \frac{\sqrt{\pi}}{2}\frac{r_{ion}}{D} q \sqrt{\frac{v}{\Delta v}}\sqrt{\frac{Q}{kTC}}\,, \tag{50}$$

where r_{ion} is the motional radius and q the charge state of the ion, D is the effective electrode distance, $v/\Delta v$ is the ratio of the ion frequency and spectral width, T is the temperature and C the capacity of the detection system. The signal of the charged particle stored in a Penning trap is picked up by means of an attached narrow-band electronic resonance circuit working under cryogenic conditions ($T = 4.2$ K). It enables the detection of a single ion as well as further successive measurements with the same ion. The invariance principle requires the measurement of all three

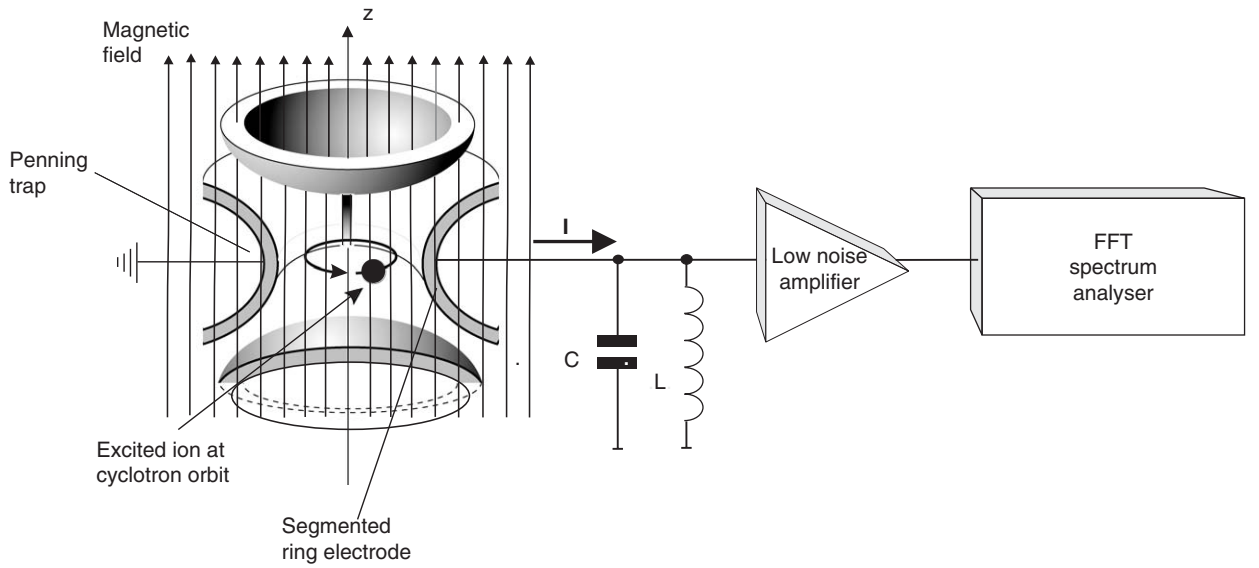

Fig. 23. Experimental setup for a sensitive, narrow-band detection of a single stored ion. Due to a tuned resonance circuit with a high quality factor Q an improved detection sensitivity is reached.

eigenfrequencies. However, generally the axial oscillation is monitored. In order to detect changes in the cyclotron orbit the modified cyclotron and the axial motion must be coupled. They are completely decoupled in the ideal trap but coupling can be achieved, for example, magnetically [36], electrostatically [165], or by side-band excitation [166,167]. In this way, a slight change in the cyclotron radius upon its excitation results in a change of the axial motion.

Another sensitive detection technique based on the measurement of image charges is called the *pulse and phase* (PNP) method [168]. Here, the ions' cyclotron motion is driven to a certain amplitude and phase at starting time $t = 0$, and then allowed to accumulate phase for some time T_{evol}, after which a π-pulse is applied in order to couple the cyclotron and axial modes. A π-pulse can be created by applying the coupling just long enough to cause the coupled modes to exactly exchange their energy. The phase of the axial signal immediately after the π-pulse is then measured with a DC-SQUID (superconducting quantum interference device) [169]. Because of the phase coherent nature of the coupling, this determines the cyclotron frequency with the same uncertainty. The ions' cyclotron frequency is obtained by measuring the accumulated phase versus evolution time T_{evol}. The PNP has the advantage of leaving the ion's motion completely unperturbed, i.e. undetected and undamped, during the cyclotron phase evolution [166].

The Schottky mass spectrometry (SMS) method in a storage ring is also based on the detection of image charges [48] and provides, as in the case of a Penning trap, single-ion sensitivity. The revolution frequency of the highly charged ions is determined from a Schottky-noise analysis, i.e., at each turn the induced mirror charges of the circulating ions on two electrostatic pick-up electrodes is monitored. Typically the 30–34th harmonics of the signals are picked up by a resonant circuit. The signals of both pick-up plates are amplified with low-noise amplifiers and then summed. The Fourier transformed signal delivers the frequency and thus the mass spectrum. At a charge state of $q = 30^{+}$ the detection sensitivity is high enough to detect single ions.

4.3. Cooling and accumulation techniques

Cooling of stored ions results in a reduction of the motional amplitudes or—in the quantum mechanical picture of ion traps—in a lowering of the quantum numbers n (see Fig. 14) of the particles oscillating in the trap potential. Cooled ions can be trapped in a much smaller volume and thus probe less of the imperfections in the trapping electric and magnetic fields. In addition beam transport of a cooled ion ensemble is much more efficient due to the reduced transverse and longitudinal emittance.

The performance of a storage ring depends strongly on the possibility of beam cooling, i.e. the enhancement of phase-space density by interaction of the ion beam with external particles or devices. The main reason is that the mass

Table 4
Different cooling techniques and their fields of application

Cooling technique	Paul/Penning trap	Storage ring
Buffer gas cooling	⋆⋆⋆	
Evaporative cooling	⋆⋆	
Resistive cooling	⋆⋆	
Electron cooling	⋆	⋆⋆⋆
Laser cooling	⋆	⋆
Stochastic cooling		⋆⋆
Sympathetic cooling	⋆	

Three stars indicate that the method is most often used, two stars indicate often usage, one star indicates rare usage, and zero stars not used so far.

resolving power is directly proportional to the relative velocity spread $\Delta v/v$, and for small particle numbers, as is the case with exotic beams, the effect of ordered-beam formation [170,171] is very favorable.

Ion cooling is therefore mandatory for high-accuracy mass spectrometry with stored ions. Quite a number of different cooling techniques have been developed during the past years. Here, only the most important cooling methods which are applied to charged particles stored in ion traps and storage rings will be discussed (see Table 4).

4.3.1. Buffer gas cooling

The most common cooling technique for radioactive ions stored in a Paul or Penning trap is buffer gas cooling in combination with radiofrequency excitation at the true cyclotron frequency ν_c. Fig. 9 shows as an example the segmented radiofrequency quadrupole as used at ISOLTRAP [132].

The effect of the buffer gas on the ion motion can be described by a viscous drag force

$$\vec{F} = -\delta m \vec{v} \ , \tag{51}$$

where $m\vec{v}$ is the ion momentum with the ion mass m and the ion velocity $\vec{v}$ and δ is the damping parameter describing the effect of the buffer gas. With the ion mobility K_{ion} the damping constant δ can be written as

$$\delta = \frac{q}{m}\frac{1}{K_{\text{ion}}}\frac{p/p_N}{T/T_N} \ . \tag{52}$$

Here, q/m is the ion's charge-to-mass ratio and p and T are the gas pressure and temperatures in units of the normal temperature T_N and pressure p_N. Usually, noble gases are used as buffer gas because of their high ionization potential and thus minimum losses due to charge exchange.

The damping of the motional amplitudes can be described as

$$\rho(t) = \rho_o \mathrm{e}^{-\alpha t} \ . \tag{53}$$

For linear oscillatory motions such as the oscillations in a Paul trap or the axial motion in a Penning trap the coefficient α is equal to the damping coefficient δ. In the cases of the magnetron and cyclotron motion in a Penning trap the damping constants are [19]

$$\alpha_\pm = \pm\delta\frac{\omega_\pm}{\omega_+ - \omega_-} \ . \tag{54}$$

The cyclotron as well as the axial oscillations are damped by buffer gas collisions. However, the negative sign of α_- results in an increase of the magnetron orbit with time since the ion loses (potential) energy by collisions with the buffer gas atoms [118,162]. This effect is shown in Fig. 24 and is in accordance with the total negative energy of the magnetron motion (see energy level diagram in Fig. 14). This drift to the ring electrodes and subsequent ion loss is counteracted by excitation of the stored ion by a quadrupolar rf-field at $\nu_c = \nu_+ + \nu_-$ that couples the modified cyclotron and the magnetron motion [118] (see also Section 4.1.2). In this way, all three quantum numbers n_+, n_z, and n_- (see Fig. 14) are driven to smaller numbers until the temperature of the ion cloud reaches that of the buffer gas and the ion sits at the trap center. It is worth noting that this cooling and centering process is mass selective because it involves the cyclotron frequency of the ion. This technique is applied in all Penning-trap mass spectrometer setups for short-lived

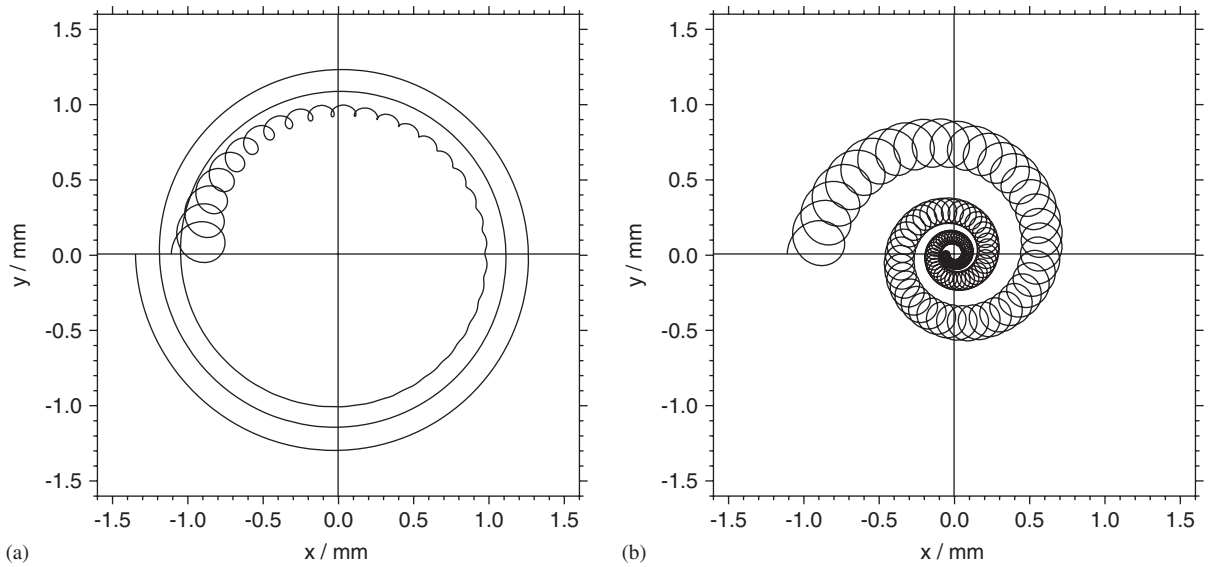

Fig. 24. Calculated radial ion trajectories in a plane perpendicular to the magnetic field. The cross marks the center of the trap. A velocity dependent damping force representing the buffer gas cooling has been included in the equations of motion. In (a) a fast damping of the cyclotron motion and a slow increase of the magnetron motion are observed. In (b) the effect of an additional excitation with an azimuthal quadrupole field of frequency ν_c is shown. Both cyclotron and magnetron motions are decreased and a mass-selective centering to the trap center is achieved.

radionuclides since the cooling process last only a few milliseconds. It is also used in many FT-ICR experiments in chemistry [164].

Trapping and buffer gas cooling in a linear radiofrequency quadrupole structure is also incorporated in the laser ion source trap (LIST) project, which has been built and is presently being tested at the University of Mainz [172]. The primary purpose of the combination of a laser ion source with a linear radiofrequency quadrupole ion trap is to decouple the evaporation and ionization processes and thus drastically improve the isobaric selectivity of laser ion sources at on-line separators based on resonance ionization [173–175]. By exploiting trapping, cooling, and bunching in a linear Paul trap LIST will deliver radioactive ion beams with selectable temporal structure from quasi-dc to pulses of microseconds duration and with an emittance that is improved by up to an order of magnitude as compared to conventional laser ion sources at on-line isotope separators [176].

4.3.2. Resistive cooling

With resistive cooling the motional energy of the stored charged particles is damped by use of an external circuit that is continuously kept in resonance with the eigenfrequency of the ions' motion. The kinetic energy of the ions is dissipated in a resistor of the circuit via the image currents induced in the trap electrodes. Finally, the energy of the ions corresponds to the temperature at which the resistor is kept (generally the temperature of liquid helium, 4.2 K), i.e., a thermal equilibrium with the environment is reached.

For simplicity we consider an ion with a charge-to-mass ratio q/m oscillating between two parallel infinite plates separated by a distance d [120]. If the velocity of the ion is v, then the induced image charges cause a current flow i through the resistor R, given by

$$i = \frac{qv}{d} \ . \tag{55}$$

This current would dissipate an energy of i^2R per unit time through Joule heating of the resistor and damps the ion motion as

$$\frac{\mathrm{d}E}{\mathrm{d}t} = -Ri^2 = -R\frac{q^2v^2}{d^2} = -R\frac{q^2E}{md^2} = -\frac{1}{\tau}E \ , \tag{56}$$

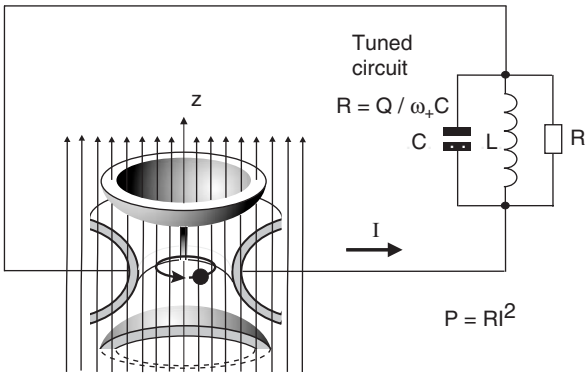

Fig. 25. Sketch of resistive cooling: The energy of the reduced cyclotron motion (ω_+) of an ion stored in a Penning trap can be dissipated through the resonant impedance of the quality $Q = \omega/\Delta\omega$.

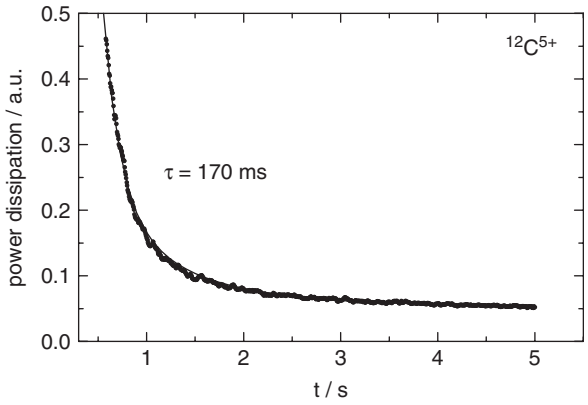

Fig. 26. Resistive cooling of the axial motion of a single $^{12}C^{5+}$ ion. The experimentally observed cooling rate of 170 ms is in agreement to the value calculated from [119]. The zero line is given by the noise power with an empty trap.

where E is the total energy of the particle. Assuming a harmonic oscillation $v = v_0 \cos^2 \omega t$ it results in $\langle mv^2 \rangle = mv_0^2 \langle \cos \omega t \rangle = \frac{1}{2} mv_0^2 = E$. The energy evolution of a single ion can thus be described by an exponential behavior $E = E_0 \exp(-\gamma t)$ where the time constant $\tau = 1/\gamma$ of the cooling process is given as

$$\tau = \frac{md^2}{Rq^2} \ . \tag{57}$$

Resistive cooling is hence especially efficient for ions with a large charge-to-mass ratio q/m and the time constant can be made small by use of a large resistor R. A possible experimental configuration for resistive cooling of radial ion motion with an external resonant circuit is shown in Fig. 25. A similar configuration can be used for axial cooling of the ions' motion. For a single stored highly charged carbon ion $^{12}C^{5+}$ with a tuned resonant circuit ($Q = 2000$, $T = 4.2$ K) a cooling constant of $\tau = 170$ ms was demonstrated (see Fig. 26) [13]. For short-lived radionuclides this cooling technique is not applicable due to the long cooling times and most often buffer gas cooling is applied (see Section 4.3.1).

Deviation from the exponential behavior as shown in Fig. 26 occurs when the cooling force is no longer proportional to the kinetic energy of the ions. A possible reason is that the ion frequency depends on the energy and therefore the effective resistance of the resonant circuit at the ion frequency changes during the cooling process. This may occur for large motional amplitudes since higher-order multipole components in the trapping potential become significant and the ion motion is no longer harmonic. In the case of a cloud of ions the situation becomes even more complicated since

only the center-of-mass mode is cooled resistively [119]. The other modes are only cooled due to their coupling to the center-of-mass mode.

Resistive cooling can be applied to the axial and modified cyclotron motion. However, as discussed above, reducing the energy of the magnetron motion would lead to an increase of the magnetron radius and finally to the loss of the ions. This can be avoided by coupling the magnetron oscillation to one of the other modes by a radiofrequency field at the sum frequency of both oscillations. This technique is often called sideband-coupling cooling.

4.3.3. Evaporative cooling

A brute force cooling technique is evaporative cooling. The process is analogous to the way a cup of hot coffee cools down by giving off the most energetic molecules as steam. As the energetic ions are removed from the trap by lowering the trapping potential, collisions readjust the remaining ions into a lower temperature thermal distribution. The ions remaining in the shallow potential well have low motional energy once the trapping voltage is returned to normal values. This procedure can be continued until only one or a few ions remain in the trap. This cooling technique is well known and widely used for magnetically trapped atoms [177]. It was developed for the pioneering efforts to achieve Bose–Einstein condensation in gaseous hydrogen [178]. It is an essential technique for atom traps and a decrease of several orders of magnitude in the temperature can be achieved within a short time, which has never been achieved with other cooling methods.

In ion traps evaporative cooling is not that efficient due to Coulomb collisions of the stored ions. For the ions produced and confined in an electron beam ion trap the steady-state evaporation of lowly charged ions is employed for cooling highly charged ions [179,180]. In the precision trap of SMILETRAP the ions are subject to an evaporation process by lowering the trap voltage from 5 to 0.1 V leaving only the coldest ions in the trap [64]. On average not more than one or two ions are left in the trap after this procedure, which is not only used for cooling but also to minimize ion–ion interactions and contamination effects.

4.3.4. Electron cooling

Electron cooling is a well-established technique to increase the phase space density of particle beams in storage rings. This is achieved by aligning the ion beam with a cold dense electron beam from a cathode. For a certain distance (about 2.5 m in the case of the experimental storage ring at GSI) the electrons are flying parallel to the ions circulating in the storage ring. The root-mean-square velocity spreads of the ions in all degrees of freedom is reduced by Coulomb interaction with the electrons. The main components of an electron cooler are shown in Fig. 27. Since its first realization by Budker in 1966 [117], the electron cooling method has been significantly developed. Demonstrated and studied in the first experiments in INP, Novosibirsk in 1974 [181], at CERN in 1980 [182], and at Fermilab in 1982 [183], this cooling method has become an efficient tool and is now a routinely used technique in storage rings and becomes more and more important in ion trap experiments. The theoretical framework was summarized in a review article by Poth [184]. The operating parameters of the electron cooler at the experimental storage ring (ESR) at GSI Darmstadt are listed in Table 5.

The principle of an electron cooler is similar to that of a heat exchanger. It relies upon the momentum exchange between “hot” ions and collinear, “cold” electrons by Coulomb collisions. Ions that are too energetic transfer kinetic energy to the electrons and get decelerated, while ions with too low energy gain kinetic energy and get accelerated. At the end of the cooling section the electrons are deflected out of the storage ring. Since electron cooling takes in general a few seconds until thermal equilibrium is reached, i.e. until the ions have the same longitudinal and transverse temperature as the electrons, this cooling technique is not suitable for very short-lived radionuclides.

Electron cooling provides brilliant beams [154] of small emittance, small momentum spread ($\Delta p/p \approx 10^{-5}$–$10^{-7}$), and high phase-space density. In a proper vacuum the storage time for longer lived nuclides exceeds many hours, even for highly charged medium-heavy ions, and the cooled particles all orbit with the same well-defined velocity.

Electron cooling in a trap has first been employed at LEAR/CERN to slow down antiprotons from an energy of 3 keV to rest [185]. This experiment aimed at an accurate mass comparison of the proton and antiproton in order to test charge conjugation, parity, and time (CPT) invariance [49]. Electron cooling of antiprotons in Penning traps [186] is one of the key processes that enabled the first production of cold antihydrogen atoms at CERN in 2002 [187–190]. Positron cooling of trapped highly charged ions has also been studied [191].

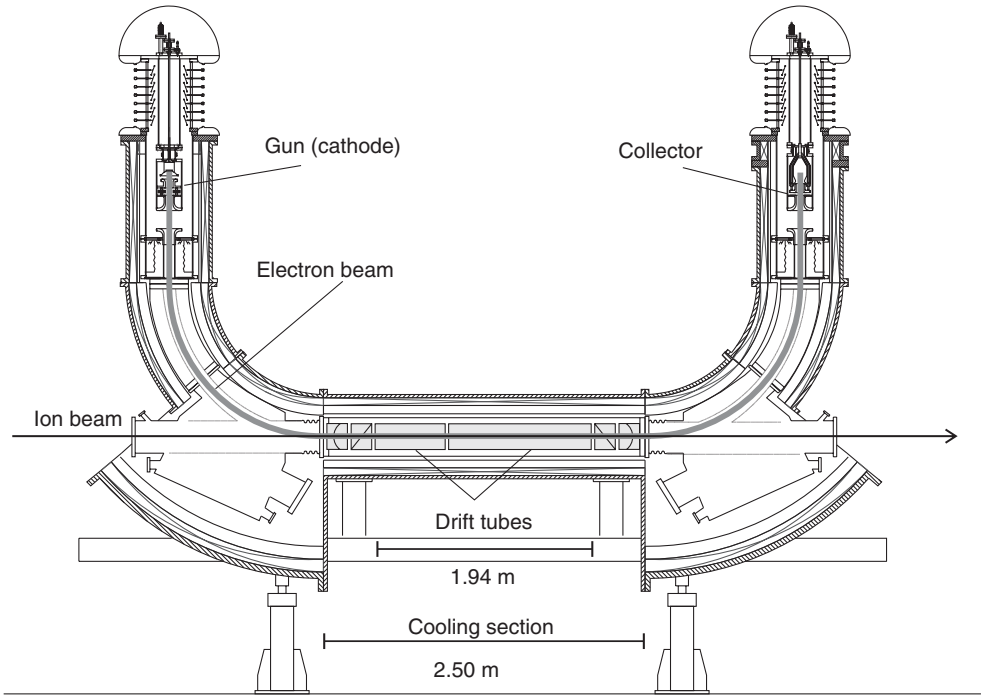

Fig. 27. Schematic view of an electron cooler. The main components are indicated.

Table 5
Operating parameters of the electron cooler at the experimental storage ring ESR at GSI Darmstadt

Electron beam		
Energy	16.5–320	keV
Diameter	50.8	mm
Electron current	max. 10	A
Transversal temperature $k_B T_\perp$	≈ 120	meV
Longitudinal temperature $k_B T_\parallel$	≈ 0.1	meV
Beam guiding		
Magnetic flux density	max. 0.25	T
Cooling section length	2500	mm
Drift tube diameter	200	mm

Compared to storage rings, electron and positron cooling in ion traps has a few peculiarities:

1. Cooling of antiprotons is caused by Coulomb interaction with electrons. Synchrotron radiation due to the high magnetic field in the trap causes the electrons to cool to the 4.2 K surroundings of the trap [36] and the Coulomb interactions bring the antiprotons into thermal equilibrium with them.
2. The electron cloud has a reversed flattened distribution of electron velocities. The longitudinal velocity spread is substantially larger than the transverse one.
3. The application of positron cooling to antiprotons requires trapping in the same place inside the trap although the particles have opposite charges. This is possible by using nested traps (see Fig. 28).

In the HITRAP project [50,51], a facility for high-accuracy experiments with trapped highly charged ions at GSI, electron cooling is applied in the storage ring as well as in the Penning trap. In the storage ring ESR the injected ions are electron cooled and decelerated to 4 MeV/u, and then injected into a linear decelerator. After deceleration to about 10 keV/q the ions are accumulated, and electron and resistively cooled in a Penning trap before they are transferred to

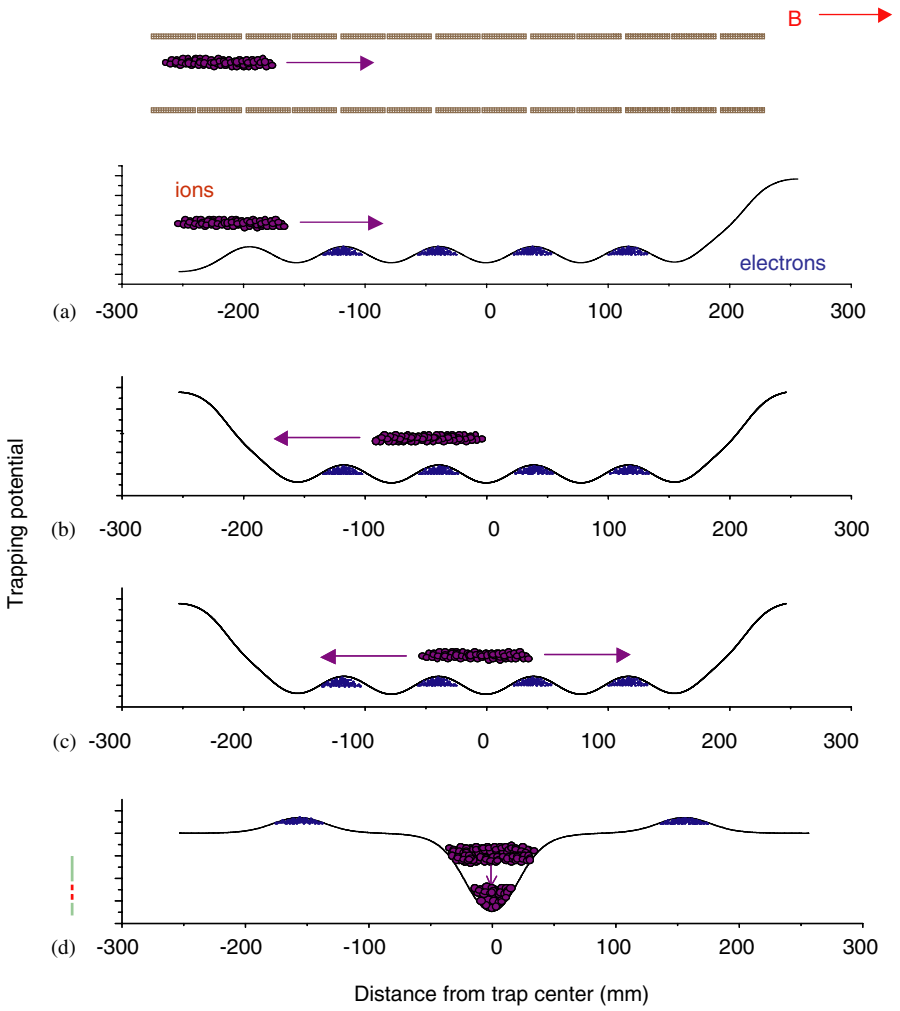

Fig. 28. Scheme showing the experimental setup of a nested Penning trap and the cooling cycle for electron cooling of highly charged ions at HITRAP [50,51]. The ions enter the trap (a), are reflected and caught after their first turn by switching the potential (b), cooled by the electron cloud (c) and finally by resistive cooling (d) after which they will be released from the cooler trap in order to be transferred to the precision experiments.

the setups for high-accuracy experiments (see Section 11). The planned cooling cycle in the HITRAP cooler Penning trap is shown in Fig. 28. The difference between cooling of highly charged ions and antiprotons is that for highly charged ions recombination processes have to be taken into account.

4.4. Mass determination and calibration issues

The mass determination in a Penning trap is based on the determination of the cyclotron frequency $\nu_c = qB/(2\pi m)$ of ions with charge q stored in a homogeneous and stable magnetic field with magnitude B. More precisely, the quantity that can be determined is the charge-to-mass ratio but normally the charge state of the ion is known.

In high-accuracy mass measurements the important relationships between the eigenfrequencies of the motion of the ion and the pure cyclotron frequency are already given in Eqs. (24) and (25). The independent determination of the eigenfrequencies and the use of these equations allow a mass determination of the stored ions when the magnetic field is known. There are two approaches: Either the eigenfrequencies can be determined by driving the corresponding motions by a dipole rf field [36] or a direct determination of the sum frequency of the magnetron and modified cyclotron motion via a quadrupole excitation [141,162].

In order to extract the atomic mass m from the measured frequency, the magnetic field has to be calibrated. This is performed by the measurement of the cyclotron frequency of a reference ion with well-known mass m_{ref}, for example, ^{23}Na, ^{85}Rb, and ^{133}Cs. These have been determined in a Penning trap experiment with a relative uncertainty of better than 2×10^{-10} [192]. If all ion species are singly charged $q = +e$, the atomic mass m of the ion of interest can be calculated by

$$m = \frac{\nu_{\mathrm{c,ref}}}{\nu_{\mathrm{c}}}(m_{\mathrm{ref}} - m_{\mathrm{e}}) + m_{\mathrm{e}} \ , \tag{58}$$

where $\nu_{\mathrm{c,ref}}$ denotes the cyclotron frequency of the reference ion, ν_{c} the cyclotron frequency of the ion of interest, m_{ref} the atomic mass of the reference ion, and m_{e} the electron mass. However, in this manner, the uncertainty of the atomic mass of the reference ion contributes to the uncertainty of the mass result as well. That is why most times the mass results obtained by Penning trap mass spectrometry are reported in terms of the ratio r of the cyclotron frequencies:

$$r = \frac{\nu_{\mathrm{c,ref}}}{\nu_{\mathrm{c}}} = \frac{m^{\mathrm{ion}}}{m^{\mathrm{ion}}_{\mathrm{ref}}} \ . \tag{59}$$

In this way, the mass of the ion of interest can be re-determined at any later time that there is a revised mass of the reference ion. While in storage ring mass spectrometry the cyclotron resonances of several ion species can be recorded at the same time since they are stored simultaneously, in Penning trap mass spectrometry the reference measurement is made in general once before and once after that of the investigated ion. The measured cyclotron frequencies are later interpolated to the time of the measurement of the ion of interest in order to eliminate drifts of the magnetic field. A complete Penning trap mass measurement thus consists of three separate cyclotron frequency determinations: That of the ion of interest, preceded and followed by that of the reference ion. Because of the mass dependence of the systematic frequency shifts caused by field imperfections (see Section 3.3.2) ideally mass doublets are used. In isochronous mass spectrometry there is often a lack of proper mass references limiting the accuracy of mass measurements far from stability.

Recently, the possibility of using carbon clusters as mass references for high-accuracy on-line mass measurements on singly charged radionuclides has been demonstrated [193]. Now at the Penning trap mass spectrometer ISOLTRAP a new magnetic-field calibration method has been installed using singly charged carbon clusters C_n^+ (n up to 20) [111]. Note, the unified atomic mass unit u is defined as 1/12 of the mass of ^{12}C [194]. The advantages of the recent development are obvious [195]: a multitude of reference masses are available that are, at most, six atomic mass units from the nuclide of interest (see Fig. 29). Thus, systematic mass dependent uncertainties that increase with the difference between the measured and the reference mass are minimized. Any uncertainty of the reference mass is eliminated by definition. As a consequence, not only direct but also absolute mass measurements can be performed since the mass of an ion of interest is related directly to the microscopic mass standard. Furthermore clusters can be used to detect systematic errors and to determine the present limit of accuracy for mass measurements [111,196]. The only remaining uncertainty is in the binding energy of the carbon atoms, which is of the order of a few eV and thus negligible on the 10^{-9} level. Sometimes also carbon hydrogen compounds are used as mass references in order to have an ideal q/A-doublet available [192].

In the case of mass spectrometry on highly charged ions as, for example, at SMILETRAP or in storage rings (see Table 2), the mass of the neutral atom m is obtained by correcting for the missing q electrons with mass m_{e} and their binding energy E_{B} according to

$$m = m_{\mathrm{ion}} + q m_{\mathrm{e}} - E_{\mathrm{B}}/c^2 \ , \tag{60}$$

where m_{ion} is the experimentally determined ion mass. The total electron binding energies were calculated by summing up the relevant experimental ionization energies tabulated for example in [197]. For ions with $Z < 20$ the relative mass uncertainty in E_{B} is $< 10^{-11}$. For heavier atoms calculated electron binding energies have to be used with uncertainties of about 100 eV [198]. For closed electron shells and for those shells having one additional or one missing electron, relativistic calculations can be made with an uncertainty of the order of 20 eV [199]. Similar to mass measurements on singly charged ions the ideal mass measurements on highly charged ions are performed by using various charge states of ^{12}C as mass references. At SMILETRAP the charge q of the $^{12}C^{q+}$ ion can be chosen such that, to the degree possible, the measurement is done with ions being q/A doublets [64].

A storage ring can be used as a high-resolution mass analyzer, and the masses are determined from the accurate measurement of their revolution frequencies. The relation between revolution frequency v, mass-to-charge ratio m/q,

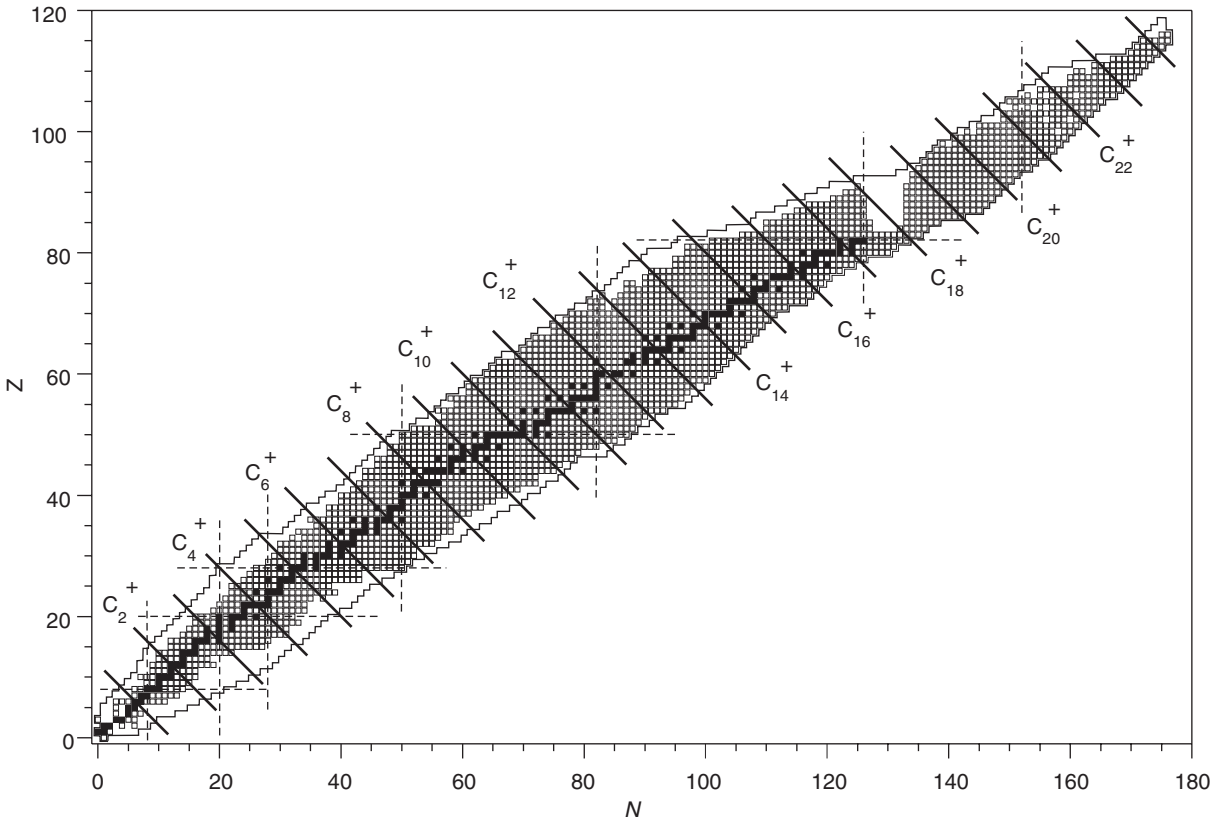

Fig. 29. Nuclear chart showing all nuclides with half-lives above 100 ms (open squares). Stable nuclides are indicated by full squares and shell closures by dashed lines. The range of known nuclides is shown by the outer lines. The diagonal solid lines indicate the isobars of carbon clusters $^{12}C_n^+$.

and velocity v of different circulating ions is given by

$$\frac{\Delta v}{v} = -\frac{1}{\gamma_t^2}\frac{\Delta(m/q)}{m/q} + \frac{\Delta v}{v}\left(1 - \frac{\gamma^2}{\gamma_t^2}\right) . \tag{61}$$

The quantity γ is the Lorentz factor of the ions and γ_t is an ion-optical parameter, which characterizes the transition point of the storage ring. For an unambiguous relation between frequency and mass, the second (velocity dependent) term on the right-hand side of Eq. (61) must be cancelled and two complementary methods apply, as shown in Fig. 30 for the experimental storage ring at GSI [200].

For Schottky mass spectrometry (SMS) [48,108,201] the storage ring is operated in the standard mode ($\gamma_t = 2.4$), electron cooling is applied so that $\Delta v/v \to 0$, and the revolution frequency is determined from a Schottky noise analysis. SMS is a versatile tool for spectroscopy on unstable, highly charged nuclides with high efficiency and resolving power, single-ion sensitivity, and in situ calibration. It enables the measurement of both the mass and the life-time of the stored ions.

The Schottky noise spectroscopy [202] is widely used for non-destructive beam diagnosis in circular accelerators and storage rings. The stored ions circulate in the storage ring with revolution frequencies of about 2 MHz. At each turn they induce mirror charges on two electrostatic pick-up electrodes which are placed in the ring aperture [203]. Because the electron-cooled ions (see Section 4.3) have a very narrow range of velocities, their revolution frequencies exhibit a one-to-one correspondence to their mass-to-charge ratios m/q. The revolution frequency is determined by the velocity of the ions and the length of their closed orbit. The signal of both pickup plates are amplified with low-noise amplifiers and then summed. Finally, the Schottky noise reveals, when Fourier transformed to the frequency space, the highly resolved masses of the various simultaneously stored and cooled ion species [153]. A typical frequency spectrum for

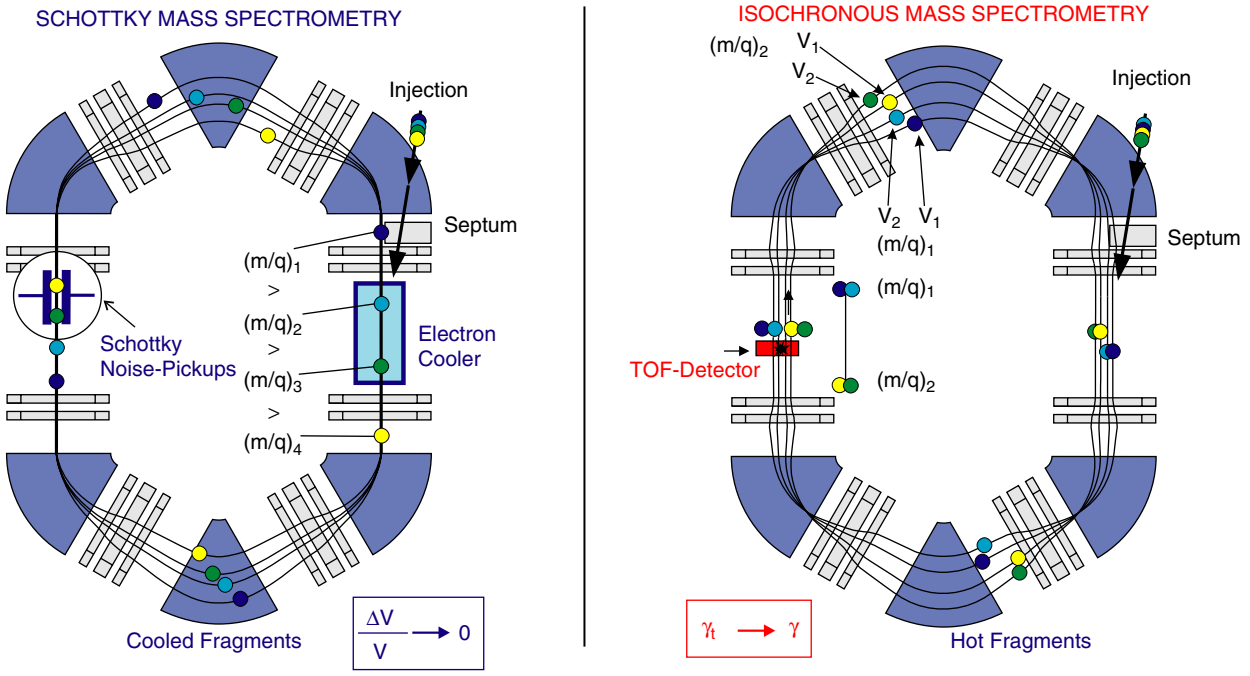

Fig. 30. (Color) Schematic view of the principle of mass measurement in the experimental storage ring at GSI. The motion of up to four different species labelled by their mass-to-charge ratio $(m/q)_{1\ldots4}$, is indicated. For Schottky mass spectrometry (left) ions are cooled by electron cooling and have the same mean velocity v whereas for isochronous mass spectrometry (right) the ions are "hot" and have different velocities.

highly charged ions of the rare earth region is shown in Fig. 31. As demonstrated in the inset of Fig. 31, SMS allows single-ion sensitivity with a high resolving power and a high efficiency. More than 100 new masses can be measured in one experiment.

The gray marked masses in Fig. 31 were previously unknown. The simultaneous storage of both unknown and known (black marked) masses allows an in-situ calibration. For two frequencies of two different ions k and l one can write in first-order approximation [48]:

$$\frac{f_k - f_l}{f_k} = -\alpha_p \frac{(m/q)_k - (m/q)_l}{(m/q)_k} , \tag{62}$$

where α_p is the momentum compaction factor, which is defined as

$$\alpha_p = \frac{dC/C}{d(B\rho)/(B\rho)} , \tag{63}$$

and which characterizes the relative variation of the orbital length (C) per relative variation of the magnetic rigidity $(B\rho)$. Typically α_p has a value of about 0.15. The width of the frequency distribution of each ion species k is given by [48]

$$\frac{\delta f_k}{f_k} = \left(\frac{1}{\gamma_k^2} - \alpha_p\right) \frac{\delta p_k}{p_k} = \left(\frac{1}{\gamma_k^2} - \alpha_p\right) \gamma_k^2 \frac{\delta v_k}{v_k} , \tag{64}$$

where $\delta p_k/p_k$ and $\delta v_i/v_i$ are the relative widths of the momentum and the velocity distributions for the kth ion species, respectively. Eqs. (62) and (64) are the basis for the Schottky mass spectrometry. They show that in order to measure masses of stored and identified ions it is sufficient to measure their orbit frequencies. The accuracy of the method can be improved by storing and studying different charge states of the same ion of interest at the same time within the accepted m/q band.

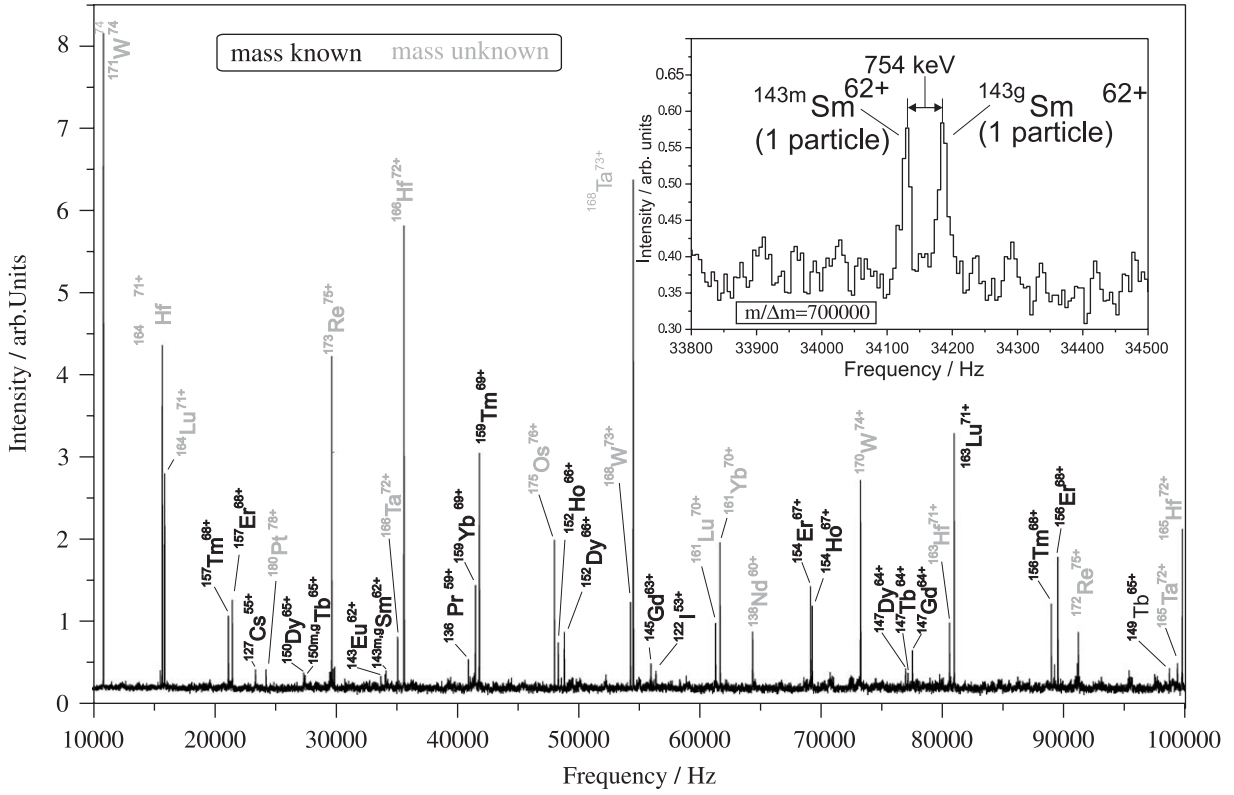

Fig. 31. Schottky spectrum of exotic nuclides simultaneously accepted and cooled in the experimental storage ring. The frequency axis shows the difference of the 32th harmonics of the corresponding revolution frequencies of the ions ($v/c \approx 0.67$) with respect to the frequency of a stabilized local oscillator operating at about 59.33 MHz. The inset shows ground and isomeric state of fully stripped ^{143}Sm. Single-ion sensitivity is obtained with Schottky mass spectrometry [200].

For isochronous mass spectrometry (IMS) [109], a technique that allows one to explore the lifetime region below one millisecond, the ESR is operated in the isochronous mode at a reduced value $\gamma_t = 1.4$. At this specific ion-optical setting the orbit frequency of ions with the same mass-to-charge ratio becomes independent of their velocity. At this so-called *transition energy* where the injected ions have a Lorentz factor of $\gamma = \gamma_t$, the ion's revolution frequency is determined from their time of flight for each turn [204]. This enables an accurate mass determination of hot uncooled nuclei [205]. The nuclides with known masses stored simultaneously with the ions under investigation are used as calibrants of the spectrum and thus the previously unknown masses can be obtained. For the detection of the circulating ions a foil is mounted in the ring aperture and delta electrons are abundantly produced at any passage of an ion through the foil. The electrons are detected by two microchannel plates (MCP) and the signals serve as time stamps for each turn of each stored ion [206]. The injected ions circulate typically a few hundred times in the storage ring with a revolution time of about 500 ns. The maximum number of observed revolutions was approximately 3500 and the masses of short-lived nuclides with half-lives as low as a few milliseconds or even in the range of microseconds (see Fig. 32) can be measured [200,205].

4.5. Resolving power and accuracy

The primary prerequisite for the accuracy of an instrument is its resolving power $\mathfrak{R}$, i.e., the line width of a resonance obtained with it [28]. Since the resolving power of a Penning trap mass spectrometer is ultimately Fourier limited, either the period of time for coherent rf-excitation T_{rf} or the observation time of the evolution of the cyclotron motion determine the line width $\Delta\nu_{\mathrm{c}}$(FWHM). According to the Rayleigh criterion, two peaks are resolved if the separation of two centroids is at least as large as the distance from either of the two centroids to its first minimum. For the resolving

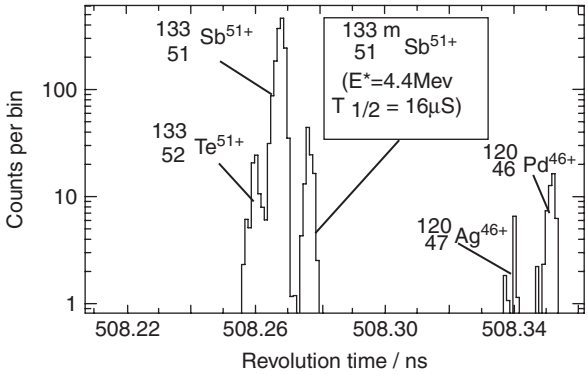

Fig. 32. A revolution-time spectrum as obtained during an experiment using the experimental storage ring in the isochronous mass mode. The capability of IMS to study nuclei with half-lives down to the microsecond range is depicted.

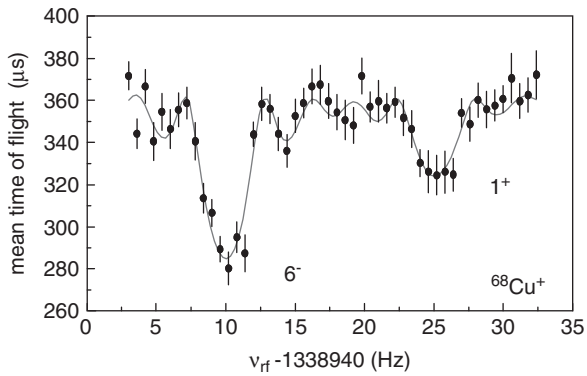

Fig. 33. Resolution of the 1^+ ground and 6^- isomeric states in ^{68}Cu. The time-of-flight resonance spectra of the ions ejected from the ISOLTRAP precision trap are plotted showing two resonances because of the mixture of two states as delivered by ISOLDE [116].

power one obtains [53]:

$$\Re = \frac{m}{\Delta m} = \frac{\nu_c}{\Delta \nu_c} \approx \nu_c T_{rf} \ . \tag{65}$$

For a singly charged ion with mass number 100 confined in a Penning trap with a magnetic field of 6 T the cyclotron frequency is about $\nu_c = 1$ MHz (see Table 3). An excitation or observation time of $T_{rf} = 1$ s results in a resolving power of typically $\Re = 10^6$. In many cases this is sufficient to separate excited long-lived nuclear states, so-called isomers, from the ground state for unambiguous state assignments [115,207] and to provide isomerically pure beams [116]. According to the energy-mass equivalence, $E = mc^2$, isomeric states are distinguished from their ground state by their additional mass. As an example, the resolution of the 1^+ ground and 6^- isomeric states in ^{68}Cu with the ISOLTRAP mass spectrometer is shown in Fig 33. In order to obtain a higher resolving power, higher cyclotron frequencies by stronger magnetic fields or higher charge states, and longer excitation or observation times are desirable. Extending for example the time of observation of the ion motion to ten seconds would increase the resolving power by an order of magnitude. This of course requires the nuclide to live and to be stored long enough. At ISOLTRAP a resolving power of about 10^7 on short-lived radionuclides was demonstrated even in the heavy mass region [114]. For light ions as in the case of the proton or antiproton the above conditions with $T_{rf} = 10$ s yields $\Re = 10^9$.

In principle the Fourier limit for frequency measurements based on Fourier analysis of detection signals can be overcome. This is the case when the integrated phase difference of the particles' motions relative to an excitation with a well-defined phase is measured [168,208]. This phase sensitive measurement technique was invented at the

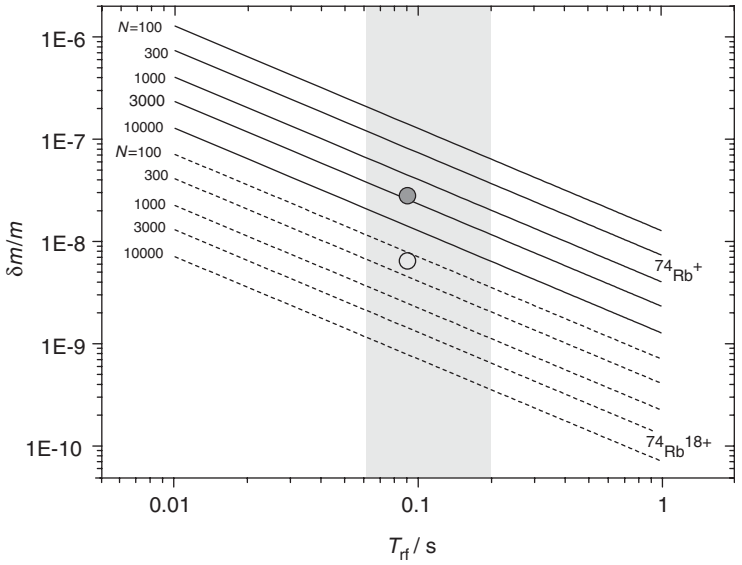

Fig. 34. Statistical mass uncertainty (see Eq. (66)) for ^{74}Rb with a half-life of $T_{1/2} = 65$ ms as a function of the excitation time in the Penning trap ($B = 5.9$ T) for two sets of charge states and different numbers of detected ions. The upper set of curves (solid lines) belongs to singly charged ions, the lower set of curves (dashed lines) to ions in the charge state 18^+. The gray-shaded area corresponds to an excitation time of about one to three times the half-life ($T_{rf} = 60$–200 ms). The full circle gives the present mass uncertainty of ^{74}Rb obtained with ISOLTRAP in 2003 [209]. The open circle indicates the accuracy limit of ISOLTRAP ($\delta m/m = 8 \times 10^{-9}$) [111], which can be reached exploiting highly charged ions with about an order of magnitude fewer ions.

MIT-TRAP (see Table 2) and is called PNP (for pulse and phase) method [168]. A similar technique is in use at the g-factor experiment at the University of Mainz [208] and is based on the fact that when the oscillation frequency of the ion is different, so is the velocity of the ion's phase evolution relative to a given initial phase. Assuming two ion species (ion of interest and reference ion) with almost identical mass, i.e. forming an excellent mass doublet, the cyclotron frequency difference can be expressed in terms of a phase difference. Thus, this scheme is not restricted by the Fourier limit.

The ability to reduce the precision beyond the line width of the centroid peak depends on the understanding of the resonance line shape, i.e. the theoretical description, as well as the statistical uncertainty of the data points that compose the measurements. Typically the center of the resonance can be determined to 10% of the full half width. In the case of Penning trap mass spectrometry and direct determination of the sum frequency via a quadrupole excitation there is an excellent understanding of the line shape [162] and the centroid can be determined to about 1% of the full half width.

For any recorded time-of-flight cyclotron resonance (see Fig. 22), the statistical uncertainty of the measured cyclotron frequency and thus of the mass of interest is given as [2,111]:

$$\left(\frac{\delta m}{m}\right)_{\text{stat}} \propto \frac{1}{\Re\sqrt{N_{\text{tot}}}} \propto \frac{m}{T_{\text{rf}} q B \sqrt{N_{\text{tot}}}}\,, \tag{66}$$

where N_{tot} is the total number of ions recorded in a single resonance and $\Re$ is the resolving power. In practise at least about 100 ions have to be measured within one resonance to get a proper fit. With the FT-ICR detection technique a complete frequency spectrum can be recorded with only a single ion stored in the trap. Here, the mass uncertainty can be reduced by measuring a sequence of N_{tot} resonances with the same stored ion. Since the resolving power is directly proportional to the observation time and the number of ions of a radionuclide being confined in the trap decreases exponentially due to radioactive decay, one can compute that the statistical accuracy is highest for an observation time that is about 2.9 times the half-life $T_{1/2}$ of the short-lived nuclide [4].

From Eq. (66), the advantage of using highly charged ions becomes obvious: For radioactive ions far from stability the interaction time is limited by the half-life while the number of detected ions depends on the production yield

Table 6
Accuracy limit $\delta m/m$, maximum resolving power $\Re$, and half-life limit $T_{1/2}$ of some of the facilities (see Table 2) performing high-accuracy mass spectrometry experiments

Name	$\delta m/m$	$\Re$	$T_{1/2}$	Ref.
CPT	1×10^{-8}	10^6–10^7	700 ms	[210,212]
ESR–IMS	1×10^{-6}	10^5	< 1 ms	[205]
ESR–SMS	2×10^{-7}	10^6	1 s	[110,115]
ISOLTRAP	8×10^{-9}	10^7	65 ms	[111,114,209]
JYFLTRAP	10^{-7}–10^{-8}	10^6–10^7	116 ms	[213]
MIT–TRAP	1×10^{-11}	$> 10^9$	stable masses	[5,7]
SHIPTRAP	10^{-7}–10^{-8}	10^6–10^7	< 1 s	[214]
SMILETRAP	3×10^{-10}	10^8	stable masses	[64]
UW–PTMS	1×10^{-11}	$> 10^9$	stable masses	[6]

In measurements on radionuclides the best values for all parameters are not achieved simultaneously in one experiment.

and the available beam time. Since highly charged ions have higher cyclotron frequencies the resolving power and the precision are increased. Alternately, a high-accuracy mass measurement can be performed in a much shorter time as compared to that for singly charged ions, which gives access to very short-lived nuclides. Fig. 34 shows the advantage of using highly charged ions with respect to precision in the case of ^{74}Rb with charge state 18^+ in a 5.9 T magnetic field.

Presently, as listed in Table 6, the achievable precision in direct mass measurements on short-lived radionuclides is about $\delta m/m = 2 \times 10^{-7}$ for storage rings [110,115] and 1×10^{-8} for Penning traps [111,210]. On stable nuclides the relative mass accuracy is between $\delta m/m = 10^{-10}$ and 10^{-11}. This is obtained either by long observation times [5,49,192,211] or by use of highly charged ions [64]. Since the ion of interest and the reference ion are not measured simultaneously, the present limit in accuracy in almost all experiments is due to fluctuations of the magnetic field. The highest accuracy obtained so far, 10^{-11} at the MIT Penning trap mass spectrometer, was achieved by parking two different ion species in a magnetron orbit at the same time and measuring their cyclotron frequency quasi-simultaneously [5]. The MIT measurement campaign was stopped in 2003 and the apparatus moved to its new location at Florida State University. After rebuilding the apparatus in Tallahassee several high-accuracy atomic mass measurements with uncertainties below 0.1 ppb have been performed and reported recently [7].

In the isochronous mode of the experimental storage ring at GSI-Darmstadt, a mass resolving power of $\Re = 110\,000$ with a mean mass accuracy of about 100 keV was demonstrated [152,205]. In the Schottky mass spectrometry mode a resolving power of up to $\Re = 2 \times 10^6$ and a relative mass accuracy of $\delta m/m = 2 \times 10^{-7}$ was obtained [110,115]. The accessible half-live in the isochronous mode of the experimental storage ring is well below one millisecond [200,205] and in the Schottky mode about one second. The latter is limited by the long time needed to cool down hot fragments, which does not allow a study of the most interesting regions of short-lived nuclei at both sides of the valley of stability.

5. Production and separation techniques for exotic nuclides

Mass spectrometry on radioactive nuclides requires their production and separation, for which several complementary techniques exist. Now, more than 3000 nuclides can be produced at the different radioactive ion beam facilities worldwide, with energies ranging from a few 10 keV to the relativistic regime. For the production of heavy, superheavy, and neutron-deficient medium-mass nuclides, heavy-ion collisions, near the energy of the Coulomb barrier, are the mechanisms of choice. This technique is exploited for example at ANL (USA) [215], GSI in Darmstadt (Germany) [216], JINR in Dubna (Russia) [217], and RIKEN (Japan) [218]. At energies above the Fermi domain, projectile fragmentation is the primary choice for the production of exotic nuclides all over the nuclear chart up to the heaviest projectile available, as it is done at GSI [219], NSCL in East Lansing (USA) [218], RIKEN [220], and GANIL in Caen [221]. Medium-mass neutron-rich nuclei can also be produced by photon, neutron, energetic-proton or heavy-ion induced fission. The facilities ISOLDE/CERN [134] and TRIUMF in Vancouver [222,223] are using among others this production technique. A survey of the different reactions themselves is given in [224]. Two general techniques used for separating the reaction products are on-line [225] and in-flight separation [226].

5.1. Isotope separation on-line

The isotope separation on-line (ISOL) technique is widely used for the production and separation of radioactive nuclides [227,228] and provided the very first exotic beams [229]. A primary beam of, for example, high-energy protons or heavy ions at energies of 100–1000 MeV/u impinges on a thick target (up to a few 100 g/cm^2) to produce large quantities of exotic nuclides. Depending on the desired radioactive species, different chemical compositions of the target, such as oxides (for example CaO and MgO), carbides (for example UC_x and ThC_x), and metals (for example Ti) are used. The desired radionuclides are produced by any suitable nuclear reaction like fission, fragmentation, spallation, fusion–evaporation, and direct reactions. The recoiling nuclei are stopped in a target matrix or a solid catcher which is thick with respect to their range in matter. By heating the matrix (sometimes up to 2000 K) the products are evaporated and diffuse out of the target towards the ion source. Chemically reactive elements such as gaseous fluorine (CF_4) are sometimes used on the target in order to produce molecular compounds such as fluorides of high vapor pressure so as to extract the chemically selected atoms as fast as possible. The radioactive atoms are ionized either by surface ionization, in a plasma, or by laser ionization before being accelerated as a quasi-dc ion beam to an energy of the order of a few 10 keV. The different methods employed for the ionization of the reaction products take advantage of physical or chemical properties of the different species to efficiently release and ionize the desired nuclide and heavily suppress all unwanted contaminants. An elaborate review on the ISOL target and ion source developments can be found in [230].

The accelerated beam is focused and mass separated using a sector magnet. Downstream of the mass separator, a beamline distributes the radioactive ion beam to the different experiments located in the experimental hall. The ion–optic elements along the beam lines for focusing and deflection are, at most of the ISOL facilities, exclusively electrostatic devices in order to assure a mass independence of the beam transport setting. The ISOL technique has the advantage of delivering beams with superior quality, which is of particular importance for high-accuracy experiments such as collinear laser spectroscopy or injection into ion traps with high efficiency.

The yields of exotic nuclei at an ISOL-type facility are primarily determined by the intensity and the energy of the primary beam, production cross-section, and target thickness. In addition, the release processes from the target–ion–source system and the transfer efficiency determine the chance of survival until arrival at the detector system. Depending on the chemical properties of the target matrix and of the ion or, respectively, the atom under investigation, the diffusion and effusion of the produced exotic nuclides out of the voluminous target matrix can take some milliseconds for ionic alkali elements, to several minutes and longer (up to infinity) for more refractory species, which restricts the nuclei that can be investigated [231]. Thus, the chemical properties and the nuclear half-lives play a crucial role in the production and the separation of exotic nuclides with the ISOL method.

Examples of ISOL-type facilities where mass measurements with ion traps have been or will be performed are ISOLDE at CERN/Geneva (Switzerland) [134,232], ISAC at TRIUMF/Vancouver (Canada) [223], and at Jyväskylä (Finland) by use of the ion guide ISOL system IGISOL [233]. The later is not limited by the release problems mentioned above. Thus, also refractory elements are accessible. At ISOLDE close to 70 elements and about 700 isotopes can presently be delivered from various ion sources (see Fig. 35). The resonance ionization laser ion source (RILIS) [173–175] is meanwhile the mostly used ionization technique at ISOLDE [234] due to its high efficiency and high elemental and isotopic selectivity.

5.2. In-flight separation

The second most prominent and complementary technique for rare isotope investigations is the in-flight separation method. In this case, a heavy, highly energetic primary beam is impinged on a target with a thickness of some grams per square centimeter and the exotic reaction products, which are partly in excited states, emerge with high kinetic energy [235,236]. Due to the kinematics of the reaction the fragments are mainly emitted in the forward direction and they can be time-tagged. After a suitable drift time at a velocity depending on the target thickness, they can be identified by their time of flight as well as standard energy-loss techniques. A main advantage here is that the reaction products have a characteristic charge-state distribution [237] that enables efficient electromagnetic separation in-flight.

Aside from the electromagnetic analysis of the radionuclides at high energy of about 30–2000 MeV/u, energy-degrader systems are used for their spatial separation, since the atomic energy loss (ΔE) of the ions penetrating through matter depends on Z^2 [238,239]. In this way the magnetic rigidity ($B\rho$) analysis is performed both before and after the degrader, and makes an unambiguous Z selection possible. This separation method is the $B\rho - \Delta E - B\rho$

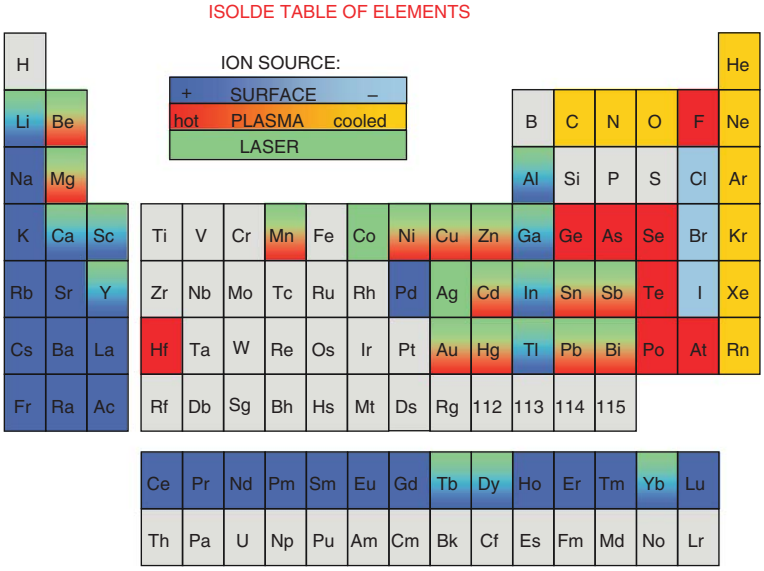

Fig. 35. (Color) Color coded periodic table of elements and the ion sources in use for their production at ISOLDE/CERN. (Courtesy of Fraile).

mode [219]. The advantage that the flight time between the production target and the exit of the separator is only in the microsecond range enables mass measurements on very short-lived nuclides.

Projectile fragmentation favors the production of exotic nuclides at relatively high energies (a few tens to a few hundred MeV/A). Due to the high velocity unambiguous Z selection is possible. At lower energies, in the range of a few MeV/u, fusion–evaporation reactions can be used in combination with in-flight separation. These are the best reactions for producing very neutron-deficient nuclides.

The in-flight separation technique is independent of the chemical properties of the elements and can therefore provide a large variety of different nuclides. Unfortunately the method of production results in a separated beam which has a large phase space. This requires spectrometers with large angular acceptance, which limits the intrinsic accuracy with which the mass might be determined. This can be compensated by coupling the in-flight facility to storage and cooler rings [240]. Major in-flight facilities based on projectile fragmentation are for example GANIL, GSI, MSU, and RIKEN.

The ISOL and in-flight separation methods are highly complementary. While the ISOL technique provides excellent beam intensities for a number of elements and superior beam qualities in respect to phase-space density, the in-flight technique allows fast, clean, and chemistry independent separation. Presently there is a completely new endeavor to construct and commission gas cells to operate at pressures as high as 1 bar so as to stop very energetic beams from a fragment separator. Fast and efficient extraction out of the gas cell is then required before the exotic beams of ISOL quality are post-accelerated [241–244].

6. Production and storage of highly charged ions

As described in Section 4.5 the resolving power and accuracy in mass spectrometry with ion traps depend on the charge state of the stored ion. To this end, the use of highly charged ions is advantageous, although charge exchange losses make the vacuum requirements for the storage device much higher than for the storage of singly charged ions. There are presently three different means to produce highly charged ions:

1. In an accelerator facility a high-energy ion beam is send through a stripper-foil and the stripped highly charged ions are injected into a storage ring [37].
2. In an EBIS or EBIT (electron beam ion source or trap, respectively, discussed in detail by Elliott [245]), an atomic vapor is stepwise ionized by impact of a high-intensity 200–300 keV electron beam and the resulting ions are stored in an ion trap or delivered to an ion trap setup for precision experiments [246].

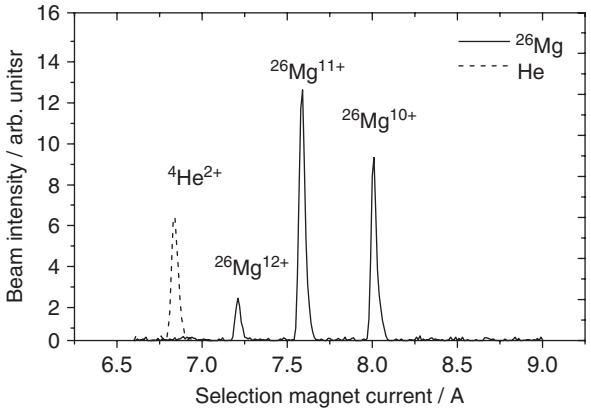

Fig. 36. Charge spectrum of $^{26}Mg^{q+}$ ions recorded in the focal plane of the double focusing magnet used for charge selection at SMILETRAP. The dotted $^{4}He^{2+}$ peak is used for calibration and only appears at an extreme concentration of helium gas in CRYSIS [252].

3. In an electron cyclotron resonance (ECR) ion source injected atoms and ions are stripped up to very high charge states by collisions with high energetic electrons of a plasma [247]. ECR ion sources are mainly used as injectors into accelerators, Van-de-Graaff generators or cyclotrons in nuclear and particle physics [248].

Since the ECR ion source has so far not been used to deliver highly charged ions to storage devices for high-accuracy mass measurements only the first two techniques will be discussed in more detail. Both techniques complement each other, each having advantages and draw-backs for specific experiments. For example, the selection of a single charge state is easy in the case of accelerated beams but difficult or even impossible in an EBIT. On the other hand, the problem of exactly determining the Doppler corrections does not exist in the case of an EBIT but it is a serious problem in storage ring experiments.

The EBIS, and similarly the EBIT, invented by Donets [249], is based on the ability of an electron beam to remove several electrons from atoms or ions trapped radially by the Coulomb interaction between a narrow beam of electrons and the ions. In the case of, for example, the CRYSIS electron beam ion trap in Stockholm [250,251], which produces highly charged ions for the SMILETRAP mass spectrometer, the electrons have an energy of 15–20 keV and the electron beam is on continuously during ion production. The axial trapping of the ions is achieved by applying suitable voltages on a set of electrodes with a total length of about 1.5 m. A strong magnetic field of typically 2 T forces the electrons into an intense beam with a diameter of only a few tenths of a mm.

Neutral atoms or molecules, or injected singly charged ions, are bombarded by dc electrons for a certain time (typically 1 s) until the charge state distribution of highly charged ions requested by the user is reached. The highest charge states that are achievable depends, of course, on the energy of the electron beam. By lowering the trapping potential applied to the electrodes the ions are then extracted as a pulse having a width of about 100 μs corresponding to the time it takes to empty the trap. A charge spectrum of ^{26}Mg ions obtained at CRYSIS with 0.4 s ion injection time, 1 s breeding time, 14.4 keV electron energy, and 138 mA electron current is shown in Fig. 36.

For the production of a clean medium-charged radioactive ion beam an electron beam ion trap [253,254] with a high-intensity electron beam, is ideally suited [255,256], since it can create high charge states in the very short time that is mandatory for short-lived nuclides. The use of non-immersed, compressed electron beams of 5 A has already been demonstrated [257]. The 6-T EBIT proposed for the Penning trap mass spectrometers TITAN [65] at TRIUMF and MATS [61] at the future international facility FAIR will provide a maximum electron beam current of 535 mA with a beam diameter in the confinement region of about 70 μm, which corresponds roughly to a current density of 14 000 A/cm^2. At the maximum electron beam energy of 50 kV, the MATS EBIT can, in principle, produce bare ions up to Xe^{54+}, and He-like ions across the periodic table. In order to increase the breeding efficiency, atomic shell closures can be used to collect most of the ions in one charge state, by appropriate adjustment of the electron beam energy [256]. Fig. 37 shows the calculated breeding for Sn-ions for moderate beam energies for Ni- and Ne-like configurations at different breeding times. High efficiencies can already be reached for short breeding times (< 50 ms). At the highest

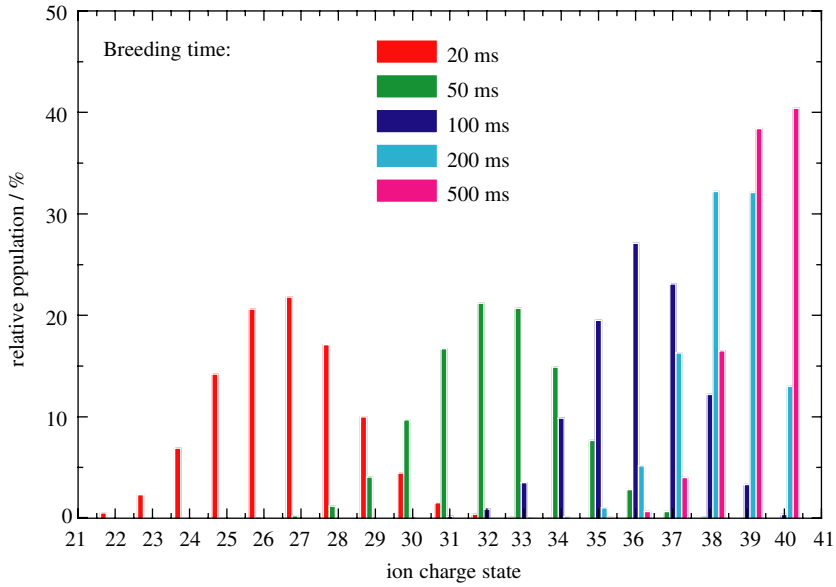

Fig. 37. (Color) Charge breeding of Sn at 6.4 keV electron beam energy, 700 A/cm^2 current density and 10^{-9} mbar gas pressure. After 500 ms, nearly 40% of the ions are in the state Sn^{39+} and 40% in the state Sn^{40+} (Na- and Ne-like configurations).

current densities, ions such as Sn^{40+} can be produced in breeding times in the order of 20 ms. An EBIS for charge breeding of short-lived radionuclides for post-acceleration is already in use at REX-ISOLDE/CERN [258].

At accelerator facilities, for example at the experimental storage ring at GSI Darmstadt, highly charged ions are produced by impinging the projectile ions on a so-called *stripper-foil*. While passing through the foil the ions lose their electrons by collisions with the target atoms and highly charged ions are created. The charge state distribution as a function of the collision energy can be well predicted for different foil materials and thicknesses. Efficient production of bare uranium ions in larger amount requires a projectile energy of at least 300 MeV/u. This is so far only possible at heavy ion accelerators like SIS at GSI Darmstadt.

7. Challenges in high-accuracy mass spectrometry with ion traps

Experiments on high-accuracy mass measurements with ion traps deal with problems common to all high-accuracy experiments. These range from mundane stability problems regarding temperature, pressure, high voltage, magnetic field, beam intensity or electronic thresholds, to the effective suppression of vibrations, electric and magnetic field inhomogeneities, and electronic noise. Some of these challenges in ion trap mass spectrometry are addressed in more detail:

1. Excellent vacuum conditions, in some cases to pressures reaching $p \leqslant 10^{-16}$ mbar, are mandatory for long storage times of the ion under investigation and to minimize background effects by collisions with rest gas atoms, especially in respect to experiments with highly charged ions.
2. Present accuracy limits of almost all Penning trap mass spectrometers are the limited temporal magnetic field stability ($(\delta B/\delta t)(1/B) \approx 10^{-9}$/h) and spatial homogeneity ($\approx \pm 0.01$ ppm measured over a 10 mm diameter spherical volume) of superconducting magnets with field amplitudes of up to 9 T, and the accurate calibration of the magnetic field amplitudes.
3. Since the accuracy and resolving power in mass measurements scale with the unperturbed observation time of the stored ion, long storage times are required.
4. Severe limitations in the precision of mass determinations with Penning traps are due to temperature and pressure fluctuations in the helium and nitrogen reservoir of the superconducting magnets. They cause changes in the

magnetic susceptibility of the materials surrounding the trap and thus in the magnetic-field homogeneity and strength. Stabilization systems with $\Delta T < 10$ mK and $\Delta p < 0.05$ mbar have been developed and implemented.
5. In all ion trap experiments, in order to confine the ions to well localized small volumes, efficient cooling techniques such as buffer gas cooling, electron cooling, resistive cooling or evaporative cooling have to be applied, sometimes to cool the ions to mK temperature.
6. Efficient destructive or non-destructive detection techniques are required to reach single-ion sensitivity and to probe precisely the ions motion in the trap.

In the case of experiments on short-lived nuclides, additional challenges to those with stable ions arise. For stable or very long-lived nuclides a high efficiency in ion production and ion capture does not play such an important role since the number of available ions is high. This is different for radionuclides, especially for those far from the valley of stability which are the most exotic and usually most interesting species. They are created in minute quantities, only at rates of a few tens of ions per second or less, and often accompanied by a large amount of contaminant ions. Since short-lived radionuclides are in general delivered as fast, quasi-continuous beams from external sources, special care has to be taken concerning efficient stopping, cooling, and bunching of the ions. Often the ion's kinetic energy has to be reduced by many orders of magnitude, in some cases from several GeV down to meV. Furthermore, to observe short-lived radionuclides which often have half-lives well below one second, a fast measurement cycle is required so as to minimize the decay losses during the measurement process. Also, the enormous mismatch between the large phase space volume of the beam and the miniscule phase space volume of the precision trap must be overcome. This is now being done by coupling the spectrometers to gas cells and gas-filled linear radiofrequency ion guides and traps [19]. The Penning trap mass spectrometer ISOLTRAP (see Table 2) was the pioneering experiment in this field, having been developed at ISOLDE/CERN over the past 20 years [53].

8. Ion trap mass spectrometers worldwide

Presently about 20 ion traps for high-accuracy mass measurements are in operation, under construction, or planned at different places worldwide (see Fig. 2 and Table 2). A brief summary of the experimental setups shall be given here, but the list might not be complete.

Penning traps can be applied to short-lived radionuclides delivered by on-line isotope separators as demonstrated first by ISOLTRAP [53]. The success of this experiment has triggered many more ion trap projects to be installed at rare-isotope facilities (see Table 2). A more complete list includes the working spectrometers Canadian Penning Trap (CPT) at Argonne [47,259,260], JYFLTRAP in Jyväskylä in Finland [54], LEBIT at the National Superconducting Cyclotron Laboratory at Michigan State University [57], and SHIPTRAP at GSI Darmstadt [63], and those to be installed such as the MAFF-TRAP [60], the RIKEN-TRAP [62], and TITAN [65]. Since all of them are based on the same measurement technique, only the ISOLTRAP experiment (see Fig. 38) will be explained in more detail while the others will be described briefly.

The ISOLTRAP apparatus shown schematically in Fig. 38 consists of three ion trap sub-systems and is fed by the 60-keV continuous ion beam from ISOLDE. First, a radiofrequency quadrupole ion trap cooler and buncher [132] stops and accumulates the ISOLDE beam and prepares it for efficient transfer into the preparation Penning trap. Short, cooled ion bunches are ejected from the RFQ and re-accelerated to an energy of about 2.7 keV by use of a pulsed drift-tube. Second, a cylindrical Penning trap [142] captures the ion bunch in flight and cools and purifies the beam by removing contaminant ions via the mass-selective buffer-gas-cooling technique [118,141] (see Section 4.3.1). Here, a resolving power of up to 10^5 is obtained, which in most cases is sufficient to resolve isobars, albeit not isomers. The ions are then transported to the third trap, a hyperboloidal precision Penning trap [261]. This is the actual mass spectrometer where the cyclotron frequency of the stored ions is determined. Both the preparation and the precision Penning trap are located in superconducting magnets with center fields of 4.7 and 5.9-T, respectively, and with a field homogeneity of 10^{-7}–10^{-8} in the precision trap [262]. The cyclotron frequencies of the ions of interest and those of the reference ions are determined by time-of-flight analysis of the cyclotron motion [107,162] (see also Section 4.2.1). As an example, the inset of Fig. 38 shows data of the short-lived radionuclide ^{63}Ga, where the mean time of flight is plotted as a function of the frequency of the quadrupolar excitation. The solid line is a fit of the theoretically expected line shape [162]

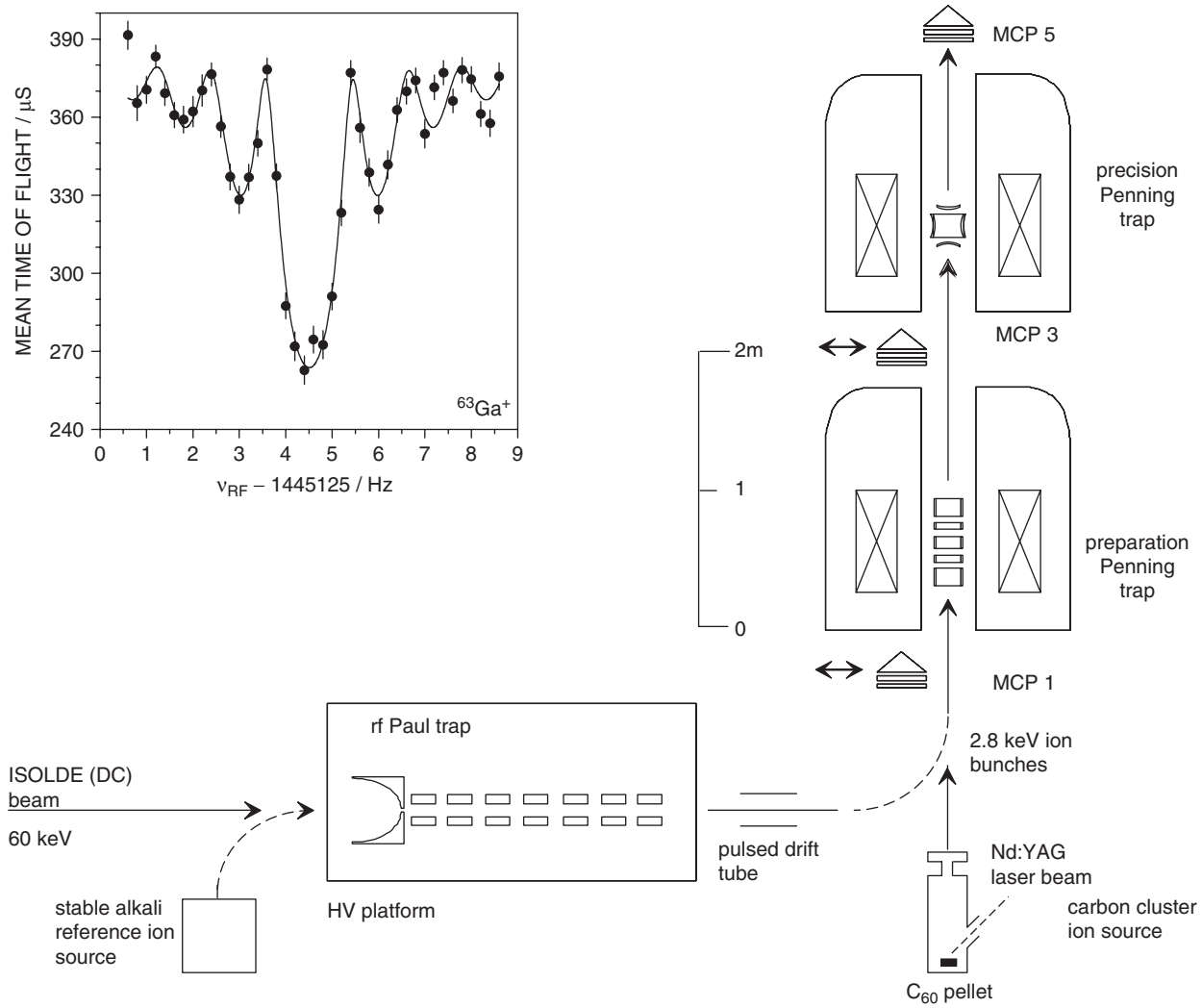

Fig. 38. General layout of the ISOLTRAP experiment. The main components are a radiofrequency quadrupole trap ion beam cooler and buncher, a preparation Penning trap for isobaric cleaning of the radioactive ion ensemble, and a 5.9 T Penning trap mass spectrometer. Micro-channel-plate (MCP) detectors are used to monitor the ion transfer as well as to record the time-of-flight resonance (MCP5) for the determination of the cyclotron frequency. The inset shows a cyclotron resonance curve for the short-lived radionuclide $^{63}Ga^+$ ($T_{1/2}$ = 31.4 s) with 900 ms duration of the quadrupolar excitation.

to the data points. The accuracy limit of ISOLTRAP was investigated in detail and found to be better than 10^{-8} [111] (see Table 6).

The second Penning trap to come into operation for mass spectrometry on radionuclides, and using the same measurement procedure as ISOLTRAP, is the Canadian Penning Trap (CPT) first developed for Chalk River and then transferred to Argonne [46,47]. Here, the projectiles from the ATLAS linear accelerator hit a target where secondary fast beams are produced by fusion reactions. After in-flight separation the energetic radioactive products are stopped in a high-pressure (100–200 mbar He) gas cell. Singly or doubly charged ions are extracted from this cell by combined static and radiofrequency electric fields. Similar gas-stopping ion guiding schemes are used at SHIPTRAP, LEBIT, and RIKEN. Subsequently, the ions enter RFQ traps which are linear gas-filled and segmented structures. From here the ions are transferred as a bunch to the actual Penning trap mass spectrometer. LEBIT recently demonstrated that rare nuclides produced by beam fragmentation at energies of 100 MeV/u can be slowed and prepared such that precision experiments with low-energy beams are possible. The development of the high-pressure He gas cell was a real challenge

since it has to be operated at a pressure as high as about 1 bar for efficient stopping of the very energetic beam from the fragment separator. LEBIT presents an important test case for the rare isotope accelerator (RIA) project in the US [41] where a gas cell is a central device for post-acceleration of secondary radioactive ion beams. Such a gas cell is presently tested at GSI by an Argonne-GSI-MSU-RIKEN collaboration.

The goal of the SHIPTRAP facility is the accurate study of properties of transactinides and superheavy nuclides. Mass spectrometry, the search for optical transitions by laser spectroscopy above einsteinium [263], decay spectroscopy, and ion chemistry are planned. At SHIPTRAP as well as at JYFLTRAP the preparation and the precision Penning trap are both placed in a single ($B = 7$ T) superconducting magnet. This tandem Penning trap system for singly charged ions allows a very compact setup. JYFLTRAP is installed at the cyclotron laboratory in Jyväskylä and gets low-energy ion beams from the IGISOL facility [264].

A rather complex apparatus is presently being set up at ISOLDE: The WITCH experiment of the Leuven group [68] aims at a measurement of the energy spectrum of the recoiling ion after β-decay. After trapping and cooling in a Penning trap the energy of the recoil ion is measured by an electrostatic retardation spectrometer similar to the one applied at the University of Mainz (Germany) to determine an upper limit of the mass of the electron antineutrino [265,266]. Contributions of a scalar interaction would show up as a change of the energy spectrum of the recoil ion. Beside angular correlation studies for tests of the Standard Model there are also plans for a mass measurement program on radionuclides at WITCH.

As already pointed out, for high resolving power and accuracy in mass spectrometry it is advantageous to use highly charged ions. Thus, at the Manne-Siegbahn Laboratory in Stockholm, the electron beam ion source CRYSIS is used for injection of stable highly charged ions into SMILETRAP, which is at present the only Penning trap mass spectrometer for highly charged heavy ions [64]. Mass measurements could be performed up to mass $A = 204$ with a typical accuracy of about $\delta m/m = 2 \times 10^{-9}$ and even an order of magnitude better in some cases where the ion of interest and the reference ion for magnetic-field calibration are q/A doublets. A similar project, where an Electron Beam Ion Trap, able to produce ions up to U^{92+}, was to be combined with a cold-bore Penning ion trap (RETRAP) was built up and put into operation at the Lawrence Livermore National Laboratory and later at Berkeley [246] before the experiment was recently stopped.

Several future Penning trap setups are presently under construction or planned with the aim of performing mass measurements on highly charged radionuclides. These are the TITAN facility at the ISAC on-line isotope separator at TRIUMF/Vancouver [65], the MAFF-TRAP at the Munich Accelerator for Fission Fragments (MAFF) to be installed at the new research reactor FRM II [60], the HITRAP facility under construction at GSI-Darmstadt [50,51], and the MATS experiment at the future international GSI facility FAIR [61]. TITAN, MAFF-TRAP, and MATS will use an electron beam ion trap for charge breeding before injecting the short-lived radionuclides into the Penning trap. In this way, higher cyclotron frequencies are obtained, resulting in higher resolving power and accuracy, or vice versa, enabling high-accuracy mass measurement in a much shorter time compared to the case of singly charged ions. This gives access to very-short lived nuclides. Aside from mass measurements, laser spectroscopy and trap-assisted nuclear decay spectroscopy experiments are also planned at these facilities. Since these three experiments are installed at radioactive ion beam facilities with different production and separation processes, the accessible nuclides are different and thus the experimental programs are complementary. HITRAP will concentrate on highly charged long-lived and stable nuclides up to fully stripped uranium that are provided by the experimental storage ring at ESR-GSI. A resolving power of 10^9 and a mass accuracy of the order of $\delta m/m = 10^{-10}$ is envisaged, as already demonstrated with the Mainz-TRAP in the GSI–Mainz experiment on the g-factor of the bound electron by measuring the cyclotron frequency of the $^{12}C^{5+}$ (see Fig. 39) [267] and $^{16}O^{7+}$ ion [167]. The Mainz-TRAP mainly concentrates on the determination of the g-factor of the bound electron for QED tests, but provide also the possibility of performing mass measurements on highly charged ions up to Ca^{19+}.

To reach relative mass uncertainties below 10^{-10} is an experimental challenge. Presently only the Penning trap mass spectrometry groups of G. Gabrielse/Harvard (Harvard-TRAP) [49], R.S. Van Dyck/Seattle (UW-PTMs [6,66,67]), D.E. Pritchard/MIT (MIT-TRAP [59,192]), and E.G. Myers/FSU (former MIT-TRAP, now moved to Tallahassee [7]) have reached such a precision. This was achieved by long observation and measurement times and special stabilization techniques for the magnetic field of the superconducting magnet. In all these experiments the non-destructive image charge detection technique is used (see Section 4.2.2). In the MIT-Trap a novel technique was recently developed to reach an accuracy below 10^{-11} [5]. This was achieved by storing the two ions to be compared in the same trap and measuring their cyclotron frequencies simultaneously, thereby almost eliminating variation in the magnetic field as

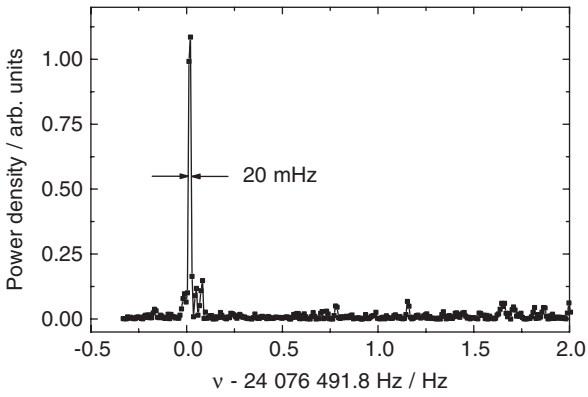

Fig. 39. Fourier transform of the current induced by the cyclotron motion of a single $^{12}C^{5+}$ ion stored in a Penning trap [13]. The resolving power $\nu_+/\Delta\nu_+$ is better than 10^9. The cyclotron energy of the ion was about 2 eV.

a source of error in the comparison. To control the effects of Coulomb interaction between the two ions they were placed in a coupled magnetron orbit: the ions orbit the center of the trap at radii of about 0.5 mm, 180 degrees apart. In the course of this work the MIT group also uncovered a small intrinsic shift of the cyclotron frequencies of ions in a Penning trap due to the ions' polarizability [441], which has consequences for high-precision mass measurements using molecular ions, but also of the mass comparison of the anti-proton to the negative hydrogen ion [49].

Today more than ten ion cooler storage rings are in operation or under construction [268]. However, only one is presently used for high-accuracy mass-spectrometry experiments (ESR-MS [48]). Such experiments are also planned for the Lanzhou-SR [55,56]. Fig. 13 shows the main components of the experimental storage ring ESR at GSI. Highly charged stable ions with energies of up to 555 MeV/u for U^{92+} from the heavy-ion synchrotron SIS or radioactive ions from the fragment separator FRS are injected into the storage ring. By sophisticated stacking, the ions are efficiently accumulated in the storage ring. By cooling (most commonly by electron cooling, see Section 4.3) the phase space volume of the stored ion beam can be compressed. As a result, new phase space becomes available for new pulses to be accumulated in principle until the space-charge limit is reached. The ions circulating in the ring with a revolution frequency of the order of 2 MHz can be observed by detecting the image charges induced in the electrodes of the Schottky detector. At the future GSI facility FAIR [40] the ILIMA (isomeric beams, lifetimes, and masses) project is proposed for the new experimental storage ring (NESR) that aims for high-accuracy measurements of nuclear masses and lifetimes of stored exotic nuclei at relativistic energies. The ILIMA goals for mass resolving power and relative mass accuracy that are about 10^6 and 1×10^{-7}, respectively [52].

With the mass spectrometers described above, close to 1000 masses of stable and radionuclides have been measured in the last few years. The results have helped to extend and refine the nuclear mass landscape. All new mass values measured until 2003 are included in the new atomic-mass evaluation AME2003 [9]. It is important to note that this atomic-mass evaluation by Audi et al. not only ensures that the consistency between masses determined via different reactions, decays and mass spectrometry methods is checked, but also provides an accompanying review of the various motivations for measuring masses. The impact of high-accuracy mass measurements on the different fields of applications in atomic and nuclear physics (see Table 1) will be discussed in detail in the following chapters.

9. Mass spectrometry on radioactive ions

The development of direct mass measurement techniques such as Penning trap and storage ring mass spectrometry has provided sensitive and high-precision tools for a detailed study of nuclear binding far from the valley of stability [1,48,226,269,270]. Mass measurements in long isotopic and isotonic chains has allowed the study of the fine structure of the mass surface and clarified discontinuities in order to extract nuclear structure information such as shell and subshell closures and the onset of deformation from binding energies [110,114,142,271–274]. Along this line it was important to demonstrate the resolution of nuclides in their ground and isomeric states [113–116,207] in order to,

for example, confirm the coexistence of nuclear shapes at nearly degenerate energies ($\approx$ 100 keV), which had been previously deduced from laser and nuclear spectroscopy [275–280]. In nucleosynthesis calculations in astrophysics, masses are among the most critical nuclear parameters [281,282]. However, many nuclei involved in these processes are still not available in sufficient amounts at radioactive ion beam facilities to perform a high-accuracy mass measurement. Therefore, mass predictions by models and mass formulae have to be employed [283–285]. Of course, the predictive power of these models and formula has to be tested in regions where masses are accurately known. In most cases of these applications a mass accuracy of the order of 10–100 keV is sufficient. The highest demand for accurate masses of short-lived nuclides is for studies of fundamental interactions and Standard Model tests, as, for example, a precise study of super-allowed β emitters [38,39]. Here, mass measurements with an accuracy of 1 keV, or less, of the parent and daughter nuclides of such transitions give stringent Q-values and complement nuclear spectroscopy measurements.

9.1. Nuclear structure studies

The contribution of mass measurements to nuclear structure studies goes back to the investigations of Aston and his discovery of the mass defect (see also Chapter 2) [73], nowadays also known as *mass excess*. The mass excess D is defined as the difference between the atomic mass (in mass units u) and the mass number A, converted to keV, $D = [m(\text{in u}) - A]$ (in keV). The missing mass of the bound system $m(N, Z)$ compared to the sum of all masses of the constituent protons Zm_p and neutrons Nm_n was later explained by the nuclear binding energy

$$B(N, Z) = (Nm_\text{n} + Zm_\text{p} - m(N, Z))c^2 \,, \tag{67}$$

which represents the sum of all the nucleonic interactions that give rise to correlations in many-body systems. As an example, the mass of the stable iron atom with mass number $A = 56$ (the nuclide with the largest binding energy per nucleon), consisting of 26 protons, 30 neutrons, and 26 electrons, is 0.51 u ($\approx$ 1%), which is 0.48 GeV, lighter than the sum of all individual masses. Since the binding energy depends on the detailed composition of protons and neutrons, the mass of each of the more than 3000 nuclides as observed to date [9] is highly specific and represents a key property of a nuclear system. Viewing these ensemble of mass data over the nuclear chart, one can examine the hills and valleys that form this surface and make hypotheses about the effects of certain nuclear configurations. To unveil these effects, mass measurements with an accuracy of $\delta m/m < 10^{-6}$ are required (see Table 1).

Differences of masses give separation energies (the energy needed to separate some nucleons from the nucleus), providing clues to shell structure and phase transitions. The most striking way in which shell structure manifests itself in mass systematics is through double differences of masses, i.e. the two-neutron separation energy

$$S_{2\text{n}}(N, Z) = B(N, Z) - B(N - 2, Z) \tag{68}$$

in the case of the neutron shells, and the two-proton separation energy

$$S_{2\text{p}}(N, Z) = B(N, Z) - B(N, Z - 2) \tag{69}$$

in the case of proton shells. Here, specific classes of interactions can be isolated [1]. The single-nucleon separation energy is a less clear-cut indication because of the pairing effect.

At an accuracy of 1×10^{-7} one becomes sensitive to localized correlations within the nuclear many-body system. Such high-accuracy for the lighter sd-shell region, at and very near the neutron number $N = 20$ for the Na and Mg nuclei, have brought evidence for a new zone of deformation, albeit very localized in (Z, N) values [276,277,286]. Another example for such a systematic survey is shown in Fig. 40 where the two-neutron separation energies in the vicinity of $Z = 82$, derived from the atomic-mass evaluation AME1995 [287] (top) and a more recent compilation including ISOLTRAP data (bottom), are compared [114].

The general trend is that $S_{2\text{n}}$ decreases as neutrons are added and deviations from this behavior points to manifestations of microscopic nuclear structure effects. For example, at $N = 126$ there is a sharp decrease of $S_{2\text{n}}$ which indicates a neutron shell closure. Also very particular effects show up as one approaches the neutron mid-shell region near $N = 104$. A possible explanation might be the presence of shape coexistence configurations in this particular mass region, which has been discussed in much detail in [276,277], and a mixing between the intruding configuration and the ground-state, causing local deviations from a smooth linear trend. This is particularly striking in the Hg and Pt nuclei and illustrates most impressively how masses give a first glimpse of nuclear structure.

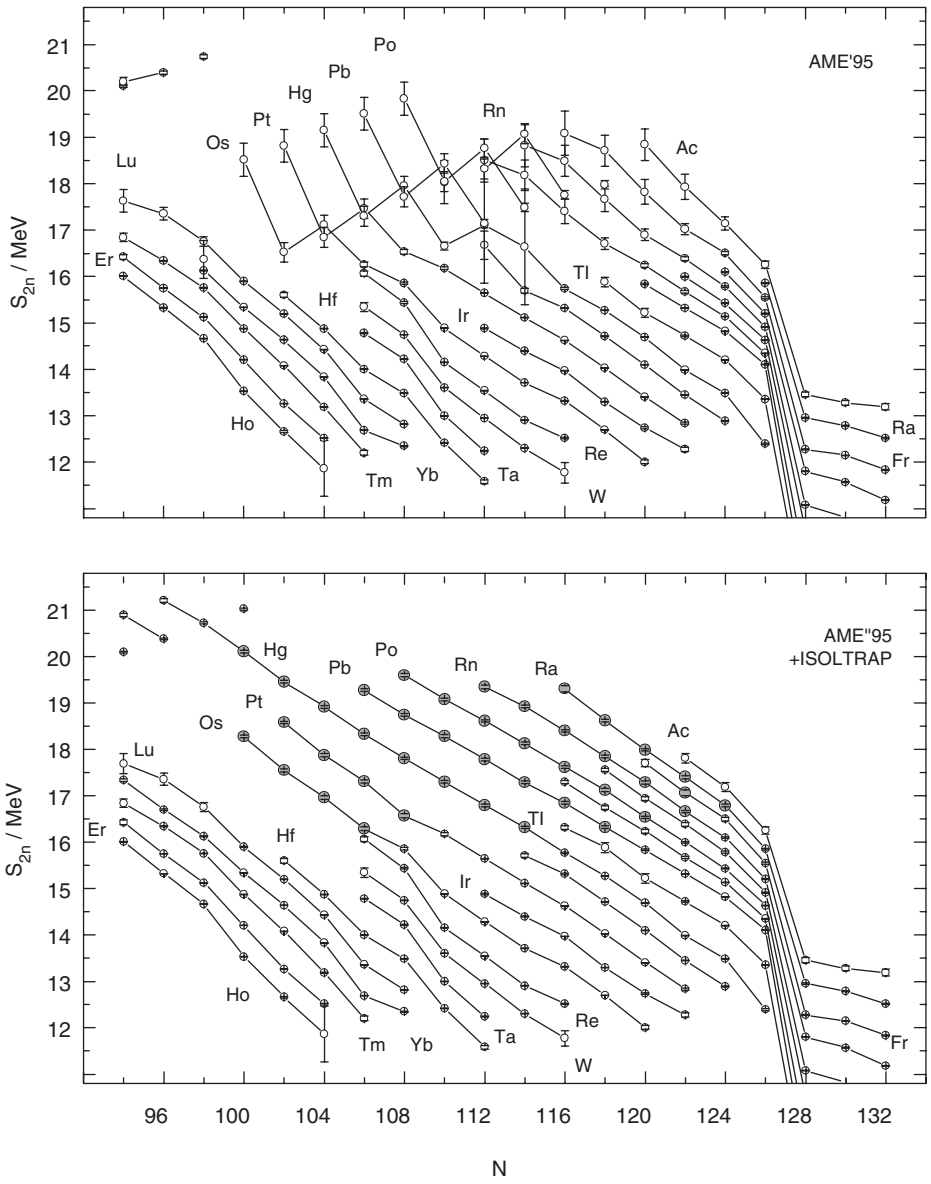

Fig. 40. Experimental two-neutron separation energies in the vicinity of $Z = 82$ as a function of neutron number. Shown are S_{2n} values derived from the atomic-mass evaluation AME1995 (top) and a more recent compilation including the new ISOLTRAP data (bottom) [114]. Full circles indicate S_{2n} values that are either obtained for the first time or whose errors were decreased by at least a factor two.

Similar investigations have been performed recently in the neutron-rich Ni–Cu–Ga mass region at ISOLTRAP [288,289] and in a long isotopic chain of neutron-rich zirconium at JYFLTRAP [274]. A large number of several hundred direct mass measurements of neutron-deficient nuclides ($30 \leqslant Z \leqslant 85$ and suburanium nuclides) obtained with the ESR–SMS method at GSI Darmstadt have been published, for example [110,273], allowing an analysis in the same context.

Another highly interesting class of interaction is that of the last proton(s) with the last neutron(s) and is called δV_{pn} [290–292]. For example δV_{pn} values show striking singularities for nuclei with $N = Z$, reflecting the isospin $T = 0$ interaction. For even–even nuclei, δV_{pn} is defined [290,293] by

$$\delta V_{\mathrm{pn}}(Z, N) = \tfrac{1}{4}[B(Z, N) - B(Z, N-2) - B(Z-2, N) - B(Z-2, N-2)] \,. \tag{70}$$

A given $\delta V_{pn}(Z, N)$ value for even-even nuclei refers to the interaction of the $(Z-1)$ and Zth protons with the $(N-1)$ and Nth neutrons.

In a recent study by Cakirli et al. [292], known masses from the new Atomic-Mass Evaluation AME2003 [9] were used to extract δV_{pn} values to highlight the variations of the p–n interaction and to interpret the very characteristic behavior. δV_{pn} values can help to explain and describe shell structure and orbit occupations near the Fermi surface, for example in the ^{208}Pb region. Since the magnitude of variations in δV_{pn} are of the order of 150–250 keV in a given region, the errors in the δV_{pn} values must be less than 30–50 keV to draw a clear conclusion. Since four masses enter in the $\delta V_{pn}(Z, N)$ equation, it becomes immediately obvious that meaningful trends can only be distinguished if the errors on each individual mass value are of the order of 10–20 keV corresponding to $\delta m \approx 5 \times 10^{-8}$ for masses above $A = 200$. Presently only Penning trap mass spectrometers can reach this accuracy and only a very small number of mass values with this accuracy exist in the heavy mass region. The analysis by Cakirli et al. [292] shows the clear need of new high-accuracy mass measurements far from stability for nuclear structure studies.

An important issue in direct mass measurements with respect to nuclear structure studies is to resolve isomeric and ground states since nearly one third of the nuclides in the nuclear chart have long-lived isomeric states with, in many cases, unknown excitation energies. In the context of nuclear physics, isomers are excited states of atomic nuclides at excitation energies ranging from 100 keV up to a few MeV. Their half-lives range from nanoseconds to beyond the age of the Universe (10^{15} years in the case of ^{180m}Ta, the only naturally occurring isomer on Earth [294]).

Direct high-accuracy mass measurements of isomeric states with ion traps have already been performed several times. The very first isolation of an isomeric state in a Penning trap was demonstrated by Bollen et al. in 1992 [113]. In that work, the ^{84m}Rb isomer could be eliminated due to its shorter half-life simply by storing the nuclei in the other state for a sufficiently long period in the trap. In the case of ^{78}Rb where this was impossible the superior resolving power of the Penning trap enabled a direct resolution of the two states ^{78}Rb and ^{78m}Rb, different by $E = 111.2$ keV. In a series of measurements several isomeric excitation energies were determined for some odd mercury isotopes ^{185m}Hg, ^{187m}Hg, ^{191m}Hg, ^{193m}Hg, and ^{197m}Hg [114]. In these cases extremely high resolving powers of up to 3.7×10^6 were applied, corresponding to excitation times of up to 8 s. Recently, the energy difference of ^{187}Pb and ^{187m}Pb was determined with Penning trap mass spectrometry to be $E = 33(13)$ keV [295]. This is the lowest isomeric excitation energy ever determined by weighing nuclei. The most intricate example is the one of ^{70}Cu [207] where a simultaneous combination of laser ionization, decay spectroscopy, and mass spectrometry succeeded in assigning the three low-lying states, the ground state and the two excited isomers with $E_m = 100.7(2.6)$ keV and $E_n = 242.0(2.7)$ keV, to the correct spin values. Also, in the experimental storage ring at GSI, ground and isomeric states of short-lived nuclides can be separated and their masses be measured, see for example [110]. In the isochronous mass spectrometry mode of the ESR, even isomers with half-lives well below 1 ms can be investigated [205].

Aside from nuclear structure studies, the extension of our knowledge at the limits of the nuclear chart is an important goal of research in nuclear physics. Foremost is the quest for the limits of bound nuclear systems, i.e., the proton and neutron drip lines [201,296,297], the proton and neutron halos [298,299], and the island of meta-stability in the superheavy-element region [300]. These investigations are closely related to mass models and formula.

9.2. Test of nuclear mass models and mass formulas

The nucleus is a self-organized, many-body quantum system that interacts through the strong, weak and electromagnetic forces. Due to the lack of an exact description of the strong interaction and the complexity of the many-body nucleonic system, the binding energy can not be described by ab-initio theories. Instead, one has to rely on mass predictions by models (with the aim of a quantitative prediction of the total binding energy of a nucleus) and formulas (with the aim of a numerical calculation of masses on a physical basis) [1]. The latter are based on a set of free parameters (up to several hundreds), which have to be constrained by local [301] or empirical [302] comparison to experimental data. In particular, data far from the valley of β-stability represent well-suited test cases for the predictive power of models. Since there was recently a very comprehensive review article by Lunney et al. [1] describing the various modern mass formulas that may be used to extrapolate from the experimental data towards the drip lines and explaining the interplay between experiment and theory, only a brief summary and very few cases of nuclear mass model and mass formula tests shall be addressed here.

Looking at nuclear models, one finds macroscopic and microscopic descriptions. The very first nuclear mass model was developed by von Weizsäcker [77] and by Bethe [78] assuming a similarity between a nucleus and a liquid drop.

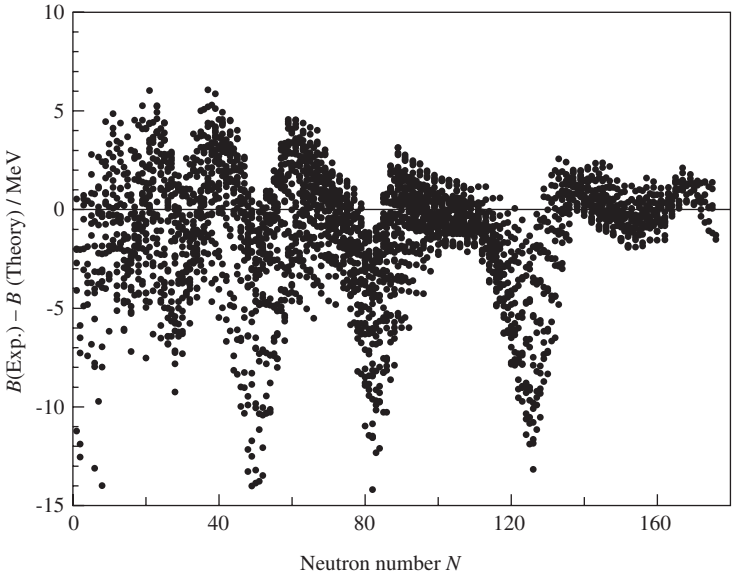

Fig. 41. Deviation between the calculated nuclear binding energies using the Bethe-Weizsäcker formula given in Eq. (71) and the experimental values taken from [9] as a function of the neutron number N.

This *liquid drop model* (LDM) describes very accurately the "bulk" properties of nuclei, i.e. the properties to which all the nucleons of the nucleus contribute, such as the nuclear mass, or equivalent, nuclear binding energy, or the derived nucleon-separation energies. The LDM describes these bulk properties "macroscopically", in terms of volume energy, surface energy, Coulomb energy, symmetry energy, and more, similar to the description of a charged liquid drop that is suspended in space. The liquid drop Bethe-Weizsäcker formula for the nuclear binding energy B is given by:

$$A = a_{\mathrm{vol}}A + a_{\mathrm{sf}}A^{2/3} + \frac{3e^2}{5r_0}Z^2A^{-1/3} + (a_{\mathrm{sym}}A \pm a_{\mathrm{ss}}A^{2/3})I^2 \tag{71}$$

with $I = (N - Z)/A$. The coefficients used for the calculations are from [303]: $a_{\mathrm{vol}} = -15.65\,\mathrm{MeV}$, $a_{\mathrm{sf}} = 17.63\,\mathrm{MeV}$, $a_{\mathrm{ss}} = -25.60\,\mathrm{MeV}$, $a_{\mathrm{sym}} = 27.72\,\mathrm{MeV}$, and $r_0 = 1.233\,\mathrm{fm}$. Fig. 41 shows the mass difference between experimental values taken from [9] and theoretical predictions of Eq. (71) for all known nuclides. One important characteristic, first noticed by this comparison, was that certain proton–neutron combinations are particular stable, resulting in strong deviations between theory and experiment. These *magic numbers* (2, 8, 20, 28, 50, 82, 126 . . .) can be explained by the so-called *nuclear shell model* (NSM), in which each nucleon moves in an orbit held by a central force calculated from the average effects of all the nucleons [304]. The NSM studies nuclear properties starting from individual nucleons and can therefore be called a "microscopic" approach. The nucleons build up in shells according to quantum mechanical principles, like electrons in atoms; the magic numbers represent fully occupied, or closed shells of protons or neutrons. According to the *Pauli principle*, which dictates that identical nucleons (protons or neutrons) cannot be described by the same set of quantum numbers, each shell can contain only a limited number of nucleons. Any nucleons orbiting beyond the outermost closed shell behave as *valence* nucleons (single particles), which can be excited to higher quantum states.

The shell model works well for most light nuclei and those with numbers of neutrons and protons near a closed shell. In the nuclear ground state, and using the most simple shell-model description, nucleons will fill orbits from the bottom of the potential up to a certain level, the *Fermi level*. When a nucleus becomes excited, it rearranges some of its nucleons from below the Fermi level up to higher-lying states. Nuclei with a magic number of protons or neutrons that fill a shell completely are extra stable because their nucleons have to bridge a large energy gap between the filled shell and the higher-lying unfilled orbitals in the next shell. For heavy nuclei, and those with nucleons not near a magic number, the interactions are best described by another class of models in which the nucleons are treated collectively as a liquid drop, held together by surface tension. This approach is similar to the one by Bethe and Weizsäcker but with additional quantum–mechanical terms arising from shell and pairing effects added to the liquid-drop energy. This is

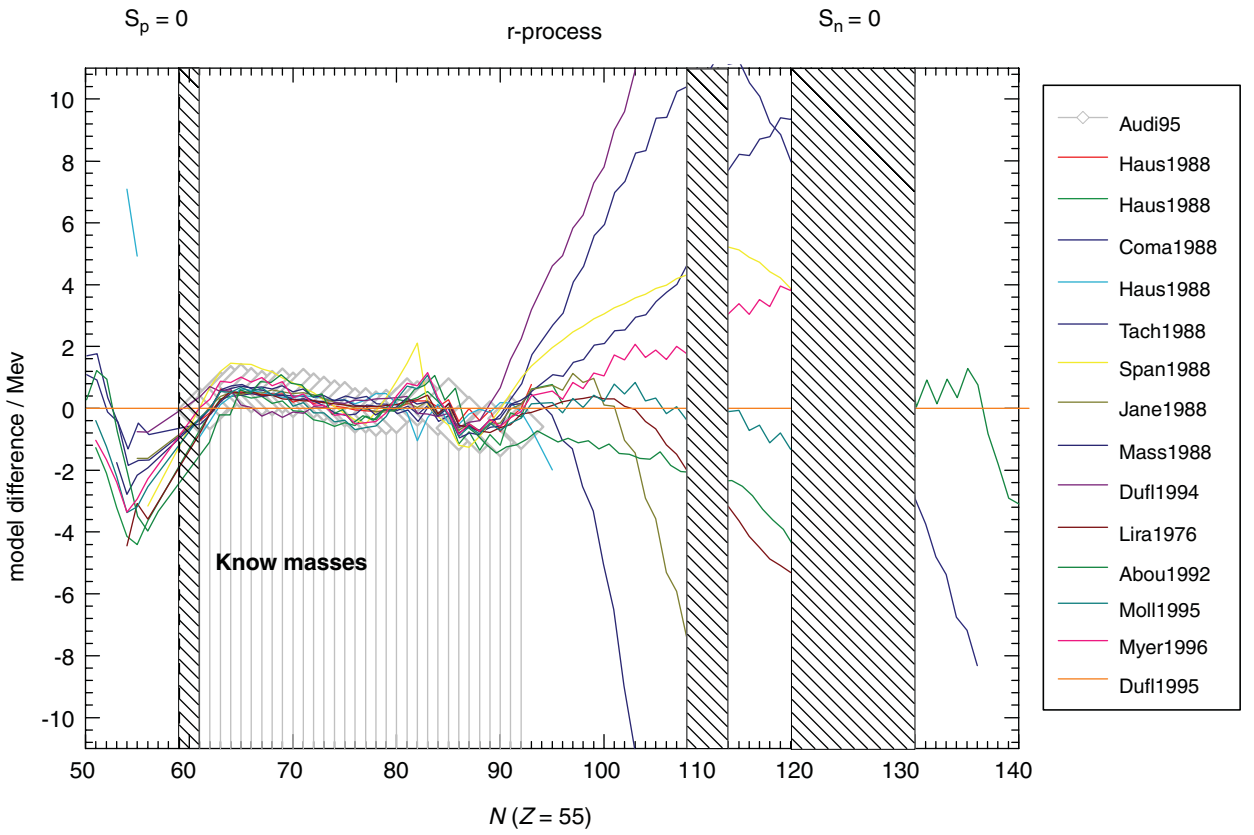

Fig. 42. (Color) Differences in mass predictions of various theoretical mass models and experimental data to predictions of the Duflo–Zucker mass model [312] as a function of N for cesium isotopes (Cs, $Z = 55$). Since the model parameters are adjusted to measured masses, the agreement is very good where masses are known. The used mass models listed in the legend are from [287,301,302,305,312–321] or private communication. The possible region where the proton S_p (around $N = 60$) and neutron S_n (around $N = 125$) separation energy gets zero is indicated. The rapid neutron capture process path could cross between $N = 108$ and 112, depending on the astrophysical conditions.

the *finite-range liquid-drop model* (FRLDM) of Möller and Nix [305]. When excited, the nucleons all move together causing the nucleus to vibrate or rotate, or even to change shape.

Another model, successful for many nuclei, describes the nucleons as pairing up into nuclear building blocks called *bosons*, which are characterized by particular quantum properties also found in the pairs of electrons responsible for superconductivity [306]. Changes in structure can then be characterized in terms of the pairs being excited or breaking up. This *interacting boson model* (IBM) truncates the number of nucleon degrees of freedom even further than the nuclear shell model [307]. The large truncation makes it possible to study heavy nuclei far from the magic numbers. *Microscopic–Macroscopic Models* try to combine the best parts of different models, for example of the Geometric Model (an extension of the LDM that emphasizes the coherent behavior in the dynamics of all the nucleons), and the NSM, especially in order to describe nuclear ground-state properties, for example nuclear masses or binding energies [308,309]. Many more nuclear models have been developed to predict properties of nuclei that have not been investigated or are not accessible nuclides. This is of special importance for nuclear astrophysics (see Section 9.3) [310,311] where masses and half-lives of very exotic nuclei have to be known. The predictive power of some of these mass models is illustrated in Fig. 42 for cesium isotopes. It is obvious that the models agree very well within the region of known masses, i.e. where experimental data exist, but differ by several MeV in the regions where the masses are unknown.

In the last few years there has been significant progress in the construction of purely microscopic mass models on the basis of self-consistent mean-field models [322]. Large-scale fits of Skyrme-type interactions to all available masses became feasible [323–325]. When including phenomenological correction terms for correlation effects, these Skyrme mass fits compete with the best available microscopic–macroscopic models. More recent theoretical developments now

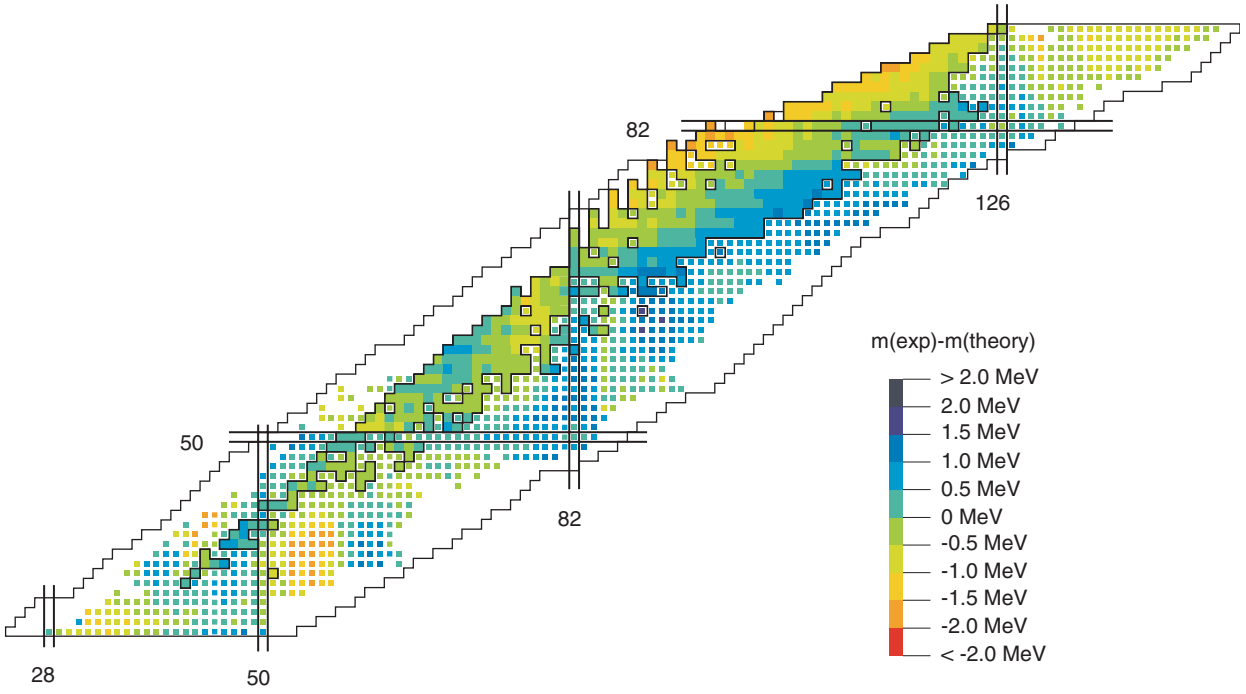

Fig. 43. (Color) Comparison of experimentally known mass values with the FRLDM mass model predictions in the range $30 \leqslant Z \leqslant 92$ [305,329,330]. The outermost full lines inclose the presently observed nuclides. Nuclides whose masses were measured in the work of Litvinov and Geissel et al. [110,331] are shown with larger squares. Each color corresponds to a change of 0.5 MeV. (Courtesy of Litvinov).

allow the large-scale microscopic calculation of correlation energies, either in the framework of a symmetry-restored generator coordinate method [326], or a microscopic Bohr–Hamiltonian [327]. Further development of the models is necessary to include all important correlation effects simultaneously, but the present results are most encouraging as they improve the masses around shell closures. For a more reliable extrapolation of masses, not only the models, but also the effective interactions used and the protocols for the adjustment of their coupling constants have to be improved. To that aim, it is highly desirable to have more data on neutron-rich nuclei beyond the neutron shell closures that separate the stable nuclei from the drip line. Their structure is mainly determined by the single-particle states above the shell closures, which are not completely constrained by the data on more stable nuclei.

For decisive tests of the predictive power of the different models mentioned above, large-scale mass measurements of exotic short-lived nuclei have been performed in recent years at the experimental storage ring at GSI-Darmstadt. A detailed comparison of the mass values as calculated from different models with experimental data is given in [115,273,328]. One example of those is shown in Fig. 43 for the FRLDM model. Note that the change of color in Fig. 43 corresponds to 0.5 MeV. Here, the rms deviation between the 310 compared experimental and theoretical masses is only 696 keV. For other models it is as large as 1.2 MeV. Surely, high-accuracy mass data will contribute to further improvement and refinement of these models and mass formulas and to more detailed understanding of the nuclear forces.

Aside from these global mass formulas there exist also a number of local mass formulas, which address the problem that what is required is often the mass of an unmeasured nucleus that lies fairly close to a considerable number of nuclei of known masses. For a detailed overview see [1]. Here, only a test of one of the most powerful local mass formula, the isobaric multiplet mass equation (IMME) [332], shall be presented. In light nuclei, isobaric analog states (IAS) have nearly identical wave functions. The charge dependent energy difference of these states can be calculated using first-order perturbation theory assuming only two-body Coulomb forces. This leads to the simple equation, noted first by Wigner [333] and Weinberg and Treiman [334], that gives the mass m of a member of an isospin multiplet as a function of its isospin projection $T_Z = (N - Z)/2$:

$$m(T_Z) = c_0 + c_1 T_Z + c_2 T_Z^2 \ . \tag{72}$$

This quadratic relation of IMME is of fundamental importance in isospin symmetry in nuclear physics [335]. Looking at the quartets [332] it was found that IMME worked very well for 21 out of 22 cases. Due to its success and lack of newer experimental data, IMME is widely used to predict masses as well as level energies, for example for the mapping of the proton drip line over a wide mass range, which is important for determining the *rp*-process path [282,336] (see also Section 9.3).

In 2001 the ISOLTRAP mass value for ^{33}Ar resulted in a breakdown of the quadratic IMME for the $A = 33$, $T = 3/2$ quartet [337]. These surprising results triggered new reaction spectroscopy experiments. The outcome was that one level energy in ^{33}Cl was inaccurate [338]. This shows the importance of refined measurements. Of course, a direct mass measurement can only determine the mass of ground state multiplet members. But these nuclei are often also the most exotic members of an isospin multiplet with a rather large mass uncertainty [335].

To test IMME with an accuracy never obtained before, ISOLTRAP performed mass measurements on the very short-lived nuclides ^{32}Ar ($T_{1/2} = 98$ ms) and ^{33}Ar ($T_{1/2} = 173$ ms) and used the mass excess values of the other states of the $T = 2$ quintet in $A = 32$ and the $T = 3/2$ quartet in $A = 33$ [339]. For the test of IMME, one allows an additional cubic term $c_3 T_Z^3$ in Eq. (72) that should fit with $c_3 = 0$ if the quadratic form of IMME is correct. The experiment yielded $c_3 = -0.11(30)$ in the case of $T = 2$, $A = 32$ and $c_3 = -0.13(45)$ in the case of $T = 3/2$, $A = 33$. Thus, in both cases the c_3 coefficient is consistent with zero within the error bars. The two multiplets that were investigated now represent the most stringent test of IMME. Even more decisive tests should come soon.

9.3. Nuclear astrophysics studies

Nuclear astrophysics needs a reliable description of the various kinds of stellar nucleosynthesis [281,282,340,341], based on key properties of unstable nuclei such as their masses, half-lives, and cross-section values. Among these ground state properties, the atomic mass is obviously the most fundamental quantity and its knowledge is indispensable to estimate the rate and energetics of any nuclear transformation and to understand the abundance distribution of the elements in the universe. Some of the most important scenarios of matter creation in stars are shown in Fig. 44:

1. slow neutron capture (s-*process*), responsible for the creation of nuclei close to the valley of β-stability,
2. explosive rapid neutron capture (r-*process*) which is thought to be the source of over half of the heavy nuclei found in the solar system, such as uranium and thorium,
3. rapid proton capture (rp-*process*) that powers, for example, type I X-ray bursts emerging from accreting neutron stars and responsible for the creation of nuclei close to the proton drip line.

Since masses contain the sum of all strong interactions, a few cases that play a key role in setting the limits of nuclear stability as well as determining the pathways of stellar nucleosynthesis shall be addressed here.

The s-process is believed to be generally understood [345], primarily because the masses and half-lives of the involved nuclei are fairly well known. However, the actual stellar site of the r-process, which is proceeding far away from the valley of stability including nuclei containing 30 or so neutrons more than the heaviest measured isotope of the same element (see Fig. 44) [281,346–348], is still unknown. It is assumed that the elements heavier than iron are produced in explosive processes in stars such as supernova explosions by an interplay of rapid neutron capture and subsequent beta-decay. The r-process path involves mostly nuclides that are not experimentally accessible at today's radioactive ion beam facilities and thus its pathway is mostly hidden. Therefore nuclear astrophysics is forced to rely on nuclear mass models and theoretical predictions, which are differing often by several MeV (see Section 9.2). The choice of models needs to be constrained and their predictions to be improved. For this, experimental data have to be obtained as far from stability as possible, which will allow a decisive test of the predictive power of the models and provide an extended and reliable basis for the adjustment of their parameters. The most important regions to provide new data are those where the r-process comes closest to stability. This is the case in the vicinity of magic neutron numbers, where the r-process slows down and proceeds towards more stable nuclei. Crucial candidates are the doubly magic ^{78}Ni, ^{132}Sn, and ^{208}Pb. It is obvious that nuclear structure effects such as the quenching of shell strength or the formation of new shell closures will have an important impact on the r-process path. Both effects are directly observable in mass measurements. While ^{78}Ni is still experimentally not accessible for mass spectrometry, the mass of the short-lived nuclide ^{132}Sn has recently been measured at ISOLTRAP with high accuracy [349] and the mass of the stable nuclide ^{208}Pb has been known for many years from reaction studies.

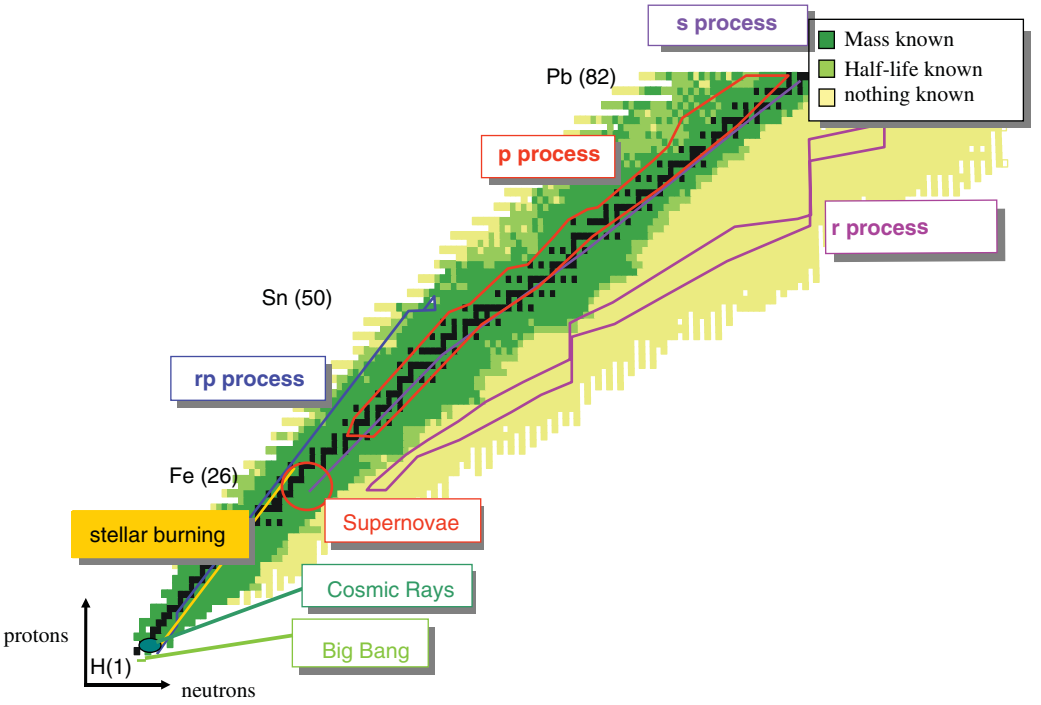

Fig. 44. (Color) Neutron- and proton-capture paths for different processes are shown in the (N, Z)-plane. The *s*-process follows a path along the stability line and finally terminates above ^{208}Bi via α-decay [342]. The r-process drives the nuclear matter far to the neutron-rich side of the stability line, and the neutron capture flows upward in the (N, Z)-plane until β-delayed fission and neutron-induced fission occur [343,344]. The rp-process on the neutron-deficient side produces nuclei close to the proton drip line [282]. (Courtesy of Langanke).

The missing mass problem is less pronounced in the synthesis of proton-rich stable nuclides on the neutron-deficient side of the nuclear chart. The available measurements extend much closer to the proton drip line than to the neutron drip line (see Fig. 44) [281,282,346]. Neutron-deficient nuclei close to the proton drip line are produced in the rp-process, where within 10–100 s hydrogen and helium are fused explosively into heavy elements up to tellurium via a sequence of rapid proton captures interrupted by slow β^+-decays. These so-called *waiting points* are near the proton drip line where further proton captures are counteracted by (γ, p) photodisintegration of weakly proton bound, or proton unbound nuclei. The waiting points delay the nuclear energy release and therefore directly affect the burst shape and duration [350–353]. For a better understanding of this sparsely explored field, among other properties, the masses of the three major waiting points, ^{64}Ge, ^{68}Se, and ^{72}Kr are needed with a relative accuracy of about 1×10^{-7}.

Recently, accurate Penning trap mass measurements of ^{68}Se and ^{72}Kr with relative uncertainties of 3×10^{-7} and 1×10^{-7}, respectively, have been performed with the Canadian Penning Trap [212] and with ISOLTRAP [285]. In both cases the range of effective lifetimes, which is the time it takes for an arbitrary initial abundance to drop by $1/e$, could be reduced by more than an order of magnitude, as shown in the case of ^{72}Kr in Fig. 45. These results lead to the belief that the 2p-capture rate on ^{68}Se and ^{72}Kr is negligible and that both are truly waiting-point nuclides and pose a significant delay in the rp-process under the assumed conditions typical for X-ray burst models (temperature of 1.5 GK, density of 10^6 g cm^{-3}, solar hydrogen abundance). ^{64}Ge still remains to be measured with an accuracy of 10^{-7}. Masses further away from the valley of stability, even reaching the proton drip line at several points around proton number $Z = 82$ and important for the rp-process, could be determined for the first time by the Schottky and isochronous mass spectrometry method at the experimental storage ring at GSI-Darmstadt [48,109]. There, they also have the possibility of generating β-unstable atoms in high atomic charge states, to store them for extended periods of time, and to measure their corresponding β lifetimes [341].

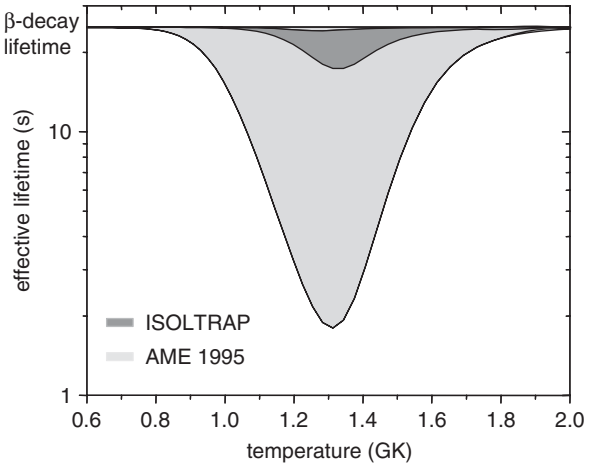

Fig. 45. The effective stellar lifetime of ^{72}Kr as a function of temperature for typical X-ray burst conditions. The light gray area marks the range of lifetimes within the old mass uncertainties [287] prior the direct Penning trap mass measurement [285], which results in the dark gray shaded range of lifetimes.

9.4. Fundamental interactions and Standard-Model tests

The CKM quark-mixing matrix V parameterizes the weak charged current interactions of quarks. The Standard Model does not predict the content of the CKM matrix, and the values of individual matrix elements are determined from weak decays of the relevant quarks.

The CKM matrix is required to be unitary. Today the only possible direct and accurate test of unitarity involves the top row of V, namely

$$|V_{ud}|^2 + |V_{us}|^2 + |V_{ub}|^2 = 1 - \Delta \ . \tag{73}$$

In the standard model with a unitary CKM matrix, Δ is zero. Presently, the unitarity test fails by up to $> 2.7\sigma$ and the origin of Δ is unclear. A deviation from unitarity has been found with nuclear β-decay [38,39,354] and neutron-β-decay data [355]. Due to its large size, a determination of V_{ud} is most important. In the CKM matrix, as assessed by the particle data group [356], the unitarity constraint has pushed $|V_{ud}|$ about two to three standard deviations higher than given by the experiments. Updates of V_{us} with revised radiative corrections [357–360] are in agreement with the current PDG value V_{us} [356] and even indicate a decrease of the central value by up to 1%. However, a recent report from E865 at BNL results in a larger V_{us} value [361]. With this value alone, one finds no significant deviation from CKM unitarity. On the other hand, the discrepancy between this BNL value and the value from K^0_{e3} is on the 3σ level. New measurements from NA48 confirm the discrepancy [362], whereas measurements from KTEV [363] find no deviation.

A violation of unitarity in the first row of the CKM matrix is a challenge to the three generation standard model. The CKM data available so far do not preclude there being more than three generations; CKM matrix entries deduced from unitarity might be altered when the CKM matrix is expanded to accommodate more generations [364,365]. A deviation Δ has been related to concepts beyond the standard model, such as couplings to exotic fermions [366,367], to the existence of an additional Z boson [368,369], to supersymmetry or to the existence of right-handed currents in the weak interaction [370].

The most precise value for the V_{ud} element can be extracted from the vector coupling constant G_V derived from the mean Ft value of *superallowed nuclear β-decay*, in conjunction with the Fermi coupling constant from muon decay G_μ: $V^2_{ud} = G^2_V/G^2_\mu$. Together with particle physics data from K and B meson decay, this can be used to test CKM unitarity.

According to the conserved-vector-current (CVC) hypothesis, the vector part of the weak interaction is not influenced by the strong interaction [371]. The comparative half-life ft of a superallowed β transition between analog states should therefore be only a function of the nuclear matrix element $\langle M_V \rangle$, that connects the two states, and the vector coupling

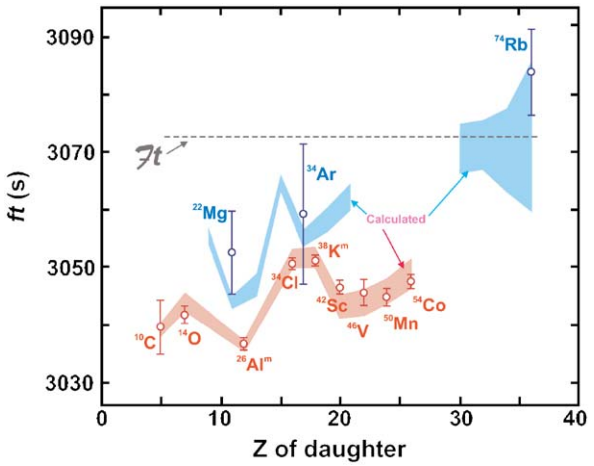

Fig. 46. Experimental *ft*-values plotted as a function of the charge on the daughter nucleus, *Z*. The bands represent the theoretical quantity $\overline{Ft}/[(1+\delta_R)(1-\delta_C)]$. The two groups distinguish those β emitters whose parent nuclei have isospin $T_z = -1$ (dark shading) from those with $T_z = 0$ (lighter shading) [374].

constant G_V [372]. It is customary to consider the so-called corrected *ft* value, denoted by the symbol *Ft*, the quantity that is expected to be constant once theoretical corrections to the nuclear matrix element and the coupling constant have been applied. The experimental *Ft* value is expressed as follows:

$$Ft \equiv ft(1+\delta_R)(1-\delta_C) = \frac{K}{2|V_{ud}|^2 G_\mu^2 (1+\Delta_R)}\ , \tag{74}$$

where t is the lifetime of the decay in question, f is the phase space factor, δ_R is the nucleus-dependent radiative correction, δ_C is the isospin-symmetry-breaking correction, and Δ_R is the nucleus-independent radiative correction, G_μ is the Fermi coupling constant from muon decay, and K is a constant. Fortunately, the three corrections δ_R, δ_C, and Δ_R are all of the order of 1% but, even so, to maintain an accuracy criterion of 0.1% they must be calculated with an accuracy of 10% of their central value. This is a demanding request, especially for the nuclear-structure-dependent corrections [38].

Experimentally, *Ft* is accessible via the following measured quantities: the decay energy Q, which enters to the fifth power into the calculation of the statistical rate function f [373], the half-life $T_{1/2}$, and the branching ratio R. By the study of superallowed β-decays the CVC hypothesis was verified to 0.026% [39]. One should note, that the uncertainty in the derivation of V_{ud} is dominated for heavier Z systems by theoretical uncertainties in the calculated corrections. Therefore part of current nuclear experiments are focused on testing and refining those correction terms that depend on nuclear structure [209]. This is illustrated in Fig. 46, where the measured *ft*-values are compared to calculated *ft*-values derived from the fixed *Ft*-value divided by the theoretical corrections [374]. The width of the colored fields shows the theoretical uncertainties. The best-known nine cases ^{10}C, ^{26m}Al, ^{34}Cl, ^{38m}K, ^{42}Sc, ^{46}V, ^{50}Mn, and ^{54}Co show that several nuclei require improved measurements (of Q-values and half-lives) to reach the situation that the uncertainties are dominated by calculations. New measurements of the masses of the radioactive nuclei ^{46}V and its daughter ^{46}Ti have been performed recently with the Canadian Penning trap mass spectrometer to an accuracy of 1×10^{-8} yielding a more accurate *Ft*-value for this superallowed transition [375]. The new *Ft*-value disagrees with the previous value and is significantly above the average. Two further series of 0^+ nuclei present themselves: For the even-Z, $T_z = -1$ cases ^{22}Mg [376] and ^{34}Ar [337] and a number of new studies such as ^{18}Ne, ^{26}Si, ^{30}S, ^{38}Ca (measurement performed at LEBIT) and ^{42}Ti are under way. Also for the odd-Z, $T_z = 0$ systems, in addition to ^{74}Rb [209] new candidates like ^{62}Ga (measurement performed at JYFLTRAP), ^{66}As and ^{70}Brwill be tested. With theses new cases, where larger theoretical variations from nuclide to nuclide are predicted, the quality of the theoretical predictions for the corrections can be judged. If the calculations agree with experiment, they will verify the reliability for the original nine transitions where the corrections are considerable smaller.

With ISOLTRAP the Q_{EC} value of three superallowed β-decays have been determined: ^{34}Ar (β^+) ^{34}Cl [337] and ^{22}Mg (β^+) ^{22}Na [376], both with an accuracy of 1×10^{-8}, and ^{74}Rb (β^+) ^{74}Kr with an accuracy of 4×10^{-8} [209]. The exotic nuclide ^{74}Rb, with a half-life of only 65 ms, is the shortest-lived nuclide on which a high-accuracy mass measurement in a Penning trap has been carried out.

Until now the parameters of twelve *superallowed nuclear β-decays* have been measured with high accuracy, yielding the most accurate value to date for the V_{ud} element $|V_{ud}| = 0.9738(4)$ [38,39]. This leads, together with the much smaller $|V_{us}| = 0.2200(26)$ from K decays and the negligibly small $|V_{ub}| = 0.00367(47)$ from B decays [356], to $\Delta = 0.0034(14)$, signalling a deviation from the unitarity condition by 2.4σ standard deviations. For many of the other potential candidates the knowledge of the Q_{EC}-value is limited. That prohibits an accurate determination of the Ft value. To reach an uncertainty level of 0.1% or better for the Ft value an uncertainty of 0.1% or better is required for half-life and branching ratio. But since the phase space factor F is proportional to Q_{EC}^5, the Q_{EC} value has to be determined with an uncertainty of better than 0.01%. This requires mass measurements of mother and daughter nuclei with relative uncertainties $\delta m/m \leqslant 3 \times 10^{-8}$. In the case that mother and daughter nuclei are short-lived this is at present only possible at the on-line Penning trap facilities CPT, ISOLTRAP, JYFLTRAP, LEBIT, and SHIPTRAP (see Table 2).

The error in $|V_{ud}|$ from nuclear $0^+ \rightarrow 0^+$ transitions is in the higher Z systems dominated by theoretical uncertainties [38]. One important point to be clarified here is the correctness of the calculated Coulomb correction δ_C. The nine well-known cases have quite low calculated Coulomb corrections of the order of 0.5%. Thus, the best candidates for testing these calculations are nuclei with Coulomb corrections predicted to be large, as for instance ^{22}Mg, ^{34}Ar, both already studied by ISOLTRAP [132,376], or ^{14}O, ^{26m}Al, and ^{30}S. Furthermore, to test new theoretical approaches as well as to probe CVC for higher Z, it is necessary to extend the study of superallowed decays beyond $A = 54$ (Co). Restoration of unitarity would require a -2.3σ shift of the theoretical corrections in nuclear decays. So far all new measurements continued to confirm the validity of the calculated correction terms. If new experimental results continue to confirm the corrections, the uncertainty of V_{ud} is likely to be reduced soon.

The newest *neutron*-decay data give $|V_{ud}| = 0.9717(13)$ [355], which leads to a deviation $\Delta = 0.0076(28)$ that is 2.7 times the stated error. Averaging over the new result [355] and previous results, the particle data group (PDG) [365] arrives at a new world average for $|V_{ud}|$ from neutron β-decay which leads to a 2.2σ deviation from unitarity.

The *pion β-decay* has been measured recently at the PSI. The pion has a different hadron structure than that of the neutron or of nucleons and it offers another possibility for determining $|V_{ud}|$. The result is $|V_{ud}| = 0.9728(30)$ [377], which is in good agreement with the neutron decay data from [355] and the PDG 2004 average, but the error is still too large for it to be a significant unitarity check.

The error in $|V_{ud}|$ from neutron decay is dominated by experimental uncertainties. Restoration of unitarity would require a -3σ shift in the present value of the β-decay asymmetry A_0, or a -8σ shift in the neutron lifetime τ. Alternatively, radiative corrections would have to be wrong by 16σ. If the deviation is due to errors in $|V_{us}|$, its presently accepted value would have to shift by $+7\sigma$ in order to explain the neutron result (by $+3\sigma$ to explain the nuclear $0^+ \rightarrow 0^+$ result). However, very recent preliminary results hint that the last word on $|V_{us}|$ has not yet been spoken, see also [378]. Further, a recent report on a new neutron lifetime measurement [379] claims a -6.5σ deviation from the world average value. If both [378,379] were true, then the problem would partly reappear, with the sign of Δ reversed. Thus, there is strong interest in several communities in resolving this problem and to continue with high-accuracy mass measurements on superallowed β-decay nuclides. At present, this is one of the most active and exciting fields of high-accuracy mass spectrometry on radionuclides.

10. Mass spectrometry on stable ions

High-accuracy mass measurements and mass comparisons of stable or very long-lived nuclides on the level of 10^{-9} and better have a wide variety of applications in physics and metrology, including new determinations of the fine structure constant [192,380–382] and a new definition of the kilogram [64,383], the provision of input data for the determination of the electron neutrino rest mass [384,385] and the search for neutrinoless double beta-decays [386,387]. Furthermore they are important for input to reliable calculations of astro-physical heavy-element formation [388], a test of the fundamental charge, parity, and time reversal symmetry [49,389], and a test of Einstein's mass-energy relationship $E = mc^2$ [390]. Some important applications are summarized in the following.

Table 7
Compilation of $(\beta^-\beta^-)$-emitters with a Q-value of at least 2 MeV

Transition	Natural abundance (%)	Q-value (keV)
$^{48}_{20}\mathrm{Ca} \rightarrow {}^{48}_{22}\mathrm{Ti}$	0.187	4273.7 (4.1)
$^{76}_{32}\mathrm{Ge} \rightarrow {}^{76}_{34}\mathrm{Se}$	7.8	2039.5 (2.3)
$^{82}_{34}\mathrm{Se} \rightarrow {}^{82}_{36}\mathrm{Kr}$	9.2	2995.7 (2.6)
$^{96}_{40}\mathrm{Zr} \rightarrow {}^{96}_{42}\mathrm{Mo}$	2.8	3349.5 (3.6)
$^{100}_{42}\mathrm{Mo} \rightarrow {}^{100}_{44}\mathrm{Ru}$	9.6	3034.0 (6.3)
$^{110}_{46}\mathrm{Pd} \rightarrow {}^{110}_{48}\mathrm{Cd}$	11.8	2004 (11)
$^{116}_{48}\mathrm{Cd} \rightarrow {}^{116}_{50}\mathrm{Sn}$	7.5	2809.1 (4.2)
$^{124}_{50}\mathrm{Sn} \rightarrow {}^{124}_{52}\mathrm{Te}$	5.64	2287.7 (2.1)
$^{130}_{52}\mathrm{Te} \rightarrow {}^{130}_{54}\mathrm{Xe}$	34.5	2530.3 (2.0)
$^{136}_{54}\mathrm{Xe} \rightarrow {}^{136}_{56}\mathrm{Ba}$	8.9	2462 (7)
$^{150}_{60}\mathrm{Nd} \rightarrow {}^{150}_{62}\mathrm{Sm}$	5.6	3367.3 (3.8)

Given are the eleven decay candidates, natural abundances of the mother nuclides, and Q-values with errors [9].

10.1. Double-beta decay and input data for neutrino mass

Double-beta decay ($\beta\beta$) is a nuclear process where the nucleus increases in charge by two when emitting two electrons. Two-neutrino double-beta decay ($2\nu\beta\beta$) is an allowed second order weak process that also emits two neutrinos. Neutrinoless double-beta decay ($0\nu\beta\beta$) can only occur if neutrinos are massive particles that are self conjugate, i.e. massive Majorana particles [391].

Since recent experimental results from atmospheric [392], solar [393], and reactor [394] neutrino sources identified neutrino oscillations and established that neutrinos have rest masses, the determination of absolute neutrino masses, together with the proof that neutrinos are Majorana particles with $\nu = \bar{\nu}$ [395], remains a great challenge. The occurrence of double-beta decay without emission of neutrinos would be a violation of the "classical" Standard Model. In order to set a reliable limit for the ($0\nu\beta\beta$) decay mode it is important to know the $Q_{\beta\beta}$ value very accurately. The current Q-values for double-beta decay deduced from [9] have a typical uncertainty of 3–7 keV. This corresponds to a relative uncertainty of about 10^{-7}–10^{-8}. The presently best-studied candidate is ^{76}Ge. The $Q_{\beta\beta}$ value of the ^{76}Ge double β decay has been determined by measuring the masses of ^{76}Ge and ^{76}Se with a relative uncertainty of better than $\delta m/m = 1 \times 10^{-9}$ using the Penning trap mass spectrometer SMILETRAP [386]. The measurement resulted in a factor of 17 improvement in the masses and a factor of 7 in the Q-value. This investigation was motivated by the fact that, for the ^{76}Ge decay search, Ge-semiconductor detectors are used. These provide the best energy resolution of all double-beta experiments but accurate knowledge of the peak position is crucial. The HEIDELBERG-MOSCOW experiment recently published that the confidence level for the neutrinoless signal in the double β decay of ^{76}Ge has been improved to 4.2σ [387,396,397], giving some indication of a non-vanishing Majorana neutrino mass. Furthermore, they deduce an effective neutrino mass of between 170 and 630 meV. However, their observed $Q_{\beta\beta}$-line of (2038.07±0.44) keV deviates by 2.1 σ from the very precise $Q_{\beta\beta}$-value of (2039.006 ± 0.050) keV obtained with SMILETRAP [386]. For ^{76}Ge some still unknown background could fake the line at $Q_{\beta\beta}$. However, it would be highly improbable that the same thing would happen for other double β-decays with very different $Q_{\beta\beta}$-values. Hence, it is desirable to extend the searches to more isotopes. This will require accurate mass determinations of those isotopes. However, despite the fact that there are 35 ($\beta\beta$) isotopes in nature, for the actual neutrino mass search only those with Q-values beyond 2 MeV are meaningful, because the decay rate scales with Q^5. This reduces the number of potentially interesting candidates to eleven. Two of them have never been seriously considered due to a lack of a feasible experimental approach. The eleven candidates and their present uncertainties in the Q-values are listed in Table 7.

Of highest importance are those where the ongoing experiments will also enable rather good energy resolution or where the use of cryogenic detectors, following extensive technical developments, will also allow to achieve rather good energy resolution in the keV range for the double-beta spectra. The two isotopes of principle interest are ^{116}Cd

used by COBRA (CdZnTe semiconductors) and ^{130}Te used by CUORICINO/CUORE (TeO_2 cryogenic bolometers) and COBRA [391,398]. Accurate knowledge of the position of the ^{130}Te energy peak is also necessary because there is a background line from ^{60}Co-decay at 2505 keV that might overlap with the ^{130}Te ($0\nu\beta\beta$)-decay region. The same argument might hold for ^{136}Xe searches.

An attractive alternative to the double-beta decay ($0\nu\beta\beta$) is the radiative neutrinoless double-electron capture, ($0\nu 2EC\gamma$). While in general this process is much slower than the ($0\nu\beta\beta$) one, it might be enhanced by several orders of magnitude due to an atomic resonance effect [399]. Candidates for such a process are ^{112}Zn, ^{136}Ce, ^{162}Er, and ^{180}W. Since the mass is a very crucial input parameter and only known to an accuracy of about $\delta m/m = 1 \times 10^{-7}$ for these four candidates, high-accuracy mass measurements are required.

A resonance enhancement in the rates for the double-electron capture modes can also occur when there is an overlap of states in the final and initial nucleus. A possible system, $^{74}_{34}\mathrm{Se} \rightarrow {}^{74}_{34}\mathrm{Ge}$, has recently been discussed as an interesting candidate [400]. However, a systematic search might reveal more candidates. One of those is ^{106}Cd were several states are close to the Q-value of the transition. A decision on the degeneracy can only be made if the Q-values are known to the level of 200 eV. Thus, for finding nuclear levels allowing for resonant enhancement, the masses of the involved nuclides have to be known with an accuracy of better than 10^{-9}.

Unprecedented mass accuracy is needed to determine the endpoint energy E_0 of the $^3\mathrm{T} \rightarrow {}^3\mathrm{He}$ decay to an uncertainty of $\Delta E_0 = 20$ meV, which corresponds to a relative mass uncertainty of $\delta m/m = 7 \times 10^{-12}$. Such a measurement is important in the context of the KArlsruhe tritium neutrino experiment KATRIN, which is designed to reach a sensitivity on the electron neutrino mass of $m(\nu_e) = 0.2$ eV [385,401]. Since E_0 is presently only known to an uncertainty of $\Delta E_0 = 1.7$ eV [8], with KATRIN it is planned to determine the endpoint energy E_0 from the fit to the beta-spectrum in a self-consistent way. If a 1 ppm accuracy in the ^{3}He–T mass difference $\Delta M(^3\mathrm{He,T})$ could be achieved, E_0 can be used as a fixed parameter and the sensitivity to m_ν could be improved. Already an accuracy of 1–10 ppm for E_0 is of great interest because the self-consistent determination of E_0 could be checked and possible sources for systematic uncertainties could be discovered [402]. Since the sensitive mass range of the KATRIN experiment covers the range of up to a few hundred meV, where the first effective neutrino masses are expected, this search looks very promising.

10.2. Test of CPT

The fundamental CPT symmetry [403,404] with its three quantum–mechanical transformations, C-charge conjugation, P-parity inversion, T-time reversal, assumes the invariance of physical laws under the combined transformation CPT to be true, despite violation of C, P, and T separately. The Lorentz invariant local field theories that describe all interactions but gravity are invariant under CPT [405]. CPT invariance implies that many measurable properties of a particle and its antiparticle are identical, for example magnitudes of the (inertial) masses, charges, mean lives, and magnetic moments. Although P, C, CP, and even T violations have all been demonstrated, CPT has been verified in every experiment so far. However, despite the fundamental importance of CPT invariance, accurate experimental tests are scarce [356]. A violation of the CPT theorem would hint to a possible failure of the Standard Model of the strong, electroweak, and gravitational interactions.

The so far most precise test of CPT in the baryonic sector was performed by a mass comparison of the proton and antiproton [49,406] using a Penning trap mass spectrometer at the low energy antiproton ring LEAR at CERN [407]. Measuring the cyclotron frequencies of a simultaneously trapped $\bar{p}$ and H^- ion established that the ratio of q/m for $\bar{p}$ and p is, within the error bar on the level of 9×10^{-11}, equal to one. At a fractional accuracy of 90 ppt there is thus no evidence for CPT violation in this baryon system. Only one lepton measurement, comparing the magnetic moment of e^+ and e^- in a Penning trap experiment to an accuracy of about 10^{-12} [11,408], and one meson mass comparison of K^0 and $\bar{K}^0$ to a unprecedented accuracy of 10^{-18} [409] are of higher precision than the barionic CPT invariance test.

Presently two other approaches to perform a stringent CPT test using stored particles in an atom or ion trap are under preparation. The first is laser spectroscopy on the 1S–2S transition in atomic hydrogen and antihydrogen. A precision of about two parts in 10^{14} has been achieved with hydrogen [410] but no laser spectroscopy measurement has so far been performed on antihydrogen. Two groups, the ATHENA [411] and the ATRAP [412] experiment, both installed at the Antiproton Decelerator (AD) at CERN [413], are aiming for such a test. So far the formation of antihydrogen by recombination of antiprotons and positrons has been demonstrated by both experiments [187,188] but storing of cooled antihydrogen has not yet been realized. This will be achieved by using a magnetic (Ioffe) trap [414]. Laser spectroscopy can be performed once trapped antihydrogen atoms are available.

The second approach using traps is a measurement of the magnetic moment of the proton and antiproton. While the magnetic moment of the proton is known to an accuracy of 10^{-8}, that of the antiproton has been determined only to an accuracy of 0.3% from the fine structure of an X-ray transition in an antiproton atom [365]. At the University of Mainz an approach, already proposed in 1993 by Quint [415], is followed using a single proton and in a later experiment an antiproton confined in a Penning trap [416]. The proton and antiproton, respectively, are resistively cooled (see Section 4.3) close to the ambient temperature of 4 K. The determination of the g-factor of the proton and antiproton results from an accurate measurement of its spin precession frequency and cyclotron frequency. The Larmor frequency of the proton and antiproton is determined by inducing transitions between the two spin states (spin up and spin down) with a radiofrequency field in the magnetic field of a Penning trap. The orientation of the proton's and antiproton's spin with respect to a magnetic field is measured via the so-called continuous Stern–Gerlach effect [416], similar to that applied in the $g-2$-experiment on free electrons by Dehmelt [408] and on hydrogen-like ions at the University of Mainz [267,417]. In this method, the spin direction is monitored by measuring the axial frequency of the trapped proton and antiproton, respectively, which depends on the spin direction due to the presence of a quadratic magnetic field component superimposed on the electric and magnetic fields of the Penning trap. A resonance spectrum of the spin precession frequency is obtained by varying the radio frequency and counting the number of spin flips for a fixed time interval. Assuming the same level of accuracy as obtained for hydrogen-like ions this method offers the possibility of a high-accuracy measurement of the magnetic moment of the proton and antiproton on the ppb-level or better. For protons the experiment can be prepared off-line. Such an accurate measurement of the proton g-factor in itself is of fundamental interest and may improve the presently known value by one order of magnitude. The proposed measurement on the antiproton would represent an improvement in accuracy by more than six orders of magnitude. Measurements on the proton will be performed at the University of Mainz (Germany) in a GSI–Mainz collaboration. The measurement on the antiproton can be performed at the present antiproton decelerator (AD) ring at CERN or at the future low-energy antiproton facility FLAIR at FAIR. Also new Penning trap mass measurements of the p and $\bar{p}$ with higher accuracy would allow for a more stringent CPT test.

10.3. Test of quantum electrodynamics in strong fields

Quantum electrodynamics (QED) is currently the most accurately tested theory in physics. It describes the interaction of electrical charges by exchange of photons and serves also as an underlying concept for all other existing field theories. Experimental studies have been carried out with an accuracy of up to 10^{-14}. For a few simple systems, this is matched by nearly equally accurate theoretical calculations, which show the power of the underlying mathematical framework of regularization, renormalization, and covariant formulation. Where the theory can not compete with the experiment, this is nowadays often caused by insufficient knowledge of other parameters such as nuclear size and structure. Even the knowledge of fundamental constants limit the predictive power of QED. The comparison of theoretical and experimental results has in turn provided the most precise values for the fine structure constant α [418] and the mass of the electron m_e [419,420] (see Section 10.5). Here, high-accuracy mass measurements can contribute to a stringent QED test, for example by measuring the binding energy of highly charged uranium, with one or a few electrons, to an uncertainty of better than 2 eV, corresponding to an accuracy of about $\delta m/m = 10^{-11}$.

Furthermore, high-accuracy measurements of the electron magnetic moment in highly charged ions provide benchmarks for bound-state quantum electrodynamics (QED) calculations in very strong electric and magnetic fields that are not accessible in any other way [421], and to derive nuclear constants of the ions under investigation. A prerequisite for these tests is the precise knowledge of the masses of the ions of interest.

So far the most stringent test of QED calculations [422] for weak electromagnetic fields is the g-factor measurement of the free electron in a Penning trap by Dehmelt et al., with an unprecedented precision of 4×10^{-12} [11,408]. The CODATA group has now used this experimental value and the calculated one, assuming QED is correct, to determine a new value for the fine structure constant α [423] (see also Section 10.5). Very recently a slightly revised α value was reported by Kinoshita [418] after correcting and extending the previous QED calculations.

In the case of a single electron bound to a nucleus, the g-factor is changed from the Dirac value $g_J = 2$ to

$$g_J = \frac{2}{3}\left(1 + 2\sqrt{1-(Z\alpha)^2}\right) + C_{\mathrm{QED}} + C_{\mathrm{fs}} + C_{\mathrm{recoil}} \tag{75}$$

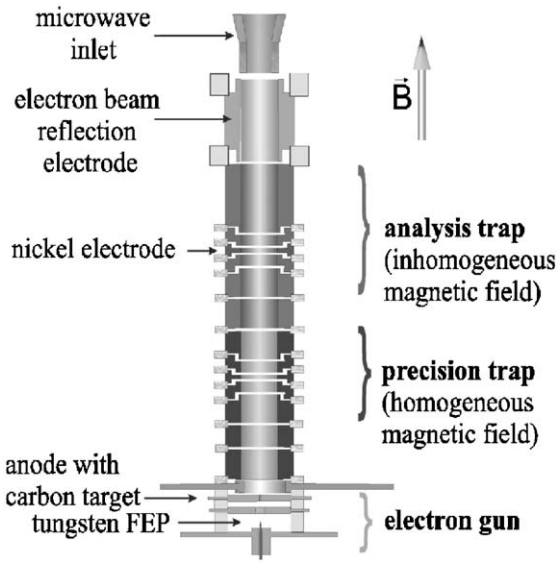

Fig. 47. Double Penning trap setup for the determination of the g-factor of the bound electron in hydrogen-like systems. In the homogeneous magnetic field of the precision trap spin-flip transitions are induced and the magnetic field is determined by measurements of the cyclotron frequency. In the analysis trap with a strong inhomogeneous magnetic field the spin direction is detected [13].

by relativistic effects, bound-state QED corrections, and small contributions for finite nuclear size and recoil corrections. For the bound electron in heavy hydrogen-like systems a perturbative treatment of the QED corrections in terms of $Z\alpha$ is no longer appropriate. Instead, the QED corrections must be calculated in a non-perturbative manner to all orders of $Z\alpha$ [424,425].

The g-factor of the bound electron can be expressed as

$$g = 2\,\frac{\omega_{\mathrm{L}}}{\omega_{\mathrm{c}}}\,\frac{qe/M}{e/m_{\mathrm{e}}}\ , \tag{76}$$

where ω_{L} is the Larmor spin precession frequency of the bound electron and ω_{c} the ion's cyclotron frequency. The Larmor frequency is measured by observing the rate of spin flips of the electron as a function of the frequency ω_{mw} of the applied microwave field. From Eq. (76) it is evident that for a g-factor determination with an uncertainty in the low ppb range, the mass M of the hydrogen-like ion has to be known to an uncertainty at the same level.

Fig. 47 shows the cryogenic double Penning trap setup of the GSI–Mainz collaboration at the Institute of Physics of the Mainz University [13]. Experiments were performed on the hydrogen-like ions $^{12}C^{5+}$ [267] and $^{16}O^{7+}$ [417] with a relative accuracy of 2×10^{-9}. The experimental g-factor values agree within the total error bars with the theoretical one, which take into account all orders in $(Z\alpha)$ for the bound-state QED contribution. For the measurement on the oxygen ion the extremely accurate mass value provided by the Seattle group [67] was taken.

When comparing the g-factors of different isotopes, a difference in the g-factor arises from the fact that the electron wave function of the lighter isotope is slightly closer to the nucleus and thus feeling a somewhat stronger Coulomb field. The size of the isotope effect can be estimated by the calculation of the g-factor correction term C_{recoil} due to the finite mass of the nucleus coming from relativistic calculations of strong-field QED [426]. This so called recoil contribution is the dominant ion mass dependent term contributing to the g-factor of the bound electron and reads

$$g_{\mathrm{recoil}} = (Z\alpha)^2\left[\left(\frac{m_{\mathrm{e}}}{M}\right) - (1+Z)\left(\frac{m_{\mathrm{e}}}{M}\right)^2\right] + (Z\alpha)^2\left(\frac{\alpha}{\pi}\right)\left[-\frac{1}{3}\left(\frac{m_{\mathrm{e}}}{M}\right) + \frac{3-2Z}{6}\left(\frac{m_{\mathrm{e}}}{M}\right)^2\right]\ . \tag{77}$$

A suitable isotope pair for a test could be ^{24}Mg and ^{26}Mg. This is because both masses are well enough known [252] to be able to extract the isotope effect in the g-factor for the two Mg isotopes as soon as the g-factors are measured. Using Eq. (77) the isotope effect in the g-factor can be estimated to be $\Delta g = 6.7\times10^{-9}$.

The method described above for the determination of the g-factor of the bound electron can be applied to any highly charged ion irrespective of the nuclear charge Z. Presently experiments are in preparation at the University of Mainz on H-like $^{40}Ca^{19+}$ with the aim to reach an accuracy on the ppb level. The required mass value of ^{40}Ca was recently determined by the SMILETRAP group with the sufficient accuracy of a few times 10^{-10}. An ultimate test of bound-state QED will become possible when the HITRAP project [50,51] is realized (see Section 11). The HITRAP facility will enable mass and g-factor measurements on highly charged ions up to hydrogen-like uranium. When the correctness of the QED, finite size, and recoil corrections is demonstrated by a g-factor measurement of very heavy hydrogen-like systems, the dominating term in Eq. (75) can be used to extract a new value of the fine structure constant α from the measured g-factor in medium-heavy ions [427].

10.4. New definition of the kilogram

A quite interesting application for high-accuracy mass measurements is the AVOGADRO project [428,429] which has the aim of replacing the kilogram artefact by a high-purity, perfect single crystal of natural or isotope-enriched silicon. To this day, the kilogram is the only base unit in the International System of Units (SI) (which followed the Meter Convention in 1960), that is still defined in term of a material prototype and not in terms of physical constants. Already Maxwell suggested in 1871: "If, then, we wish to obtain standards of length, time, and mass which shall be absolutely permanent, we must seek them not in the dimensions, or the motion or the mass of our planet, but in the wavelength, the period of vibration, and the absolute mass of these imperishable and unalterable and perfectly similar molecules.", i.e., the kilogram should be based on atomic quantities. The presently used Pt–Ir kilogram is a rather arbitrary standard and suffers a loss of weight each time it is cleaned. Great efforts are therefore made to replace the ur-kilogram. The approach of the AVOGADRO project for the new definition of the kilogram is a high-accuracy determination of the Avogadro constant N_A with an assigned uncertainty of 10^{-8}. Via the relation $1\,\mathrm{kg} = \{N_A\,\mathrm{kmol}\}\mathrm{u}$, with the atomic mass unit being $\mathrm{u} = 1/12\,m(^{12}\mathrm{C})$, a new kilogram definition can be established. The determination of a more accurate Avogadro constant can be based on a silicon single-crystal of known volume V, mass m, molar Mass $M(\mathrm{Si})$, and volume V_0 of the unit cell (with n atoms):

$$N_A = \frac{nM(\mathrm{Si})V}{V_0 m}\ . \tag{78}$$

Several such spherical crystals have been made in Australia and are used at PTB in Braunschweig, Germany. Its macroscopic radius can be determined by an interference method and knowing its lattice constant, it should then be possible to "count" the number of Si atoms with high accuracy. Given this number of silicon atoms, it should then be multiplied with the atomic average weight of Si. Therefore it is a prerequisite to perform high-accuracy mass measurements on the stable silicon atoms ^{28,29,30}Si. All three of them have been measured by the MIT-TRAP and SMILETRAP (using highly charged ions in the charge state 12+, 13+, and 14+) to a relative mass uncertainty of better than 10^{-9} [59,64,383,430]. The remaining problem in the AVOGADRO project until the new definition of the kilogram can be accepted is the accurate determination of the isotopic composition of the silicon spheres.

10.5. Fundamental constants

The dimensionless fine structure constant $\alpha = e^2/4\pi\epsilon_0\hbar c$ determines the strength of the electromagnetic interaction and, in a truly universal way, enters equations from many different subfields of physics. If the values of α measured by different techniques are compared, as shown in Fig. 48, one finds that they significantly deviate within the given error bars. The reasons have to be clarified and it is mandatory to measure α more accurately with different techniques to see if one gets better agreement with the so far most accurate value, which is derived from $g-2$ in QED [431].

The fine structure constant α can be expressed in terms of other quantities, for example [431,432]:

$$\alpha^2 = \left(\frac{2R_\infty}{c}\right)\left(\frac{h}{m_e}\right) = \left(\frac{2R_\infty}{c}\right)\left(\frac{h}{m_{Cs}}\right)\left(\frac{m_{Cs}}{m_p}\right)\left(\frac{m_p}{m_e}\right) \tag{79}$$

which allows its determination by different phenomena, as shown in Fig. 48, and represents the second most accurate value for α. In the most recent listing of the fundamental physical constants [433], the Rydberg constant $R_\infty = m_e e^4/8\epsilon_0^2 h^3 c$ is given with a relative uncertainty of 3.3×10^{-9}. The velocity of light is defined by $c = 299\ 792\ 458\,\mathrm{m/s}$.

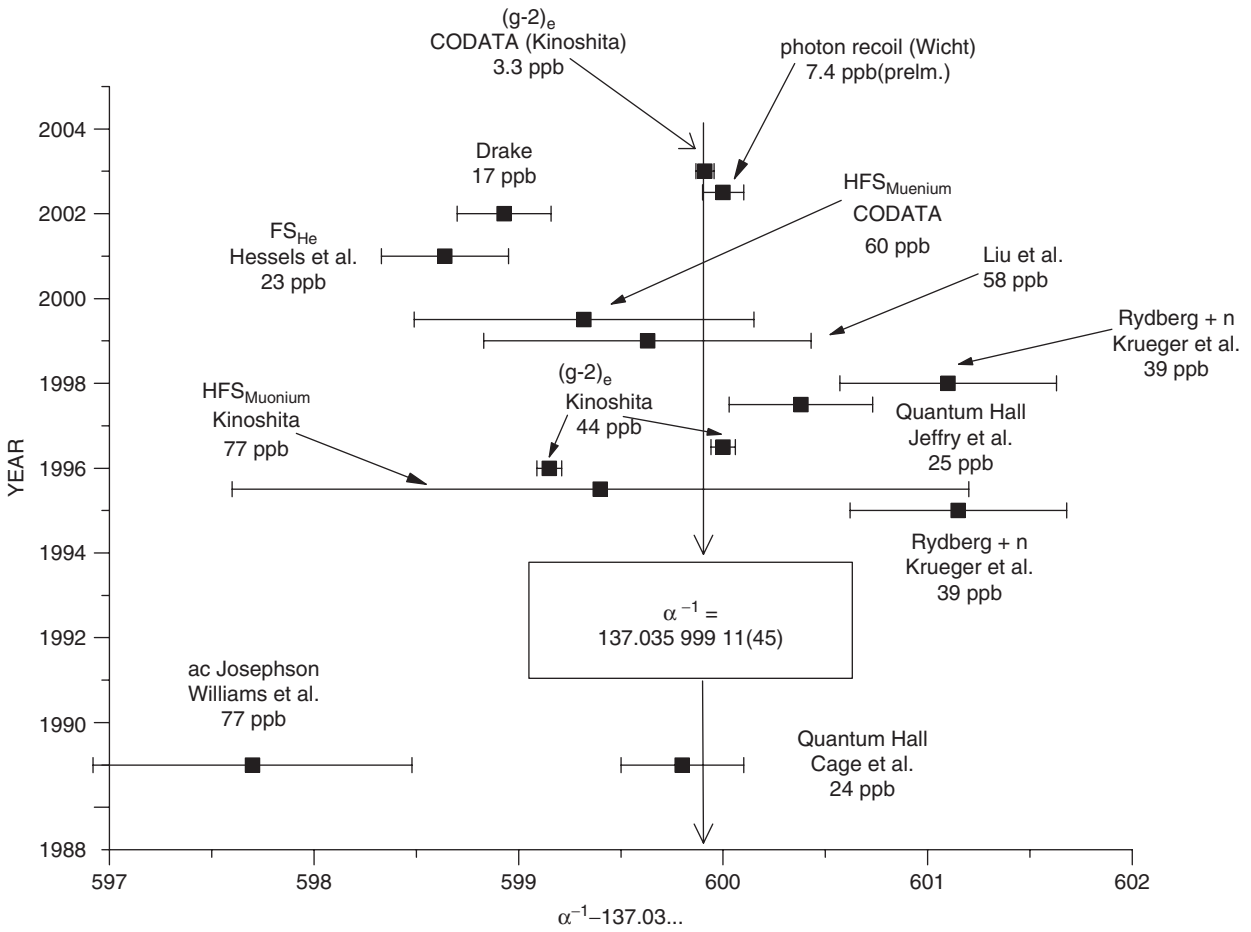

Fig. 48. Relative deviations of present values of the fine structure constant α as obtained with different experimental approaches (see for example [431,433–436]).

Therefore the accuracy of the ratio (h/m_e) to within 6.7×10^{-9} [433] presently determines the accuracy of α. However, it may be related to other ratios, for example to mass ratios, as shown in the second part of the formula. Recently Wicht et al. [382] performed a measurement of the photon recoil on cesium atoms (h/m_{Cs}), but other systems resulting in other mass ratios are of interest as well.

One possibility for improving the accuracy of α is to determine the molar Planck constant $N_A h$ combining a mass difference measurement between highly charged nuclides differing by one neutron in a Penning trap with wavelength measurements of corresponding capture γ-rays. $N_A h$ can be determined using the relation:

$$(M(n) + M(A) - M(A+1))uc^2 = \sum_i \frac{(hc)}{\lambda_i} \ . \tag{80}$$

Here u is the atomic mass unit in SI units with $u = 10^{-3}/N_A$ [kg]. $M(A)$ is the mass of the nucleus A and λ_i are the wavelengths of a γ cascade after neutron capture. Since the molar electron mass $M_e = m_e N_A$ is known to $\Delta M_e/M_e = 4.4 \times 10^{-10}$ [433] the accuracy of $(N_A h/M_e)$ is presently determined by the molar Planck constant with $\Delta(N_A h)/N_A h = 6.7 \times 10^{-9}$ [433]. By measuring $N_A h$ to 10^{-8} the fine structure constant α can be determined to within 10^{-8}. At the GAMS facility at the ILL reactor (Grenoble) the wavelengths of γ rays after neutron capture are measured presently to an accuracy of 4×10^{-7} and it is foreseen to reach $\leqslant 1 \times 10^{-8}$ by 2006. The masses of the highly charged nuclides to be measured are ^{36,37}Cl, ^{48,49}Ti, ^{156,157}Er. This means that this new way of measuring the molar Planck constant in a completely different way would lead to a similar error, but can be surely improved in

the future. Presently, the Avogadro number N_A is known to $\Delta N_A/N_A = 1.7 \times 10^{-7}$ [433] and correspondingly the Planck constant h is known to $\Delta h/h = 1.7 \times 10^{-7}$ [433]. Since an improvement of the Avogadro number is expected in the near future, using isotopically pure Si, a contribution to an improved measurement of the Planck constant by improving the measurement of the molar Planck constant is possible.

The last application of high-accuracy mass measurements for the determination of fundamental constants to be presented here is the electron mass itself. The accurate knowledge of m_e is of vital importance for metrology, because the electron mass enters the expressions from which a number of fundamental constants are derived [437]. For example, the Rydberg constant, which is known to an accuracy of 0.008 ppb [438], is related to the fine structure constant α and Planck's constant h via $R = \alpha^2 m_e/(2h)$. Attempts to reduce the uncertainty of the electron mass are required in view of ongoing experiments to determine the fine structure constant with improved accuracy from the photon recoil on cesium atoms [439,382] (see Fig. 48) and from the electron mass through the relationship with Rydberg constant. If the photon recoil measurement can be improved to the sub-ppb level, the present value for the electron mass would represent the term with the largest error bar and any improvement would reduce the overall uncertainty for α.

A new possibility of determining the electron mass arises from Penning trap experiments which have been performed at the University of Mainz in a GSI–Mainz collaboration (see also Section 10.3). The mass of the electron is determined by comparing the Larmor precession frequency of the spin of the bound electron with the cyclotron frequency of a H-like ion. The result of the determination of the electron mass, which was obtained from measurements on H-like carbon $^{12}C^{5+}$ [267] and H-like oxygen $^{16}O^{7+}$ [417], is $m_e = 0.0005485799092(3)u$. The fractional uncertainty of this determination of the electron mass of 0.4 ppb represents an improvement in accuracy by a factor of four [419] compared to the previous value, which was mainly based on a mass measurement of the electron in a Penning trap [211].

11. Future projects

High-accuracy mass spectrometry especially of radionuclides appears to have a very bright future. There are at least eight new proposed mass measurement projects, six based on Penning traps (HITRAP, MAFF-TRAP, MATS, RIKEN-TRAP, SPIRAL2-TRAP, TITAN), two on storage rings (ILIMA, Lanzhou-SR), some of which are scheduled for data taking within the next few years. They are listed in Table 2 and briefly described in Chapter 8. Common to all projects are the aims to get access to even shorter-lived nuclides, to reach higher resolving power and mass accuracy, and to perform measurements on nuclides much further away from stability than presently possible. This should be achieved mostly by technical improvements such as charge breeding and electron and laser cooling of the stored ions. Another technical challenge is the construction and use of cryogenic Penning trap mass spectrometers for radionuclides where the ions of interest are delivered from external sources.

The first Penning trap mass spectrometer using highly charged short-lived radionuclides will be TITAN [65] at the ISAC on-line isotope separator at TRIUMF/Vancouver. The setup will be similar to the ISOLTRAP mass spectrometer. However, an electron beam ion trap (EBIT) is placed between the radiofrequency quadrupole trap and the Penning trap, which is used for charge breeding. Similar plans exist for MAFF-TRAP to be installed at the new research reactor FRM II [60]. Here, especially the neutron-rich fission fragments produced from a uranium target by thermal neutrons can be investigated and used for fusion reactions after post-acceleration.

However, one can still not get access to a large number of nuclides for which the production rate is far too weak. Part of the solution is reserved for planned new facilities, such as EURISOL (Europe) [440], FAIR (Germany) [40], RIA (USA) [41], and RIKEN (Japan) [42]. At FAIR for example an enhancement of primary ion beams by a factor of 100, and of stored secondary beams by a factor of 10 000 is foreseen, due to much improved techniques and new capabilities of ion sources, synchrotrons, fragment separators and storage rings. For each of these new facilities ambitious mass measurement projects are planned. In the case of FAIR even three new trap experiments are proposed, the storage ring project ILIMA and the two Penning trap mass spectrometers HITRAP and MATS. HITRAP will already be in operation within the next two years at the present GSI facility and will therefore be discussed here in more detail.

In the HITRAP project [51] (see Fig. 49) highly charged ions are produced by stripping the relativistic ion beams delivered by the GSI accelerator complex. These ions are injected into the experimental storage ring ESR. After electron cooling and deceleration to 4 MeV/u the ions are injected into a linear decelerator. After deceleration to about 10 keV/q the ions are accumulated and electron cooled in a cylindrical Penning trap before they are further transferred to different setups for experiments including g-factor measurements and high-accuracy mass spectrometry. In the later case a relative

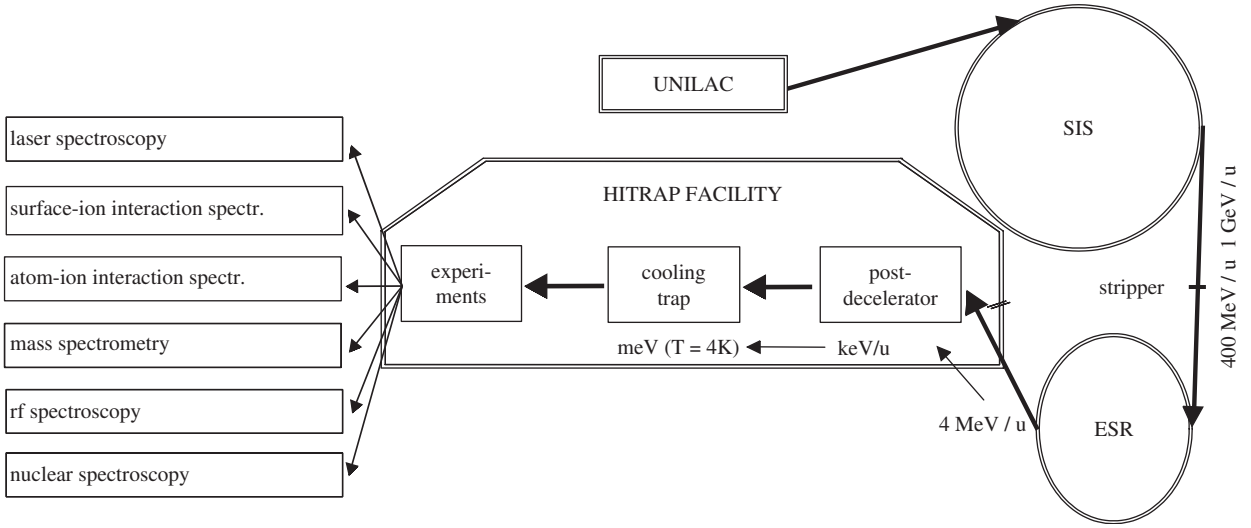

Fig. 49. Overview of the planned HITRAP facility at GSI and FAIR for experiments with highly charged ions at nearly rest in space.

mass accuracy of 10^{-11} or better is envisaged. In order to minimize uncertainties in the mass determination due to fluctuation of the electromagnetic fields, ion–ion interactions, and field inhomogeneities, a novel four-trap system (two hyperbolical precision Penning traps in the center and one cylindrical Penning trap on each side) to be installed in a superconducting magnet with high field stability ($((\delta B/\delta t)(1/B) \leqslant 10^{-10}/h$) and homogeneity ($\leqslant \pm 0.01$ ppm measured over a 10 mm diameter spherical volume) is proposed. Non-destructive phase-sensitive cyclotron frequency measurements, i.e. a measurement of the integrated phase difference of the particles' motions relative to an excitation with a well-defined phase, will be performed. Thereby, the classical Fourier-limit for frequency measurements based on Fourier-analysis of detection signals, already mentioned, can be overcome. By simultaneously storing the two resistively cooled ions in different traps but within the same homogeneous region of the magnet ion–ion interactions are avoided and one can expect that magnetic-field changes as well as systematic errors in the measured frequency ratios will, to a large extent, be canceled. HITRAP will have only access to longer lived ($T_{1/2} > 10$ s) or stable nuclides due to the slow electron cooling process in the experimental storage ring and the cooling Penning trap. At a later stage the ion of interest and the reference ion can be cooled below millikelvin temperatures by exchange of energy with an ion (preferably $^{24}Mg^{+}$), which has been laser-cooled to the zero-point state. The laser cooling of $^{24}Mg^{+}$ will take place in the preparation traps since no extreme field homogeneity is needed.

Aside from enabling high-accuracy experiments, ion traps have been proven to be extremely efficient devices for (radioactive) ion beam manipulation as, for example, accumulation, cooling, beam cleaning, charge breeding, and bunching [18,19]. This advantage becomes more and more important for the planned high-accuracy ion trap experiments and the future radioactive beam facilities. With all these ongoing experiments and new projects the community of atomic, nuclear, and astrophysicists requiring accurate mass data of stable and short-lived nuclides are in an excellent position. For sure we will soon see exciting new results from the field of high-accuracy mass spectrometry with storage rings and Penning traps.

12. Concluding remarks

This review has summarized the state-of-the art in high-accuracy ion trap mass spectrometry, a field that started about 20 years ago and that has now a large variety of exciting applications in different fields of science. The main focus was put on Penning trap mass spectrometry since it provides the highest mass accuracy, but the importance of storage ring mass spectrometry was pointed out as well. The basics of ion trapping, cooling, and detection techniques and their applications are described. Trapping and cooling of charged particles in ion traps have now become a versatile tool at

accelerators that provides extreme accuracy and sensitivity as well as new approaches not only for mass spectrometry but also for atomic and nuclear physics experiments in general.

Mass spectrometry of radionuclides and stable ions in storage rings and Penning traps is performed or planned at many radioactive beam facilities and university institutes. The accurate mass values are or will be applied in the near future to high-accuracy proofs of the weak interaction, to test the conserved-vector-current hypothesis and the unitarity of the CKM matrix, to test symmetries and CPT invariance, to determine fundamental constants, or to provide high-accuracy proofs of quantum electrodynamics in strong fields.

Since next generation radioactive beam production facilities are in the planning, design, and construction stages as, for example, EURISOL, FAIR, RIA, and SPRIAL2, many more ion traps with novel cooling and detection techniques and a wide variety of applications in ion manipulation and high-accuracy mass spectrometry will be built. They aim for shorter half-lives, higher resolving powers, and even higher mass accuracies with relative uncertainties as low as 10^{-9} for radionuclides and 10^{-12} for stable masses. In case somebody asks why higher and higher accuracy is needed, the best answer was already given by Heinz Maier–Leibniz (1911–2000): "Whenever you invent a method ten or a hundred times better than the existing ones, you can be sure that this will lead to new science!".

Acknowledgements

I have been grateful to many colleagues over the years for their input into high-accuracy mass spectrometry with ion traps. I am particularly indebted to H.-J. Kluge (GSI Darmstadt, Germany) for his permanent support and advice during all the years we worked together. The author thank many people from different facilities for providing me with material to be included into this review and especially G. Werth (University of Mainz, Germany) and R.B. Moore (McGill University, Canada) for their many detailed and useful comments which significantly improved the manuscript. The support of the Helmholtz Association of National Research Centres (HGF) under contract number VH-NG-037 and of the Gesellschaft für Schwerionenforschung (GSI) Darmstadt is acknowledged.

References

[1] D. Lunney, J.M. Pearson, C. Thibault, Rev. Mod. Phys. 75 (2003) 1021.
[2] G. Bollen, Nucl. Phys. A 693 (2001) 3.
[3] F. Herfurth, F. Ames, G. Audi, D. Beck, K. Blaum, G. Bollen, A. Kellerbauer, H.-J. Kluge, M. Kuckein, D. Lunney, R.B. Moore, M. Oinonen, D. Rodríguez, E. Sauvan, C. Scheidenberger, S. Schwarz, G. Sikler, C. Weber, ISOLDE Collaboration, J. Phys. B 36 (2003) 931.
[4] A. Kellerbauer, Int. J. Mass Spectr. 229 (2003) 107.
[5] S. Rainville, J.K. Thompson, D.E. Pritchard, Science 303 (2004) 334.
[6] R.S. Van Dyck Jr., S.L. Zafonte, S. Van Liew, D.B. Pinegar, P.B. Schwinberg, Phys. Rev. Lett. 92 (2004) 220802.
[7] W. Shi, M. Redshaw, E.G. Myers, Phys. Rev. A 72 (2005) 022510.
[8] A.H. Wapstra, G. Audi, C. Thibault, Nucl. Phys. A 729 (2003) 129.
[9] G. Audi, A.H. Wapstra, C. Thibault, Nucl. Phys. A 729 (2003) 337.
[10] K. Blaum, G. Audi, D. Beck, G. Bollen, P. Delahaye, S. George, C. Guénaut, F. Herfurth, A. Herlert, A. Kellerbauer, H.-J. Kluge, D. Lunney, M. Mukherjee, S. Schwarz, L. Schweikhard, C. Yazidjian, Nucl. Phys. A 752 (2005) 317c.
[11] H. Dehmelt, Rev. Mod. Phys. 62 (1990) 525.
[12] G. Werth, H. Häffner, W. Quint, Adv. At. Mol. Opt. Phys. 48 (2002) 191.
[13] H. Häffner, T. Beier, S. Djekić, N. Hermanspahn, H.-J. Kluge, W. Quint, S. Stahl, J. Verdú, T. Valenzuela, G. Werth, Eur. Phys. J. D 22 (2003) 163.
[14] T.W. Hänsch, H. Walther, Rev. Mod. Phys. 71 (1999) S242.
[15] D. Leibfried, R. Blatt, C. Monroe, D. Wineland, Rev. Mod. Phys. 75 (2003) 281.
[16] H. Walther, Adv. At. Mol. Opt. Phys. 31 (1993) 137.
[17] M. Block, P. Seibert, O. Rehm, G. Werth, Eur. Phys. J. D 7 (1999) 461.
[18] H.-J. Kluge, K. Blaum, F. Herfurth, W. Quint, Phys. Scr. T 104 (2003) 167.
[19] G. Bollen, Lect. Notes Phys. 651 (2004) 169.
[20] P.H. Dawson (Ed.), Quadrupole Mass Spectrometry and its Applications, American Institute of Physics, New York, 1995 (originally published by Elsevier, Amsterdam, 1976).
[21] R.E. March, J.F. Todd (Eds.), Practical Aspects of Ion Trap Mass Spectrometry, vols. 1–3, second ed., CRC Press, Boca Raton, Florida, 1995.
[22] H.-J. Kluge, K. Blaum, Nucl. Phys. A 746 (2004) 200c.
[23] D.H. Dubin, D. Schneider, (Eds.), in: Proceedings of the Trapped Charged Particles and Fundamental Physics, Asilomar, CA, USA, 1998 (AIP Conference Proceedings, vol. 457, 1999).

[24] D. Lunney, G. Audi, H.-J. Kluge (Eds.), in: Proceedings of the Atomic Physics at Accelerators: Mass Spectrometry (APAC 2000), Cargèse, France, 2000 (Hyperfine Interactions 132 (2001)).
[25] J.M. D'Auria, J. Thomson, M. Comyn (Eds.), in: Proceedings of the 4th International Conference on Electromagnetic Isotope Separation and Techniques Related to their Applications (EMIS-14) Conference, Victoria, Canada, 2002 (Nucl. Instr. and Meth. B 204 (2003)).
[26] M. Groß, D. Habs, W. Lange, U. Schramm, H. Walther (Eds.), in: Proceedings of the Trapped Charged Particles and Fundamental Interactions (TCPFI 2002) Conference Wildbad Kreuth, Germany, 2002 (J. Phys. B 36 (2003)).
[27] C. Gross, W. Nazarewicz, (Eds.), Proceedings of the Fourth International Conference on Exotic Nuclei and Atomic Masses (ENAM2004), Callaway Gardens, Pine Mountain, Georgia, USA, 2004 (Eur. Phys. J. A 25 (2005)).
[28] D. Lunney, G. Bollen, Hyperfine Interactions 129 (2000) 249.
[29] D. Lunney, G. Audi, H. Doubre, S. Henry, C. Monsanglant, M. de Saint Simon, C. Thibault, C. Toader, C. Borcea, G. Bollen, Phys. Rev. C 64 (2001) 054311.
[30] L. Bianchi, B. Fernandez, J. Gastebois, A. Gillibert, W. Mittig, J. Barrette, Nucl. Instr. and Meth. A 276 (1989) 509.
[31] G.F. Lima, A. Lépine-Szily, G. Audi, W. Mittig, M. Chartier, N.A. Orr, R. Lichtenthaler, J.C. Angelique, J.M. Casandjian, A. Cunsolo, C. Donzaud, A. Foti, A. Gillibert, M. Lewitowicz, S. Lukyanov, M. MacCormick, D.J. Morrissey, A.N. Ostrowski, B.M. Sherrill, C. Stephan, T. Suomijarvi, L. Tassan-Got, D.J. Vieira, A.C.C. Villari, J.M. Wouters, Phys. Rev. C. 65 (2002) 044618.
[32] G. Auger, W. Mittig, A. Lépine-Szily, L.K. Fifield, M. Bajard, E. Baron, D. Bibet, P. Bricault, J.M. Casandjian, M. Chabert, M. Chartier, J. Fermé, L. Gaudard, A. Gillibert, M. Lewitowicz, M.H. Moscatello, N.A. Orr, E. Plagnol, C. Ricault, A.C.C. Villari, Y.Y. Feng, Nucl. Instr. and Meth. A 350 (1994) 235.
[33] M. Chartier, G. Auger, W. Mittig, A. Lépine-Szily, L.K. Fifield, J.M. Casandjian, M. Chabert, J. Fermé, A. Gillibert, M. Lewitowicz, M. MacCormick, M.H. Moscatello, O.H. Odland, N.A. Orr, G. Politi, C. Spitaels, A.C.C. Villari, Phys. Rev. Lett. 77 (1996) 2400.
[34] C. Scheidenberger, Eur. Phys. J. A 15 (2002) 7.
[35] W. Paul, Rev. Mod. Phys. 62 (1990) 531.
[36] L.S. Brown, G. Gabrielse, Rev. Mod. Phys. 58 (1986) 233.
[37] B. Franzke, Nucl. Instr. and Meth. B 24/25 (1987) 18.
[38] J.C. Hardy, I.S. Towner, Phys. Rev. C 71 (2005) 055501.
[39] J.C. Hardy, I.S. Towner, Phys. Rev. Lett. 94 (2005) 092502.
[40] http://www.gsi.de/fair/
[41] http://www.phy.anl.gov/ria/
[42] http://www.riken.jp/
[43] http://www.ganil.fr/research/developments/spiral2/
[44] J.J. Thomson, Phil. Mag. 3 (1897) 293.
[45] J.J. Thomson, Phil. Mag. 5 (1899) 547.
[46] K.S. Sharma, R.C. Barber, F. Buchinger, J.E. Crawford, X. Feng, H. Fukutani, S. Gulick, G. Hackman, J.C. Hardy, D. Hofman, J.K.P. Lee, P. Martinez, R.B. Moore, G. Savard, D. Seweryniak, J. Uusitalo, Proc. of the International Conference on Exotic Nuclei and Atomic Masses (ENAM1998) Bellaire, Ed. Michigan, B.M. Sherill, D.J. Morissey, C.M. Davids, AIP Conf. Proc. 455 (1998) 130.
[47] G. Savard, R.C. Barber, C. Boudreau, F. Buchinger, J. Caggiano, J. Clark, J.E. Crawford, H. Fukutani, S. Gulick, J.C. Hardy, A. Heinz, J.K.P. Lee, R.B. Moore, K.S. Sharma, J. Schwartz, D. Seweryniak, G.D. Sprouse, J. Vaz, Hyperfine Interactions 132 (2001) 221.
[48] T. Radon, H. Geissel, G. Münzenberg, B. Franzke, Th. Kerscher, F. Nolden, Yu.N. Novikov, Z. Patyk, C. Scheidenberger, F. Attallah, K. Beckert, T. Beha, F. Bosch, H. Eickhoff, M. Falch, Y. Fujita, M. Hausmann, F. Herfurth, H. Irnich, H.C. Jung, O. Klepper, C. Kozhuharov, Yu.A. Litvinov, K.E.G. Löbner, F. Nickel, H. Reich, W. Schwab, B. Schlitt, M. Steck, K. Sümmerer, T. Winkler, H. Wollnik, Nucl. Phys. A 677 (2000) 75.
[49] G. Gabrielse, A. Khabbaz, D.S. Hall, C. Heimann, H. Kalinowsky, W. Jhe, Phys. Rev. Lett. 82 (1999) 3198.
[50] W. Quint, J. Dilling, S. Djekic, H. Häffner, N. Hermanspahn, H.-J. Kluge, G. Marx, R. Moore, D. Rodríguez, J. Schönfelder, G. Sikler, T. Valenzuela, J. Verdú, C. Weber, G. Werth, Hyperfine Interactions 132 (2001) 453.
[51] F. Herfurth, T. Beier, L. Dahl, S. Eliseev, S. Heinz, O. Kester, H.-J. Kluge, C. Kozhuharov, G. Maero, W. Quint, and the HITRAP Collaboration, in: Proceeding of the Workshop on Physics with Ultra Slow Antiproton Beams, RIKEN, AIP Conference Proceedings 793 (2005) 278.
[52] Yu.N. Novikov for the ILIMA Collaboration, submitted to GSI/FAIR Darmstadt, 2005, Technical Proposal.
[53] G. Bollen, S. Becker, H.-J. Kluge, M. König, R.B. Moore, T. Otto, H. Raimbault-Hartmann, G. Savard, L. Schweikhard, H. Stolzenberg, ISOLDE Collaboration, Nucl. Instr. and Meth. A 368 (1996) 675.
[54] V.S. Kolhinen, S. Kopecky, T. Eronen, U. Hager, J. Hakala, J. Huikari, A. Jokinen, A. Nieminen, S. Rinta-Antila, J. Szerypo, J. Äystö, Nucl. Instr. and Meth. A 528 (2004) 776.
[55] X.W. Ma, Hyperfine Interactions 115 (1998) 107.
[56] W.L. Zhan, Proceedings of the International Conference on Nuclear Physics at Storage Rings (STORI2005), Jülich, Germany, 2005.
[57] G. Bollen, S. Schwarz, D. Davies, P. Lofy, D. Morrissey, R. Ringle, P. Schury, T. Sun, L. Weissman, Nucl. Instr. and Meth. A 532 (2004) 203.
[58] S. Brunner, T. Engel, A. Schmitt, G. Werth, Eur. Phys. J. D 15 (2001) 181.
[59] F. DiFilippo, V. Natarajan, M. Bradley, F. Palmer, D.E. Pritchard, Phys. Scr. T 59 (1995) 144.
[60] J. Szerypo, D. Habs, S. Heinz, J. Neumayr, P. Thirolf, A. Wilfart, F. Voit, Nucl. Instr. and Meth. B 204 (2003) 512.
[61] K. Blaum for the MATS Collaboration, submitted to GSI/FAIR Darmstadt, 2005, Technical Proposal.
[62] M. Wada, Y. Ishida, T. Nakamura, Y. Yamazaki, T. Kambara, H. Ohyama, Y. Kanai, T.M. Kojima, Y. Nakai, N. Ohshima, A. Yoshida, T. Kubo, Y. Matsuo, Y. Fukuyama, K. Okada, T. Sonoda, S. Ohtani, K. Noda, H. Kawakami, I. Katayama, Nucl. Instr. and Meth. B 204 (2003) 570.
[63] G. Marx, D. Ackermann, J. Dilling, F.P. Hessberger, S. Hoffmann, H.-J. Kluge, R. Mann, G. Münzenberg, Z. Qamhieh, W. Quint, D. Rodriguez, M. Schädel, J. Schönfelder, G. Sikler, C. Toader, C. Weber, O. Engels, D. Habs, P. Thirolf, H. Backe, A. Dretzke, W. Lauth, W. Ludolphs, M. Sewtz, Hyperfine Interactions 132 (2001) 459.

[64] I. Bergström, C. Carlberg, T. Fritioff, G. Douysset, J. Schönfelder, R. Schuch, Nucl. Instr. and Meth. A 487 (2002) 618.
[65] J. Dilling, P. Bricault, M. Smith, H.-J. Kluge, TITAN Collaboration, Nucl. Instr. and Meth. B 204 (2003) 492.
[66] R.S. Van Dyck Jr., D.L. Farnham, S.L. Zafonte, P.B. Schwinberg, Rev. Scientific Instr. 70 (1999) 1665.
[67] R.S. Van Dyck Jr., S.L. Zafonte, P.B. Schwinberg, Hyperfine Interactions 132 (2001) 163.
[68] M. Beck, F. Ames, D. Beck, G. Bollen, B. Delauré, V.V. Golovko, V.Yu. Kozlov, I.S. Kraev, A. Lindroth, T. Phalet, W. Quint, P. Schuurmans, N. Severijns, B. Vereecke, S. Versyck, Nucl. Instr. and Meth. A 503 (2003) 567.
[69] J.J. Thomson, Phil. Mag. 13 (1907) 561.
[70] J.J. Thomson, Phil. Mag. 24 (1912) 209/669.
[71] F.W. Aston, Phil. Mag. 38 (1919) 707.
[72] F.W. Aston, Nature (London) 195 (1920) 617.
[73] F.W. Aston, Proc. Phys. Soc. 115 (1927) 484.
[74] A. Einstein, Annal. Phys. 18 (1905) 639.
[75] F.W. Aston, Mass Spectra and Isotopes, second ed., Edward Arnold, London, 1942.
[76] G. Gamow, Proc. R. Soc. London, Ser. A 126 (1930) 632.
[77] C.F. von Weizsäcker, Z. Phys. 96 (1935) 431.
[78] H.A. Bethe, R.F. Bacher, Rev. Mod. Phys. 8 (1936) 82.
[79] A.J. Dempster, Proc. Amer. Phil. Soc. 75 (1935) 755.
[80] K.T. Bainbridge, E.B. Jordan, Phys. Rev. 50 (1936) 282.
[81] J.H.E. Mattauch, Phys. Rev. 50 (1936) 617.
[82] J.H.E. Mattauch, Ergeb. exakt. Naturwissenschaften 19 (1940) 170.
[83] A.O. Nier, T.R. Roberts, Phys. Rev. 81 (1951) 507.
[84] H.E. Duckworth, Rev. Sci. Instr. 21 (1950) 54.
[85] H.E. Duckworth, Phys. Rev. 78 (1950) 386.
[86] O. Haxel, J.H.D. Jensen, H.E. Suess, Naturwissenschaften 35 (1948) 376.
[87] O. Haxel, J.H.D. Jensen, H.E. Suess, Naturwissenschaften 36 (1949) 153.
[88] O. Haxel, J.H.D. Jensen, H.E. Suess, Naturwissenschaften 36 (1949) 155.
[89] O. Haxel, J.H.D. Jensen, H.E. Suess, Phys. Rev. 75 (1949) 1766.
[90] O. Haxel, J.H.D. Jensen, H.E. Suess, Z. Phys. 128 (1950) 295.
[91] M.G. Mayer, Phys. Rev. 74 (1948) 235.
[92] M.G. Mayer, Phys. Rev. 75 (1949) 1969.
[93] M.G. Mayer, Phys. Rev. 78 (1950) 16.
[94] C. Thibault, R. Klapisch, C. Rigaud, A.M. Poskanzer, R. Prieels, L. Lessard, W. Reisdorf, Phys. Rev. C 12 (1975) 644.
[95] W. Paul, H. Steinwedel, Z. Naturf. 8a (1953) 448.
[96] W. Paul, M. Raether, Z. Phys. 140 (1955) 262.
[97] W. Paul, H.P. Reinhard, U.v. Zahn, Z. Phys. 152 (1958) 143.
[98] E. Fischer, Z. Phys. 156 (1959) 1.
[99] F.M. Penning, Physica 3 (1936) 563.
[100] J.R. Pierce, in: Theory and Design of Electron Beams, D. van Nostrand Co., New York 1949 (Chapter 3).
[101] N.F. Ramsey, Rev. Mod. Phys. 62 (1990) 541.
[102] L.G. Smith, Rev. Sci. Instr. 27 (1956) 638.
[103] L.G. Smith, Conf. Nuclidic Masses Winnipeg 811 (1967).
[104] G. Bollen, P. Dabkievicz, P. Egelhof, T. Hilberath, H. Kalinowsky, F. Kern, H.-J. Kluge, R.B. Moore, H. Schnatz, L. Schweikhard, H. Stolzenberg, G. Temmer, G. Ulm, ISOLDE Collaboration, Hyperfine Interactions 38 (1987) 793.
[105] R.S. Van Dyck Jr., D.L. Farnham, P.B. Schwinberg, in: R. Neugart, A. Wöhr (Eds.), Proceedings of the Conference on Nuclei Far from Stability, Bernkastel, Germany, 1992 (Inst. Phys. Conf. Series 132 (1992) 3).
[106] V. Natarajan, K.R. Boyce, F. DiFilippo, D.E. Pritchard, in: R. Neugart, A. Wöhr (Eds.), Proceedings of the Conference on Nuclei far from Stability, Bernkastel, Germany, 1992 (Inst. Phys. Conf. Series 132 (1992) 3).
[107] G. Gräff, H. Kalinowsky, J. Traut, Z. Phys. A 297 (1980) 35.
[108] B. Franzke, K. Beckert, H. Eickhoff, F. Nolden, H. Reich, U. Schaaf, B. Schlitt, A. Schwinn, M. Steck, Th. Winkler, Phys. Scr. T 59 (1995) 176.
[109] M. Hausmann, F. Attallah, K. Beckert, F. Bosch, A. Dolinskiy, H. Eickhoff, M. Falch, B. Franczak, B. Franzke, H. Geissel, Th. Kerscher, O. Klepper, H.-J. Kluge, C. Kozhuharov, K.E.G. Löbner, G. Münzenberg, F. Nolden, Yu.N. Novikov, T. Radon, H. Schatz, C. Scheidenberger, J. Stadlmann, M. Steck, T. Winkler, H. Wollnik, Nucl. Instr. and Meth. A 446 (2000) 569.
[110] Yu.A. Litvinov, H. Geissel, T. Radon, F. Attallah, G. Audi, K. Beckert, F. Bosch, M. Falch, B. Franzke, M. Hausmann, M. Hellström, Th. Kerscher, O. Klepper, H.-J. Kluge, C. Kozhuharov, K.E.G. Löbner, G. Münzenberg, F. Nolden, Yu.N. Novikov, W. Quint, Z. Patyk, H. Reich, C. Scheidenberger, B. Schlitt, M. Steck, K. Sümmerer, L. Vermeeren, M. Winkler, Th. Winkler, H. Wollnik, Nucl. Phys. A 756 (2005) 3.
[111] A. Kellerbauer, K. Blaum, G. Bollen, F. Herfurth, H.-J. Kluge, M. Kuckein, E. Sauvan, C. Scheidenberger, L. Schweikhard, Eur. Phys. J. D 22 (2003) 53.
[112] K. Blaum, G. Bollen, F. Herfurth, A. Kellerbauer, H.-J. Kluge, M. Kuckein, S. Heinz, P. Schmidt, L. Schweikhard, J. Phys. B 36 (2003) 921.
[113] ISOLDE Collaboration, G. Bollen, H.-J. Kluge, M. König, T. Otto, G. Savard, H. Stolzenberg, R.B. Moore, G. Rouleau, G. Audi, Phys. Rev. C 46 (1992) R2140.

[114] S. Schwarz, F. Ames, G. Audi, D. Beck, G. Bollen, C. De Coster, J. Dilling, O. Engels, R. Fossion, J.-E. Garcia Ramos, S. Henry, F. Herfurth, K. Heyde, A. Kellerbauer, H.-J. Kluge, A. Kohl, E. Lamour, D. Lunney, I. Martel, R.B. Moore, M. Oinonen, H. Raimbault-Hartmann, C. Scheidenberger, G. Sikler, J. Szerypo, C. Weber, ISOLDE Collaboration, Nucl. Phys. A 693 (2001) 533.
[115] Yu.A. Litvinov, H. Geissel, Yu.N. Novikov, Z. Patyk, T. Radon, C. Scheidenberger, F. Attallah, K. Beckert, F. Bosch, M. Falch, B. Franzke, M. Hausmann, Th. Kerscher, O. Klepper, H.-J. Kluge, C. Kozhuharov, K.E.G. Löbner, G. Münzenberg, F. Nolden, M. Steck, H. Wollnik, Nucl. Phys. A 734 (2004) 473.
[116] K. Blaum, D. Beck, G. Bollen, P. Delahaye, C. Guénaut, F. Herfurth, A. Kellerbauer, H.-J. Kluge, D. Lunney, S. Schwarz, L. Schweikhard, C. Yazidjian, Europhys. Lett. 67 (2004) 586.
[117] G.I. Budker, in: Proceedings of the International Symposium on Electron and Positron Storage Rings, Saclay, 1966, p. II-I-I; Sov. At. Energy, 22 (1967) 346 (in Russian).
[118] G. Savard, St. Becker, G. Bollen, H.-J. Kluge, R.B. Moore, Th. Otto, L. Schweikhard, H. Stolzenberg, U. Wiess, Phys. Lett. A 158 (1991) 247.
[119] D.J. Wineland, H.G. Dehmelt, J. Appl. Phys. 46 (1975) 919.
[120] Ion Traps, P.K. Ghosh, International Series of Monographs on Physics, vol. 90, Clarendon Press, Oxford, 1995.
[121] F.G. Major, V.N. Gheorghe, G. Werth, Charged Particle Traps, Physics and Techniques of Charged Particle Field Confinement, Springer Series on Atomic, Optical, and Plasma Physics, vol. 37, Springer, Berlin, 2005.
[122] E. Fischer, O. Osberghaus, W. Paul, Forsch.-Ber. d. Wirtsch. Ministeriums Nordrhein-Westfalen, Nr. 415 (1958).
[123] K. Blaum, C. Geppert, P. Müller, W. Nörtershäuser, E.W. Otten, A. Schmitt, N. Trautmann, K. Wendt, B.A. Bushaw, Int. J. Mass Spec. Ion Process. 181 (1998) 67.
[124] N.W. McLachlan, in: Theory and Application of Mathieu-Functions, Clarendon-Press, Oxford, 1947.
[125] V.V. Titov, J. Am. Soc. Mass Spectr. 9 (1998) 50.
[126] V.V. Titov, J. Am. Soc. Mass Spectr. 9 (1998) 70.
[127] K. Blaum, Ch. Geppert, P. Müller, W. Nörtershäuser, K. Wendt, B.A. Bushaw, Int. J. Mass Spec. Ion Process. 202 (2000) 81.
[128] P. Müller, B.A. Bushaw, K. Blaum, S. Diel, Ch. Geppert, A. Nähler, N. Trautmann, W. Nörtershäuser, K. Wendt, Fres. J. Anal. Chem. 370 (2001) 508.
[129] K. Blaum, C. Geppert, W.G. Schreiber, J.G. Hengstler, P. Müller, W. Nörtershäuser, K. Wendt, B.A. Bushaw, Anal. Bioanal. Chem. 372 (2002) 759.
[130] K. Wendt, N. Trautmann, Int. J. Mass Spectr. 242 (2005) 161.
[131] A. Nieminen, J. Huikari, A. Jokinen, J. Äystö, P. Campbell, E.C.A. Cochrane, EXOTRAPS Collaboration, Nucl. Instr. and Meth. A 469 (2001) 244.
[132] F. Herfurth, J. Dilling, A. Kellerbauer, G. Bollen, S. Henry, H.-J. Kluge, E. Lamour, D. Lunney, R.B. Moore, C. Scheidenberger, S. Schwarz, G. Sikler, J. Szerypo, Nucl. Instr. and Meth. A 469 (2001) 254.
[133] A. Kellerbauer, T. Kim, R.B. Moore, P. Varfalvy, Nucl. Instr. and Meth. A 469 (2001) 276.
[134] E. Kugler, Hyperfine Interactions 129 (2000) 23.
[135] R.E. March, R.J. Hughes, J.F.J. Todd, in: Quadrupole Storage Mass Spectrometry, Wiley, New York, 1989, p. 31.
[136] E. Teloy, D. Gerlich, Chem. Phys. 4 (1974) 417.
[137] D. Gerlich, Adv. Chem. Phys. 82 (1992) 1.
[138] A.G. Marshall, C.L. Hendrickson, G.S. Jackson, Mass Spectr. Rev. 17 (1998) 1.
[139] T. Gudjons, B. Hilbert, P. Seibert, G. Werth, Europhys. Lett. 33 (1996) 595.
[140] L.S. Brown, G. Gabrielse, Phys. Rev. A 25 (1982) 2423.
[141] G. Bollen, R.B. Moore, G. Savard, H. Stolzenberg, J. Appl. Phys. 68 (1990) 4355.
[142] H. Raimbault-Hartmann, D. Beck, G. Bollen, M. König, H.-J. Kluge, E. Schark, J. Stein, S. Schwarz, J. Szerypo, Nucl. Instr. and Meth. B 126 (1997) 378.
[143] R.S. Van Dyck Jr., F.L. Moore, D.L. Farnham, P.B. Schwinberg, Phys. Rev. A 40 (1989) 6308.
[144] P.W. Anderson, Phys. Rev. Lett. 9 (1962) 309.
[145] P.W. Anderson, Y.B. Kim, Rev. Mod. Phys. 39 (1964) 39.
[146] R.S. Van Dyck Jr., D.L. Farnham, P.B. Schwinberg, J. Mod. Opt. 39 (1992) 243.
[147] K. Jungmann, J. Hoffnagle, R.G. DeVoe, R.G. Brewer, Phys. Rev. A 36 (1987) 3451.
[148] J.B. Jeffries, S.E. Barlow, G.H. Dunn, Int. J. Mass Spectr. Ion Process. 54 (1983) 169.
[149] G. Gabrielse, W. Jhe, D. Phillips, W. Quint, L. Haarsma, K. Abdullah, H. Kalinowsky, J. Gröbner, Hyperfine Interactions 81 (1993) 5.
[150] D. Beck, F. Ames, M. Beck, G. Bollen, B. Delauré, P. Schuurmans, S. Schwarz, P. Schmidt, N. Severijns, O. Forstner, Hyperfine Interactions 132 (2001) 469.
[151] J.V. Porto, Phys. Rev. A 64 (2001) 023403.
[152] F. Bosch, Nucl. Phys. A 701 (2002) 509c.
[153] B. Schlitt, K. Beckert, F. Bosch, H. Eickhoff, B. Franzke, Y. Fujita, H. Geissel, M. Hausmann, H. Irnich, O. Klepper, H.-J. Kluge, C. Kozhuharov, G. Kraus, G. Münzenberg, F. Nickel, F. Nolden, Z. Patyk, T. Radon, H. Reich, C. Scheidenberger, W. Schwab, M. Steck, K. Sümmerer, Th. Winkler, T. Beha, M. Falch, Th. Kerscher, K.E.G. Löbner, H.C. Jung, H. Wollnik, Yu. Novikov, Nucl. Phys. A 626 (1997) 315c.
[154] M. Steck, Nucl. Phys. A 626 (1997) 473c.
[155] W.M. Itano, D.J. Wineland, Phys. Rev. A 25 (1982) 35.
[156] V. Fock, Z. Phys. 47 (1928) 446.
[157] C.G. Darwin, Proc. Cambridge Phil. Soc. 27 (1930) 86.
[158] A.A. Sokolov, Y.G. Pavlenko, Opt. Spectrosc. (USSR) 22 (1967) 1.
[159] G. Gräff, E. Klempt, G. Werth, Z. Phys. 222 (1969) 201.

[160] M. Kretzschmar, Phys. Scr. 46 (1992) 544.
[161] M. Kretzschmar, in: Proceedings of the Conference on Trapped Charged Particles and Fundamental Physics, Asilomar, California, AIP Conference Proceedings 457 (1999) 242.
[162] M. König, G. Bollen, H.-J. Kluge, T. Otto, J. Szerypo, Int. J. Mass Spectr. Ion Process. 142 (1995) 95.
[163] M.B. Comisarow, A.G. Marshall, Chem. Phys. Lett. 25 (1974) 282.
[164] L. Schweikhard, S. Guan, A.G. Marshall, Int. J. Mass Spec. Ion Process. 120 (1992) 71.
[165] R.S. Van Dyck Jr., D.L. Farnham, P.B. Schwinberg, Phys. Rev. Lett. 70 (1993) 2888.
[166] E.A. Cornell, R.M. Weisskoff, K.R. Boyce, D.E. Pritchard, Phys. Rev. A 41 (1990) 312.
[167] J.L. Verdú, S. Djekić, S. Stahl, T. Valenzuela, M. Vogel, G. Werth, H.-J. Kluge, W. Quint, Phys. Scr. T 112 (2004) 68.
[168] E.A. Cornell, R.M. Weisskoff, K.R. Boyce, R.W. Flanagan, G.P. Lafyatis, D.E. Pritchard, Phys. Rev. Lett. 63 (1989) 1674.
[169] S. Rainville, M.P. Bradley, J.V. Porto, J.K. Thomson, D.E. Pritchard, Hyperfine Interactions 132 (2001) 177.
[170] M. Steck, K. Beckert, H. Eickhoff, B. Franzke, F. Nolden, H. Reich, B. Schlitt, T. Winkler, Phys. Rev. Lett. 77 (1996) 3803.
[171] M. Steck, P. Beller, K. Beckert, B. Franzke, F. Nolden, Nucl. Instr. and Meth. A 532 (2004) 357.
[172] K. Blaum, C. Geppert, H.-J. Kluge, M. Mukherjee, S. Schwarz, K. Wendt, Nucl. Instr. and Meth. B 204 (2003) 331.
[173] H.-J. Kluge, F. Ames, W. Ruster, K. Wallmeroth, in: Proc. Acc. Radioact. Beams WS, TRIUMF 85-1, 1985, p. 119.
[174] V.N. Fedoseyev, G. Huber, U. Köster, J. Lettry, V.I. Mishin, H. Ravn, V. Sebastian, Hyperfine Interactions 127 (2000) 409.
[175] U. Köster, V.N. Fedoseyev, V.I. Mishin, Spectrochim. Acta B 58 (2003) 1047.
[176] K. Wendt, K. Blaum, K. Brück, Ch. Geppert, H.-J. Kluge, M. Mukherjee, G. Passler, S. Schwarz, S. Sirotzki, K. Wies, Nucl. Phys. A 746 (2004) 47c.
[177] W. Ketterle, N.J. van Druten, Adv. At. Mol. Opt. Phys. 37 (1996) 181.
[178] T. Greytak, in: A. Griffin, D. Snoke, S. Stringari (Eds.), Bose–Einstein Condensation, Cambridge University, Cambridge, England, 1995.
[179] M.B. Schneider, M.A. Levine, C.L. Bennett, J.R. Henderson, D.A. Knapp, R.E. Marrs, in: A. Hershcovitch (Ed.), Electron Beam Ion Sources and Their Applications, AIP Conference Proceedings, vol. 188, American Institute of Physics, New York, 1989, p. 158.
[180] B.M. Penetrante, D. Schneider, R.E. Marrs, J.N. Bardsley, Rev. Scientific Instr. 63 (1992) 2806.
[181] V.V. Anashin, G.I. Budker, N.S. Dikansky, et al., in: Proceedings of the Fourth All-Union Conference on Charged Particle Accelerators, vol. 2, Nauka, Moscow, 1975, p. 308.(in Russian).
[182] M. Bell, J. Chaney, H. Herr, F. Krienen, P. Møller-Petersen, G. Petrucci, Nucl. Instr. and Meth. 190 (1981) 237.
[183] T. Ellison, W. Kells, V. Kerner, P. McIntyre, F. Mills, L. Oleksiuk, A. Ruggiero, IEEE Trans. Nucl. Sci. NS-30 (1983) 2370.
[184] H. Poth, Phys. Rep. 196 (1990) 135.
[185] G. Gabrielse, X. Fei, L.A. Orozco, R.L. Tjoelker, J. Haas, H. Kalinowsky, T.A. Trainor, W. Kells, Phys. Rev. Lett. 63 (1989) 1360.
[186] D.S. Hall, G. Gabrielse, Phys. Rev. Lett. 77 (1996) 1962.
[187] M. Amoretti, C. Amsler, G. Bonomi, A. Bouchta, P. Bowe, C. Carraro, C.L. Cesar, M. Charlton, M.J.T. Collier, M. Doser, V. Filippini, K.S. Fine, A. Fontana, M.C. Fujiwara, R. Funakoshi, P. Genova, J.S. Hangst, R.S. Hayano, M.H. Holzscheiter, L.V. Jørgensen, V. Lagomarsino, R. Landua, D. Lindelöf, E.L. Rizzini, M. Macrì, N. Madsen, G. Manuzio, M. Marchesotti, P. Montagna, H. Pruys, C. Regenfus, P. Riedler, J. Rochet, A. Rotondi, G. Rouleau, G. Testera, A. Variola, T.L. Watson, D.P. van der Werf, Nature 419 (2002) 456.
[188] G. Gabrielse, N.S. Bowden, P. Oxley, A. Speck, C.H. Storry, J.N. Tan, M. Wessels, D. Grzonka, W. Oelert, G. Schepers, T. Sefzick, J. Walz, H. Pittner, T.W. Hänsch, E.A. Hessels, Phys. Rev. Lett. 89 (2002) 213401.
[189] M. Amoretti, C. Amsler, G. Bonomi, A. Bouchta, P.D. Bowe, C. Carraro, M. Charlton, M.J.T. Collier, M. Doser, V. Filippini, K.S. Fine, A. Fontana, M.C. Fujiwara, R. Funakoshi, P. Genova, A. Glauser, D. Grögler, J.S. Hangst, R.S. Hayano, H. Higaki, M.H. Holzscheiter, W. Joffrain, L.V. Jørgensen, V. Lagomarsino, R. Landua, C. Lenz Cesar, D. Lindelöf, E. Lodi Rizzini, M. Macrì, N. Madsen, G. Manuzio, P. Montagna, H. Pruys, C. Regenfus, P. Riedler, J. Rochet, A. Rotondi, G. Rouleau, G. Testera, D.P. van der Werf, A. Variola, T.L. Watson, T. Yamazaki, Y. Yamazaki, The ATHENA Collaboration, Nucl. Instr. and Meth. A 518 (2004) 679.
[190] M.H. Holzscheiter, M. Charlton, M.M. Nieto, Phys. Rep. 402 (2004) 1.
[191] N. Oshima, T.M. Kojima, M. Niigaki, A. Mohri, K. Komaki, Y. Iwai, Y. Yamazaki, Nucl. Instr. and Meth. B 205 (2003) 178.
[192] M.P. Bradley, J.V. Porto, S. Rainville, J.K. Thompson, D.E. Pritchard, Phys. Rev. Lett. 83 (1999) 4510.
[193] K. Blaum, G. Bollen, F. Herfurth, A. Kellerbauer, H.-J. Kluge, M. Kuckein, E. Sauvan, C. Scheidenberger, L. Schweikhard, Eur. Phys. J. A 15 (2002) 245.
[194] T.J. Quinn, I.M. Mills, in: The International System of Units (SI), The SI Brochure, 7th Edition, Bureau International des Poids et Mesures, Sèvres, France, 1998, p. 152.
[195] K. Blaum, G. Huber, H.-J. Kluge, L. Schweikhard, Eur. Phys. J. D 24 (2003) 145.
[196] K. Blaum, A. Herlert, G. Huber, H.-J. Kluge, J. Maul, L. Schweikhard, Anal. Bioanal. Chem. 377 (2003) 1133.
[197] R.L. Kelly, J. Phys. Chem. Ref. Data 16 (Suppl 1) (1987) 1.
[198] J. Scofield, in: Ionization Energies, LLNL Internal Report, Livermore, 94550 California, USA, 2001.
[199] G.C. Rodrigues, M.A. Ourdane, J. Bieron, P. Indelicato, E. Lindroth, Phys. Rev. A. 63 (2001) 012510.
[200] H.-J. Kluge, K. Blaum, C. Scheidenberger, Nucl. Instr. and Meth. A 532 (2004) 48.
[201] T. Radon, Th. Kerscher, B. Schlitt, K. Beckert, T. Beha, F. Bosch, H. Eickhoff, B. Franzke, Y. Fujita, H. Geissel, M. Hausmann, H. Irnich, H.C. Jung, O. Klepper, H.-J. Kluge, C. Kozhuharov, G. Kraus, K.E.G. Löbner, G. Münzenberg, Yu. Novikov, F. Nickel, F. Nolden, Z. Patyk, H. Reich, C. Scheidenberger, W. Schwab, M. Steck, K. Sümmerer, H. Wollnik, Phys. Rev. Lett. 78 (1997) 4701.
[202] J. Borer et al., in: Proc. IXth Conference on High Energy Accelerators, Stanford, 1974, p. 53.
[203] K. Beckert, S. Cocher, B. Franzke, U. Schaaf (Darmstadt, GSI), in: P. Marin, P. Mandrillon (Eds.), EPAC 90—Proceedings of the Second European Part. Accel. Conference, Nice, 1990, Éditions Frontières, Gif-sur-Yvette, 1990.

[204] J. Trötscher, K. Balog, H. Eickhoff, B. Franczak, B. Franzke, Y. Fujita, H. Geissel, Ch. Klein, J. Knollmann, A. Kraft, K.E.G. Löbner, A. Magel, G. Münzenberg, A. Przewloka, D. Rosenauer, H. Schäfer, M. Sendor, D.J. Vieira, B. Vogel, Th. Winkelmann, H. Wollnik, Nucl. Instr. and Meth. B 70 (1992) 455.
[205] J. Stadlmann, M. Hausmann, F. Attallah, K. Beckert, P. Beller, F. Bosch, H. Eickhoff, M. Falch, B. Franczak, B. Franzke, H. Geissel, T. Kerscher, O. Klepper, H.-J. Kluge, C. Kozhuharov, Yu.A. Litvinov, K.E.G. Löbner, M. Matoš, G. Münzenberg, N. Nankov, F. Nolden, Yu.N. Novikov, T. Ohtsubo, T. Radon, H. Schatz, C. Scheidenberger, M. Steck, H. Weick, H. Wollnik, Phys. Lett. B 586 (2004) 27.
[206] M. Hausmann, J. Stadlmann, F. Attallah, K. Beckert, P. Beller, F. Bosch, H. Eickhoff, M. Falch, B. Franczak, B. Franzke, H. Geissel, T. Kerscher, O. Klepper, H.-J. Kluge, C. Kozhuharov, Y.A. Litvinov, K.E.G. Löbner, G. Münzenberg, N. Nankov, F. Nolden, Y.N. Novikov, T. Ohtsubo, T. Radon, H. Schatz, C. Scheidenberger, M. Steck, Z. Sun, H. Weick, H. Wollnik, Hyperfine Interactions 132 (2001) 289.
[207] J. Van Roosbroeck, C. Guénaut, G. Audi, D. Beck, K. Blaum, G. Bollen, J. Cederkall, P. Delahaye, H. De Witte, D. Fedorov, V.N. Fedoseyev, S. Franchoo, H. Fynbo, M. Gorska, F. Herfurth, K. Heyde, M. Huyse, A. Kellerbauer, H.-J. Kluge, U. Köster, K. Kruglov, D. Lunney, A. De Maesschalck, V.I. Mishin, W.F. Müller, S. Nagy, S. Schwarz, L. Schweikhard, N.A. Smirnova, K. Van de Vel, P. Van Duppen, A. Van Dyck, W.B. Walters, L. Weissmann, C. Yazidjian, Phys. Rev. Lett. 92 (2004) 112501.
[208] S. Stahl, J. Alonso, S. Djekic, H.-J. Kluge, W. Quint, J. Verdu, M. Vogel, G. Werth, J. Phys. B: At. Mol. Opt. Phys. 38 (2005) 297.
[209] A. Kellerbauer, G. Audi, D. Beck, K. Blaum, G. Bollen, B.A. Brown, P. Delahaye, C. Guénaut, F. Herfurth, H.-J. Kluge, D. Lunney, S. Schwarz, L. Schweikhard, C. Yazidjian, Phys. Rev. Lett. 93 (2004) 072502.
[210] G. Savard, J.A. Clark, F. Buchinger, J.E. Crawford, S. Gulick, J.C. Hardy, A.A. Hecht, V.E. Iacob, J.K.P. Lee, A.F. Levand, B.F. Lundgren, N.D. Scielzo, K.S. Sharma, I. Tanihata, I.S. Towner, W. Trimble, J.C. Wang, Y. Wang, Z. Zhou, Phys. Rev. C 70 (2004) 042501 (R).
[211] D.L. Farnham, R.S. Van Dyck Jr., P.B. Schwinberg, Phys. Rev. Lett. 75 (1995) 3598.
[212] J.A. Clark, G. Savard, K.S. Sharma, J. Vaz, J.C. Wang, Z. Zhou, A. Heinz, B. Blank, F. Buchinger, J.E. Crawford, S. Gulick, J.K.P. Lee, A.F. Levand, D. Seweryniak, G.D. Sprouse, W. Trimble, Phys. Rev. Lett. 92 (2004) 192501.
[213] A. Jokinen, University of Jyväskylä, Finland, Private communication, 2005.
[214] M. Block, GSI Darmstadt, Germany, Private communication, 2005.
[215] C.N. Davids, B.B. Back, K. Bindra, D.J. Henderson, W. Kutschera, T. Lauritsen, Y. Nagame, P. Sugathan, A.V. Ramayya, W.B. Walters, Nucl. Instr. and Meth. B 70 (1992) 358.
[216] S. Hofmann, G. Münzenberg, Rev. Mod. Phys. 72 (2000) 733.
[217] Yu.Ts. Oganessian, V.K. Utyonkoy, Yu.V. Lobanov, F.Sh. Abdullin, A.N. Polyakov, I.V. Shirokovsky, Yu.S. Tsyganov, G.G. Gulbekian, S.L. Bogomolov, A.N. Mezentsev, S. Iliev, V.G. Subbotin, A.M. Sukhov, A.A. Voinov, G.V. Buklanov, K. Subotic, V.I. Zagrebaev, M.G. Itkis, J.B. Patin, K.J. Moody, J.F. Wild, M.A. Stoyer, N.J. Stoyer, D.A. Shaughnessy, J.M. Kenneally, R.W. Lougheed, Phys. Rev. C 69 (2004) 021601.
[218] D.J. Morrissey, B.M. Sherrill, M. Steiner, A. Stolz, I. Wiedenhover, Nucl. Instr. and Meth. B 204 (2003) 90.
[219] H. Geissel, P. Armbruster, K.H. Behr, A. Brünle, K. Burkard, M. Chen, H. Folger, B. Franczak, H. Keller, O. Klepper, B. Langenbeck, F. Nickel, E. Pfeng, M. Pfützner, E. Roeckl, K. Rykaczewski, I. Schall, D. Schardt, C. Scheidenberger, K.-H. Schmidt, A. Schröter, T. Schwab, K. Sümmerer, M. Weber, G. Münzenberg, T. Brohm, H.-G. Clerc, M. Fauerbach, J.-J. Gaimard, A. Grewe, E. Hanelt, B. Knödler, M. Steiner, B. Voss, J. Weckenmann, C. Ziegler, A. Magel, H. Wollnik, J.P. Dufour, Y. Fujita, D.J. Vieira, B. Sherrill, Nucl. Instr. and Meth. B 70 (1992) 286.
[220] T. Kubo, M. Ishihara, N. Inabe, H. Kumagai, I. Tanihata, K. Yoshida, T. Nakamura, H. Okuno, S. Shimoura, K. Asahi, Nucl. Instr. and Meth. B 70 (1992) 309.
[221] http://www.ganil.fr/
[222] H.A. Grunder, Nucl. Phys. A 701 (2002) 43.
[223] P. Bricault, R. Baartman, M. Dombsky, A. Hurst, C. Mark, G. Stanford, P. Schmor, Nucl. Phys. A 701 (2002) 49.
[224] K.-H. Schmidt, J. Benlliure, T. Enqvist, A.R. Junghans, F. Rejmund, M.V. Ricciardi, Nucl. Phys. A 701 (2002) 115.
[225] A. Lépine-Szily, Hyperfine Interactions 132 (2001) 35.
[226] W. Mittig, A. Lépine-Szily, N.A. Orr, Annu. Rev. Nucl. Sci. 47 (1997) 27.
[227] H.L. Ravn, P. Bricault, G. Ciavola, P. Drumm, B. Fogelberg, E. Hagebø, M. Huyse, R. Kirchner, W. Mittig, A. Mueller, H. Nifenecker, E. Roeckl, Nucl. Instr. and Meth. B 88 (1994) 441.
[228] U. Köster, in: Ausbeuten und Spektroskopie radioaktiver Isotope bei LOHENGRIN und ISOLDE, Ph.D. Thesis, Technische Universität, München, 2000.
[229] B. Jonson, A. Richter, Hyperfine Interactions 129 (2000) 1.
[230] R. Kirchner, Nucl. Instr. and Meth. B 204 (2003) 179.
[231] U. Köster, Eur. Phys. J. A 15 (2002) 255.
[232] M. Lindroos, The CERN ISOLDE team, the REX-ISOLDE Collaboration, the ISOLDE Collaboration, Nucl. Instr. and Meth. B 204 (2003) 730.
[233] J. Äystö, Nucl. Phys. A 693 (2001) 477.
[234] U. Köster, V.N. Fedoseyev, A.N. Andreyev, U.C. Bergmann, R. Catherall, J. Cederkäll, M. Dietrich, H. De Witte, D.V. Fedorov, L. Fraile, S. Franchoo, H. Fynbo, U. Georg, T. Giles, M. Gorska, M. Hannawald, M. Huyse, A. Joinet, O.C. Jonsson, K.L. Kratz, K. Kruglov, Ch. Lau, J. Lettry, V.I. Mishin, M. Oinonen, K. Partes, K. Peräjärvi, B. Pfeiffer, H.L. Ravn, M.D. Seliverstov, P. Thirolf, K. Van de Vel, P. Van Duppen, J. Van Roosbroeck, L. Weissman, IS365, IS387, IS393, ISOLDE Collaborations, Nucl. Instr. and Meth. B 204 (2003) 347.
[235] H. Geissel, G. Münzenberg, K. Riisager, Annu. Rev. Nucl. Part. Sci. 45 (1995) 163.
[236] D.J. Morrissey, Eur. Phys. J. A 15 (2002) 105.
[237] C. Scheidenberger, Th. Stöhlker, W.E. Meyerhof, H. Geissel, P.H. Mokler, B. Blank, Nucl. Instr. and Meth. B 142 (1998) 441.
[238] H.A. Bethe, Z. Phys. 76 (1932) 293.
[239] C. Scheidenberger, H. Geissel, Nucl. Instr. and Meth. B 135 (1998) 25.

[240] H. Geissel, K. Beckert, F. Bosch, H. Eickhoff, B. Franczak, B. Franzke, M. Jung, O. Klepper, R. Moshammer, G. Münzenberg, F. Nickel, F. Nolden, U. Schaaf, C. Scheidenberger, P. Spädtke, M. Steck, K. Sümmerer, A. Magel, Phys. Rev. Lett. 68 (1992) 3412.
[241] H. Geissel, G. Münzenberg, H. Weick, Nucl. Phys. A 701 (2002) 259c.
[242] G. Savard, J. Clark, C. Boudreau, F. Buchinger, J.E. Crawford, H. Geissel, J.P. Greene, S. Gulick, A. Heinz, J.K.P. Lee, A. Levand, M. Maier, G. Münzenberg, C. Scheidenberger, D. Seweryniak, K.S. Sharma, G. Sprouse, J. Vaz, J.C. Wang, B.J. Zabransky, Z. Zhou, The S258 Collaboration, Nucl. Instr. and Meth. B 204 (2003) 582.
[243] L. Weissman, D.A. Davies, P.A. Lofy, D.J. Morrissey, Nucl. Instr. and Meth. A 531 (2004) 416.
[244] W. Trimble, G. Savard, B. Blank, J.A. Clark, F. Buchinger, T. Cocolios, J.E. Crawford, A. Frankel, J.P. Greene, S. Gulick, J.K.P. Lee, A. Levand, M. Portillo, K.S. Sharma, J.C. Wang, B.J. Zabransky, Z. Zhou, The S258 Collaboration, Nucl. Phys. A 746 (2004) 415c.
[245] S.R. Elliot, Nucl. Instr. and Meth. B 98 (1995) 114.
[246] L. Gruber, J.P. Holder, D. Schneider, Phys. Scr. 71 (2005) 60.
[247] R. Geller, Annu. Rev. Nucl. Part. Sci. 40 (1990) 15.
[248] A. Girard, G. Melin, Nucl. Instr. and Meth. A 382 (1996) 252.
[249] E.D. Donets, Phys. Scr. T 3 (1983) 11.
[250] E. Beebe, L. Liljeby, Å. Engström, M. Björkhage, Phys. Scr. 47 (1993) 469.
[251] I. Bergström, M. Björkhage, H. Danared, H. Cederquist, T. Fritioff, L. Liljeby, R. Schuch, in: K. Prelec (Ed.), Electron Beam Ion Sources and Traps and Their Applications, AIP Conference Proceedings, vol. 572, American Institute of Physics, New York, 2001, p. 20.
[252] I. Bergström, M. Björkhage, K. Blaum, H. Bluhme, T. Fritioff, Sz. Nagy, R. Schuch, Eur. Phys. J. D 22 (2003) 41.
[253] M.A. Levine, R.E. Marrs, J.R. Henderson, D.A. Knapp, M.B. Schneider, Phys. Scr. T 22 (1988) 157.
[254] R.E. Marrs, M.A. Levine, D.A. Knapp, J.R. Henderson, Phys. Rev. Lett. 60 (1988) 1715.
[255] J.R. Crespo López-Urrutia, B. Bapat, I. Draganic, A. Werdich, J. Ullrich, Phys. Scr. T 92 (2001) 110.
[256] J.R. Crespo López-Urrutia, J. Braun, G. Brenner, H. Bruhns, A. Lapierre, A.J. González Martínez, V. Mironov, R. Soria Orts, H. Tawara, M. Trinczek, J. Ullrich, Rev. Scientific Instr. 75 (2004) 1560.
[257] J.R. Crespo López-Urrutia, MPI Heidelberg, Germany, private communication (2005).
[258] D. Habs, O. Kester, T. Sieber, H. Bongers, S. Emhofer, P. Reiter, P.G. Thirolf, G. Bollen, J. Aystö, O. Forstner, H. Ravn, T. Nilsson, M. Oinonen, H. Simon, J. Cederkall, F. Ames, P. Schmidt, G. Huber, L. Liljeby, O. Skeppstedt, K.G. Rensfelt, F. Wenander, B. Jonson, G. Nyman, R. von Hahn, H. Podlech, R. Repnow, C. Gund, D. Schwalm, A. Schempp, K.-U. Kühnel, C. Welsch, U. Ratzinger, G. Walter, A. Huck, K. Kruglov, M. Huyse, P. Van den Bergh, P. Van Duppen, L. Weissman, A.C. Shotter, A.N. Ostrowski, T. Davinson, P.J. Woods, J. Cub, A. Richter, G. Schrieder, Hyperfine Interactions 129 (2000) 43.
[259] G. Savard, R.C. Barber, D. Beeching, F. Buchinger, J.E. Crawford, S. Gulick, X. Feng, E. Hagberg, J.C. Hardy, V.T. Koslowsky, J.K.P. Lee, R.B. Moore, K.S. Sharma, M. Watson, Nucl. Phys. A 626 (1997) 353c.
[260] J. Clark, R.C. Barber, C. Boudreau, F. Buchinger, J.E. Crawford, S. Gulick, J.C. Hardy, A. Heinz, J.K.P. Lee, R.B. Moore, G. Savard, D. Seweryniak, K.S. Sharma, G. Sprouse, J. Vaz, J.C. Wang, Z. Zhou, Nucl. Instr. and Meth. 204 (2003) 487.
[261] St. Becker, G. Bollen, F. Kern, H.-J. Kluge, R.B. Moore, G. Savard, L. Schweikhard, H. Stolzenberg, ISOLDE Collaboration, Int. J. Mass Spectr. Ion Proc. 99 (1990) 53.
[262] K. Blaum, D. Beck, G. Bollen, F. Herfurth, A. Kellerbauer, H.-J. Kluge, R.B. Moore, E. Sauvan, C. Scheidenberger, S. Schwarz, L. Schweikhard, Nucl. Instr. and Meth. B 204 (2003) 478.
[263] H. Backe, M. Hies, H. Kunz, W. Lauth, O. Curtze, P. Schwamb, M. Sewtz, W. Theobald, R. Zahn, K. Eberhard, N. Trautmann, D. Habs, R. Repnow, B. Fricke, Phys. Rev. Lett. 80 (1998) 920.
[264] H. Penttilä, P. Dendooven, A. Honkanen, M. Huhta, P.P. Jauho, A. Jokinen, G. Lhersonneau, M. Oinonen, J.-M. Parmonen, K. Peräjärvi, J. Äystö, Nucl. Instr. and Meth. B 126 (1997) 213.
[265] J. Bonn, B. Bornschein, L. Bornschein, L. Fickinger, B. Flatt, A. Kovalik, Ch. Kraus, B. Müller, E.W. Otten, J.P. Schall, Th. Thümmler, H. Ulrich, Ch. Weinheimer, Prog. Part. Nucl. Phys. 48 (2002) 133.
[266] Ch. Kraus, B. Bornschein, L. Bornschein, J. Bonn, B. Flatt, A. Kovalik, B. Ostrick, E.W. Otten, J.P. Schall, Th. Thümmler, Ch. Weinheimer, Eur. Phys. J. C 40 (2005) 447.
[267] H. Häffner, T. Beier, N. Hermanspahn, H.-J. Kluge, W. Quint, S. Stahl, J. Verdú, G. Werth, Phys. Rev. Lett. 85 (2000) 5308.
[268] T. Katayama, T. Koseki (Eds.), in: Proceedings of the International Workshop on Beam Cooling and Related Topcs (COOL 2003), Lake Yamanaka, Yamanashi, Japan, 2003 (Nucl. Instr. and Meth. A 532 (2004)).
[269] G. Bollen, Nucl. Phys. A 626 (1997) 297c.
[270] C. Scheidenberger, Nucl. Phys. A 751 (2005) 209c.
[271] F. Ames, G. Audi, D. Beck, G. Bollen, M. de Saint Simon, R. Jertz, H.-J. Kluge, A. Kohl, M. König, D. Lunney, I. Martel, R.B. Moore, T. Otto, Z. Patyk, H. Raimbault-Hartmann, G. Rouleau, G. Savard, E. Schark, S. Schwarz, L. Schweikhard, H. Stolzenberg, J. Szerypo, ISOLDE Collaboration, Nucl. Phys. A 651 (1999) 3.
[272] D. Beck, F. Ames, G. Audi, G. Bollen, F. Herfurth, H.-J. Kluge, A. Kohl, M. König, D. Lunney, I. Martel, R.B. Moore, H. Raimbault-Hartmann, E. Schark, S. Schwarz, M. de Saint Simon, ISOLDE Collaboration, J. Szerypo, Eur. Phys. J. A 8 (2000) 307.
[273] Yu.N. Novikov, F. Attallah, F. Bosch, M. Falch, H. Geissel, M. Hausmann, Th. Kerscher, O. Klepper, H.-J. Kluge, C. Kozhuharov, Yu.A. Litvinov, K.E.G. Löbner, G. Münzenberg, Z. Patyk, T. Radon, C. Scheidenberger, A.H. Wapstra, H. Wollnik, Nucl. Phys. A 697 (2002) 92.
[274] S. Rinta-Antila, S. Kopecky, V.S. Kolhinen, J. Hakala, J. Huikari, A. Jokinen, A. Nieminen, J. Äystö, Phys. Rev. C 70 (2004) 011301(R).
[275] P. Dabkiewicz, F. Buchinger, H. Fischer, H.-J. Kluge, H. Kremmling, T. Kühl, A.C. Müller, H.A. Schuessler, Phys. Lett. B 82 (1979) 199.
[276] K. Heyde, P. Van Isacker, M. Waroquier, J.L. Wood, R.A. Meyer, Phys. Rep. 102 (1983) 291.
[277] J.L. Wood, K. Heyde, W. Nazarewicz, M. Huyse, P. van Duppen, Phys. Rep. 215 (1992) 101.
[278] E.W. Otten, in: D. Allan Bromley (Ed.), Treatise on Heavy-ion Science, eighth ed., Plenum Press, New York, 1989, p. 515.

[279] A.N. Andreyev, M. Huyse, P. van Duppen, L. Weissman, D. Ackermann, J. Gerl, F.P. Hessberger, S. Hofmann, A. Kleinböhl, G. Münzenberg, S. Reshitko, C. Schlegel, H. Schaffner, P. Cagarda, M. Matos, S. Saro, A. Keenan, C. Moore, C.D. O'Leary, R.D. Page, M. Taylor, H. Kettunen, M. Leino, A. Lavrentiev, R. Wyss, K. Heyde, Nature 405 (2000) 430.
[280] H.-J. Kluge, W. Nörtershäuser, Spectrochim. Acta B 58 (2003) 1031.
[281] G. Wallerstein, I. Iben, P. Parker, A.M. Boesgaard, G.M. Hale, A.E. Champagne, C.A. Barnes, F. Käppeler, V.V. Smith, R.D. Hoffmann, F.X. Timmes, C. Sneden, R.N. Boyd, B.S. Meyer, D.L. Lambert, Rev. Mod. Phys. 69 (1997) 995.
[282] H. Schatz, A. Aprahamian, J. Görres, M. Wiescher, T. Rauscher, J.F. Rembges, F.-K. Thielemann, B. Pfeiffer, P. Möller, K.-L. Kratz, H. Herndl, B.A. Brown, H. Rebel, Phys. Rep. 294 (1998) 167.
[283] S. Goriely, M. Arnould, Astron. Astrophys. J. 312 (1996) 327.
[284] B. Pfeiffer, K.-L. Kratz, F.-K. Thielemann, W.B. Walters, Nucl. Phys. A 693 (2001) 282.
[285] D. Rodríguez, V.S. Kolhinen, G. Audi, J. Äystö, D. Beck, K. Blaum, G. Bollen, F. Herfurth, A. Jokinen, A. Kellerbauer, H.-J. Kluge, M. Oinonen, H. Schatz, E. Sauvan, S. Schwarz, Phys. Rev. Lett. 93 (2004) 161104.
[286] E.K. Warburton, J.A. Becker, B.A. Brown, Phys. Rep. 41 (1990) 1147.
[287] G. Audi, A.H. Wapstra, Nucl. Phys. A 595 (1995) 409.
[288] C. Guénaut, G. Audi, D. Beck, K. Blaum, G. Bollen, P. Delahaye, F. Herfurth, A. Kellerbauer, H.-J. Kluge, D. Lunney, S. Schwarz, L. Schweikhard, C. Yazidjian, Eur. Phys. J. A 25 (s01) (2005) 33.
[289] C. Guénaut, G. Audi, D. Beck, K. Blaum, G. Bollen, P. Delahaye, F. Herfurth, A. Kellerbauer, H.-J. Kluge, D. Lunney, S. Schwarz, L. Schweikhard, C. Yazidjian, submitted to Phys. Rev. C (2005).
[290] J.-Y. Zhang, R.F. Casten, D.S. Brenner, Phys. Lett. B 227 (1989) 1.
[291] P. Van Isacker, D.D. Warner, D.S. Brenner, Phys. Rev. Lett. 74 (1995) 4607.
[292] R.B.Cakirli, D.S. Brenner, R.F. Casten, E.A. Millman, Phys. Rev. Lett. 94, 2005, 092501 and Phys. Rev. Lett. 95 (2005) 119903.
[293] D.S. Brenner, C. Wesselborg, R.F. Casten, D.D. Warner, J.-Y. Zhang, Phys. Lett. B 243 (1990) 1.
[294] G. Audi, O. Bersillon, J. Blachot, A.H. Wapstra, Nucl. Phys. A 729 (2003) 3.
[295] C. Weber, G. Audi, D. Beck, K. Blaum, G. Bollen, F. Herfurth, A. Kellerbauer, H.-J. Kluge, D. Lunney, S. Schwarz, Phys. Lett. A 347 (2005) 81.
[296] H.K. Carter, J.H. Hamilton, A.V. Ramayya, E.F. Zganjar (Eds.), Proceedings of the Third International Conference on Fission and Properties of Neutron-Rich Nuclei, ICFPNRN 2002, Sanibel Island, Florida, World Scientific, Singapore, 2003.
[297] T. Baumann, N. Frank, B.A. Luther, D.J. Morrissey, J.P. Seitz, B.M. Sherrill, M. Steiner, J. Stetson, A. Stolz, M. Thoennessen, I. Wiedenhöver, Phys. Rev. C 67 (2003) 061303.
[298] P.G. Hansen, A.S. Jensen, B. Jonson, Annu. Rev. Nucl. Part. Sci. 45 (1995) 591.
[299] B. Jonson, Phys. Rep. 389 (2004) 1.
[300] S. Hofmann, Rep. Prog. Phys. 61 (1998) 639.
[301] J. Jänecke, P.J. Masson, At. Data Nucl. Data Tab. 39 (1988) 265.
[302] T. Tachibana, M. Uno, M. Yamada, S. Yamada, At. Data Nucl. Data Tab. 39 (1988) 251.
[303] J.M. Pearson, Hyperfine Interactions 132 (2001) 59.
[304] K. Heyde, The Nuclear Shell-model, Springer, Berlin, Heidelberg, New York, 1994.
[305] P. Møller, J.R. Nix, W.D. Myers, W.J. Swiatecki, At. Data Nucl. Data Tab. 59 (1995) 185.
[306] R. Fossion, C. de Coster, J.E. Garcia-Ramos, T. Werner, K. Heyde, Nucl. Phys. A 697 (2002) 703.
[307] F. Iachello, A. Arima, The Interacting Boson Model, Cambridge University Press, Cambridge, 1987.
[308] V.M. Strutinsky, Nucl. Phys. A 95 (1967) 420.
[309] V.M. Strutinsky, Nucl. Phys. A 122 (1968) 1.
[310] S. Goriely, Hyperfine Interactions 132 (2001) 105.
[311] S. Goriely, Nucl. Phys. A 752 (2005) 560c.
[312] J. Duflo, A.P. Zuker, Phys. Rev. C 52 (1995) R23.
[313] S. Liran, N. Zeldes, At. Data Nucl. Data Tab. 17 (1976) 431.
[314] E. Comay, I. Kelson, A. Zidon, At. Data Nucl. Data Tab. 39 (1988) 235.
[315] P.E. Haustein, At. Data Nucl. Data Tab. 39 (1988) 185.
[316] L. Spanier, S.A.E. Johansson, At. Data Nucl. Data Tab. 39 (1988) 259.
[317] P.J. Masson, J. Jänecke, At. Data Nucl. Data Tab. 39 (1988) 273.
[318] Y. Aboussir, J.M. Pearson, A.K. Dutta, F. Tondeur, Nucl. Phys. A 549 (1992) 155.
[319] J. Duflo, Nucl. Phys. A 576 (1994) 29.
[320] H.v. Groote, E.R. Hilf, K. Takahashi, At. Data Nucl. Data Tab. 17 (1976) 418.
[321] W.D. Myers, W.J. Swiatecki, Nucl. Phys. A 601 (1996) 141.
[322] M. Bender, P.-H. Heenen, P.-G. Reinhard, Rev. Mod. Phys. 75 (2003) 121.
[323] F. Tondeur, S. Goriely, J.M. Pearson, M. Onsi, Phys. Rev. C 62 (2000) 024308.
[324] M. Samyn, S. Goriely, P.-H. Heenen, J.M. Pearson, F. Tondeur, Nucl. Phys. A 700 (2002) 142.
[325] S. Goriely, M. Samyn, M. Bender, J.M. Pearson, Phys. Rev. C 68 (2003) 054325.
[326] M. Bender, G.F. Bertsch, P.-H. Heenen, Phys. Rev. Lett. 94 (2005) 102503.
[327] P. Fleischer, P. Klüpfel, P.-G. Reinhard, J.A. Maruhn, Phys. Rev. C 70 (2004) 054321.
[328] Yu.A. Litvinov, F. Attallah, K. Beckert, F. Bosch, M. Falch, B. Franzke, H. Geissel, M. Hausmann, Th. Kerscher, O. Klepper, H.-J. Kluge, C. Kozhuharov, K.E.G. Löbner, G. Münzenberg, F. Nolden, Yu.N. Novikov, Z. Patyk, W. Quint, T. Radon, C. Scheidenberger, M. Steck, L. Vermeeren, H. Wollnik, Hyperfine Interactions 132 (2001) 283.

[329] P. Møller, J.R. Nix, At. Data Nucl. Data Tab. 26 (1981) 165.
[330] P. Møller, J.R. Nix, Nucl. Phys. A 361 (1981) 117.
[331] H. Geissel, Yu.A. Litvinov, F. Attallah, K. Beckert, P. Beller, F. Bosch, D. Boutin, T. Faestermann, M. Falch, B. Franzke, M. Hausmann, M. Hellström, E. Kaza, Th. Kerscher, O. Klepper, H.-J. Kluge, C. Kozhuharov, K.-L. Kratz, S.A. Litvinov, K.E.G. Löbner, L. Maier, M. Matoš, G. Münzenberg, F. Nolden, Yu.N. Novikov, T. Ohtsubo, A. Ostrowski, Z. Patyk, B. Pfeiffer, M. Portillo, T. Radon, C. Scheidenberger, V. Shishkin, J. Stadlmann, M. Steck, D.J. Viera, H. Weick, M. Winkler, H. Wollnik, T. Yamaguchi, Nucl. Phys. A 746 (2004) 150c.
[332] W. Benenson, E. Kashy, Rev. Mod. Phys. 51 (1979) 527.
[333] E.P. Wigner, in: W.O. Millikan (Ed.), Proceedings of the Robert A. Welch Foundation Conference on Chemical Research, Houston, vol. 1, Robert A. Welch Foundation, Houston, 1957.
[334] S. Weinberg, S.B. Treiman, Phys. Rev. 116 (1959) 465.
[335] J. Britz, A. Pape, M. Antony, At. Data Nucl. Data Tab. 69 (1998) 125.
[336] W.E. Ormand, Phys. Rev. C 55 (1997) 2407.
[337] F. Herfurth, J. Dilling, A. Kellerbauer, G. Audi, D. Beck, G. Bollen, H.-J. Kluge, D. Lunney, R.B. Moore, C. Scheidenberger, S. Schwarz, G. Sikler, J. Szerypo, ISOLDE Collaboration, Phys. Rev. Lett. 87 (2001) 142501.
[338] M.C. Pyle, A. García, E. Tatar, J. Cox, B.K. Nayak, S. Triambak, B. Laughman, A. Komives, L.O. Lamm, J.E. Rolon, T. Finnessy, L.D. Knutson, P.A. Voytas, Phys. Rev. Lett. 88 (2002) 122501.
[339] K. Blaum, G. Audi, D. Beck, G. Bollen, F. Herfurth, A. Kellerbauer, H.-J. Kluge, E. Sauvan, S. Schwarz, Phys. Rev. Lett. 91 (2003) 260801.
[340] C.E. Rolfs, W.S. Rodney, Cauldrons in the Cosmos—Nuclear Astrophysics, University of Chicago Press, Chicago and London, 1988.
[341] F. Bosch, J. Phys. B 36 (2003) 585.
[342] D.D. Clayton, M.E. Rassbach, Astrophys. J. 148 (1967) 69.
[343] F.K. Thielemann, J. Metzinger, V. Klapdor, Z. Phys. A 309 (1983) 301.
[344] F.K. Thielemann, J. Metzinger, V. Klapdor, Z. Astr. Ap. 123 (1983) 162.
[345] F. Kaeppeler, F.K. Thielemann, M. Wiescher, Annu. Rev. Nucl. Part. Sci. 48 (1998) 175.
[346] M. Arnould, K. Takahashi, Rep. Prog. Phys. 62 (1999) 395.
[347] K.-L. Kratz, B. Pfeiffer, F.-K. Thielemann, W.B. Walters, Hyperfine Interactions 129 (2000) 185.
[348] S. Goriely, Nucl. Phys. A 718 (2003) 287c.
[349] G. Sikler, G. Audi, D. Beck, K. Blaum, G. Bollen, F. Herfurth, A. Kellerbauer, H.-J. Kluge, D. Lunney, M. Oinonen, C. Scheidenberger, S. Schwarz, J. Szerypo, C. Weber, Nucl. Phys. A 763 (2005) 45.
[350] O. Koike, M. Hashimoto, K. Arai, S. Wanajo, Astron. Astrophys. 342 (1999) 464.
[351] H. Schatz, A. Aprahamian, V. Barnard, L. Bildsten, A. Cumming, M. Ouellette, T. Rauscher, F.-K. Thielemann, M. Wiescher, Phys. Rev. Lett. 86 (2001) 3471.
[352] B.A. Brown, R.R.C. Clement, H. Schatz, A. Volya, W.A. Richter, Phys. Rev. C 65 (2002) 045802.
[353] J.L. Fisker, F.-K. Thielemann, Astrophys. J. 608 (2004) L61.
[354] I.S. Towner, J.C. Hardy, J. Phys. G 29 (2003) 197.
[355] H. Abele, M. Astruc Hoffmann, S. Baeßler, D. Dubbers, F. Glück, U. Müller, V. Nesvizhevsky, J. Reich, O. Zimmer, Phys. Rev. Lett. 88 (2002) 211801.
[356] Particle Data Group, Phys. Lett. B 592 (2004) 1.
[357] G. Calderón, G. López Castro, Phys. Rev. D 65 (2002) 073032.
[358] V. Cirigliano, M. Knecht, H. Neufeld, H. Rupertsberger, P. Talavera, Eur. Phys. J. C 23 (2002) 121.
[359] V. Bytev, E. Kuraev, A. Baratt, J. Thompson, Eur. Phys. J. C 27 (2003) 57.
[360] J. Bijnens, P. Talavera, Nucl. Phys. B 669 (2003) 341.
[361] A. Sher, R. Appel, G.S. Atoyan, B. Bassalleck, D.R. Bergman, N. Cheung, S. Dhawan, H. Do, J. Egger, S. Eilerts, H. Fischer, W. Herold, V.V. Issakov, H. Kaspar, D.E. Kraus, D.M. Lazarus, P. Lichard, J. Lowe, J. Lozano, H. Ma, W. Majid, S. Pislak, A.A. Poblaguev, P. Rehak, X. Aleksey Sher, J.A. Thompson, P. Truöl, M.E. Zeller, Phys. Rev. Lett. 91 (2003) 261802.
[362] A. Lai, D. Marras, A. Bevan, R.S. Dosanjh, T.J. Gershon, B. Hay, G.E. Kalmus, C. Lazzeroni, D.J. Munday, E. Olaiya, M.A. Parker, T.O. White, S.A. Wotton, G. Barr, G. Bocquet, A. Ceccucci, T. Cuhadar-Dönszelmann, D. Cundy, G. D'Agostini, N. Doble, V. Falaleev, L. Gatignon, A. Gonidec, B. Gorini, G. Govi, P. Grafström, W. Kubischta, A. Lacourt, A. Norton, S. Palestini, B. Panzer-Steindel, H. Taureg, M. Velasco, H. Wahl, C. Cheshkov, A. Gaponenko, P. Hristov, V. Kekelidze, L. Litov, D. Madigojine, N. Molokanova, Yu. Potrebenikov, S. Stoynev, G. Tatishvili, A. Tkatchev, A. Zinchenko, I. Knowles, V. Martin, R. Sacco, A. Walker, M. Contalbrigo, P. Dalpiaz, J. Duclos, P.L. Frabetti, A. Gianoli, M. Martini, F. Petrucci, M. Savrié, A. Bizzeti, M. Calvetti, G. Collazuol, G. Graziani, E. Iacopini, M. Lenti, F. Martelli, M. Veltri, H.G. Becker, K. Eppard, M. Eppard, H. Fox, A. Kalter, K. Kleinknecht, U. Koch, L. Köpke, P. Lopes da Silva, P. Marouelli, I. Pellmann, A. Peters, B. Renk, S.A. Schmidt, V. Schönharting, Y. Schué, R. Wanke, A. Winhart, M. Wittgen, J.C. Chollet, L. Fayard, L. Iconomidou-Fayard, J. Ocariz, G. Unal, I. Wingerter-Seez, G. Anzivino, P. Cenci, E. Imbergamo, P. Lubrano, A. Mestvirishvili, A. Nappi, M. Pepe, M. Piccini, R. Casali, C. Cerri, M. Cirilli, F. Costantini, R. Fantechi, L. Fiorini, S. Giudici, G. Lamanna, I. Mannelli, G. Pierazzini, M. Sozzi, J.B. Cheze, J. Cogan, M. De Beer, P. Debu, A. Formica, R. Granier de Cassagnac, E. Mazzucato, B. Peyaud, R. Turlay, B. Vallage, M. Holder, A. Maier, M. Ziolkowski, R. Arcidiacono, C. Biino, N. Cartiglia, R. Guida, F. Marchetto, E. Menichetti, N. Pastrone, J. Nassalski, E. Rondio, M. Szleper, W. Wislicki, S. Wronka, H. Dibon, G. Fischer, M. Jeitler, M. Markytan, I. Mikulec, G. Neuhofer, M. Pernicka, A. Taurok, L. Widhalm, NA48 Collaboration, Phys. Lett. B 602 (2004) 41.
[363] T. Alexopoulos, M. Arenton, R.F. Barbosa, A.R. Barker, L. Bellantoni, A. Bellavance, E. Blucher, G.J. Bock, E. Cheu, S. Childress, R. Coleman, M.D. Corcoran, B. Cox, A.R. Erwin, R. Ford, A. Glazov, A. Golossanov, J. Graham, J. Hamm, K. Hanagaki, Y.B. Hsiung, H. Huang, V. Jejer, D.A. Jensen, R. Kessler, H.G.E. Kobrak, K. Kotera, J. LaDue, A. Ledovskoy, P.L. McBride, E. Monnier, K.S. Nelson, H. Nguyen, R. Niclasen, V. Prasad, X.R. Qi, E.J. Ramberg, R.E. Ray, M. Ronquest, E. Santos, P. Shanahan, J. Shields, W. Slater, D. Smith, N. Solomey, E.C. Swallow,

P.A. Toale, R. Tschirhart, Y.W. Wah, J. Wang, H.B. White, J. Whitmore, M. Wilking, B. Winstein, R. Winston, E.T. Worcester, T. Yamanaka, E.D. Zimmerman, Phys. Rev. Lett. 93 (2004) 181802.
[364] W.J. Marciano, A. Sirlin, Phys. Rev. Lett. 56 (1986) 22.
[365] Particle Data Group, Phys. Rev. D 66 (2002) 010001.
[366] P. Langacker, D. London, Phys. Rev. D 38 (1988) 886.
[367] J. Maalampi, M. Roos, Phys. Rep. 186 (1990) 53.
[368] P. Langacker, M. Luo, Phys. Rev. D 45 (1992) 278.
[369] W.J. Marciano, A. Sirlin, Phys. Rev. D 35 (1987) 1672.
[370] B.R. Holstein, S.B. Treiman, Phys. Rev. D 16 (1977) 2369.
[371] J.C. Hardy, I.S. Towner, Hyperfine Interactions 132 (2001) 115.
[372] W.E. Ormand, B.A. Brown, B.R. Holstein, Phys. Rev. C 40 (1989) 2914.
[373] M.A. Preston, in: Physics of the Nucleus, Addison-Wesley, Reading, MA, 1962.
[374] J.C. Hardy, Nucl. Phys. A 752 (2005) 101c.
[375] G. Savard, F. Buchinger, J.A. Clark, J.E. Crawford, S. Gulick, J.C. Hardy, A.A. Hecht, J.K.P. Lee, A.F. Levand, N.D. Scielzo, H. Sharma, K.S. Sharma, I. Tanihata, A.C.C. Villari, Y. Wang, Phys. Rev. Lett. 95 (2005) 102501.
[376] M. Mukherjee, A. Kellerbauer, D. Beck, K. Blaum, G. Bollen, F. Carrel, P. Delahaye, J. Dilling, S. George, C. Guénaut, F. Herfurth, A. Herlert, H.-J. Kluge, U. Köster, D. Lunney, S. Schwarz, L. Schweikhard, C. Yazidjian, Phys. Rev. Lett. 93 (2004) 150801.
[377] D. Počanić, E. Frlež, V.A. Baranov, W. Bertl, Ch. Brönnimann, M. Bychkov, J.F. Crawford, M. Daum, N.V. Khomutov, A.S. Korenchenko, S.M. Korenchenko, T. Kozlowski, N.P. Kravchuk, N.A. Kuchinsky, W. Li, R.C. Minehart, D. Mzhavia, B.G. Ritchie, S. Ritt, A.M. Rozhdestvensky, V.V. Sidorkin, L.C. Smith, I. Supek, Z. Tsamalaidze, B.A. VanDevender, Y. Wang, H.-P. Wirtz, K.O.H. Ziock, Phys. Rev. Lett. 93 (2004) 181803.
[378] N. Cabibbo, E.C. Swallow, R. Winston, Phys. Rev. Lett. 92 (2004) 251803.
[379] A. Serebrov, V. Varlamov, A. Kharitonov, A. Fomin, Yu. Pokotilovski, P. Geltenbort, J. Butterworth, I. Krasnoschekova, M. Lasakov, R. Tal'daev, A. Vassiljev, O. Zherebtsov, Phys. Lett. B 605 (2005) 72.
[380] E. Kruger, W. Nistler, W. Weirauch, Metrologia 35 (1998) 203.
[381] C. Carlberg, T. Fritioff, I. Bergström, Phys. Rev. Lett. 83 (1999) 4506.
[382] A. Wicht, J.M. Hensley, E. Sarajlic, S. Chu, Phys. Scr. T 102 (2002) 82.
[383] F. DiFilippo, V. Natarajan, K.R. Boyce, D.E. Pritchard, Phys. Rev. Lett. 73 (1994) 1481.
[384] V.M. Lobashev, Nucl. Phys. A 719 (2003) 153c.
[385] L. Bornschein, for the KATRIN-Collaboration, Nucl. Phys. A 752 (2005) 14c.
[386] G. Douysset, T. Fritioff, C. Carlberg, Phys. Rev. Lett. 86 (2001) 4259.
[387] H.V. Klapdor-Kleingrothaus, I.V. Krivosheina, A. Dietz, O. Chkvorets, Phys. Lett. B 586 (2004) 198.
[388] B. Fogelberg, K.A. Meyilev, H. Mach, V.I. Isakov, J. Slovova, Phys. Rev. Lett. 82 (1999) 1823.
[389] G. Werth, J. Phys. G 20 (1994) 1865.
[390] G.L. Greene, M.S. Dewey, E.G. Kessler Jr., E. Fischbach, Phys. Rev. D 44 (1991) R2216.
[391] J.D. Vergados, Phys. Rep. 361 (2002) 1.
[392] T. Kajita, Y. Totsuka, Rev. Mod. Phys. 73 (2001) 85.
[393] S. Fukuda, et al., Phys. Rev. Lett. 86 (2001) 5651, 5656.
[394] F. Boehm, J. Busenitz, B. Cook, G. Gratta, H. Henrikson, J. Kornis, D. Lawrence, K.B. Lee, K. McKinny, L. Miller, V. Novikov, A. Piepke, B. Ritchie, D. Tracy, P. Vogel, Y.-F. Wang, J. Wolf, Phys. Rev. D 64 (2001) 112001.
[395] S.R. Elliot, P. Vogel, Annu. Rev. Nucl. Part. Sci. 52 (2002) 115.
[396] H.V. Klapdor-Kleingrothaus, A. Dietz, H.L. Harney, I.V. Krivosheina, Mod. Phys. Lett. A 16 (2001) 2409.
[397] H.V. Klapdor-Kleingrothaus, A. Dietz, I.V. Krivosheina, O. Chkvorets, Nucl. Instr. and Meth. A 522 (2004) 371.
[398] Y. Zdesenko, Rev. Mod. Phys. 74 (2002) 663.
[399] Z. Sujkowski, S. Wycech, Phys. Rev. C 70 (2004) 052501.
[400] D. Frekers, Phys. Lett. B, 2005, submitted, hep-ex/0506002.
[401] J. Angrik et al., KATRIN Design Report 2004, FZKA Scientific Report 7090 (2005).
[402] C. Weinheimer, Private communication, University of Münster, Germany, 2005.
[403] J.S. Bell, Proc. Roy. Soc. A 231 (1955) 479.
[404] W. Pauli (Ed.), Niels Bohr and the Development of Physics, Pergamon, New York, 1964 and references therein.
[405] G. Luders, K. Dan, Vidensk. Selsk. Mat. Fys. Medd. 28 (1954) 5.
[406] G. Gabrielse, Adv. At. Mol. Opt. Phys. 45 (2000) 1.
[407] R. Billinge, in: U. Gastaldi, R. Klapisch, J.M. Richard, J. Tran Thanh Van (Eds.), Physics with Antiprotons at LEAR in the ACOL Era, Éditions Frontières, Gif-sur-Yvette, 1985, p. 13.
[408] R.S. Van Dyck Jr., P.B. Schwinberg, H.G. Dehmelt, Phys. Rev. Lett. 59 (1987) 26.
[409] L.K. Gibbons, A.R. Barker, R.A. Briere, G. Makoff, V. Papadimitriou, J.R. Patterson, B. Schwingenheuer, S.V. Somalwar, Y.W. Wah, B. Winstein, R. Winston, M. Woods, H. Yamamoto, G.J. Bock, R. Coleman, J. Enagonio, Y.B. Hsiung, E.J. Ramberg, K. Stanfield, R. Tschirhart, T. Yamanaka, E.C. Swallow, G.D. Gollin, M. Karlsson, J.K. Okamitsu, P. Debu, B. Peyaud, R. Turlay, B. Vallage, Phys. Rev. D 55 (1997) 6625.
[410] M. Fischer, N. Kolachevsky, M. Zimmermann, R. Holzwarth, Th. Udem, T.W. Hänsch, M. Abgrall, J. Grünert, I. Maksimovic, S. Bize, H. Marion, F. Pereira Dos Santos, P. Lemonde, G. Santarelli, P. Laurent, A. Clairon, C. Salomon, M. Haas, U.D. Jentschura, C.H. Keitel, Phys. Rev. Lett. 92 (2004) 230802.

[411] L.V. Jørgensen, D.P. van der Werf, T.L. Watson, M. Charlton, M.J.T. Collier, in: F. Anderegg, C.F. Driscoll, L. Schweikhard (Eds.), Non-neutral Plasma Physics IV, AIP Conference Proceedings, vol. 606, American Institute of Physics, New York, 2002, p. 35.
[412] G. Gabrielse, J. Estrada, J.N. Tan, P. Yesley, N.S. Bowden, P. Oxley, T. Roach, C.H. Storry, M. Wessels, J. Tan, D. Grzonka, W. Oelert, G. Schepers, T. Sefzick, W.H. Breunlich, M. Cargnelli, H. Fuhrmann, R. King, R. Ursin, J. Zmeskal, H. Kalinowsky, C. Wesdorp, J. Walz, K.S.E. Eikema, T.W. Hänsch, Phys. Lett. B 507 (2001) 1.
[413] S. Baird, D. Berlin, J. Boillot, J. Bosser, M. Brouet, J. Buttkus, F. Caspers,V. Chohan, O. Dekkers, T. Eriksson, R. Garoby, R. Giannini, O. Gröbner, J. Gruber, J.Y. Hémery, H. Koziol, R. Maccaferri, S. Maury, C. Metzger, K.D. Metzmacher, D. Möhl, H. Mulder, M. Paoluzzi, F. Pedersen, J.P. Riunaud, C. Serre, D.J. Simon, G. Tranquille, J.W.N. Tuyn, B. Williams, Design Study of the Antiproton Decelerator: AD, CERN Report CERN-PS-96-043-AR, 1996.
[414] J.T.M. Walraven, Hyperfine Interactions 76 (1993) 205.
[415] W. Quint, G. Gabrielse, Hyperfine Interactions 76 (1993) 379.
[416] W. Quint, J. Alonso, S. Djekić, H.-J. Kluge, S. Stahl, T. Valenzuela, J. Verdú, M. Vogel, G. Werth, Nucl. Instr. and Meth. B 214 (2004) 207.
[417] J. Verdú, S. Djekić, S. Stahl, T. Valenzuela, M. Vogel, G. Werth, T. Beier, H.-J. Kluge, W. Quint, Phys. Rev. Lett. 92 (2004) 093002.
[418] T. Kinoshita, M. Nio, Phys. Rev. Lett. 90 (2003) 021803.
[419] T. Beier, H. Häffner, N. Hermanspahn, S.G. Karshenboim, H.-J. Kluge, W. Quint, S. Stahl, J. Verdú, G. Werth, Phys. Rev. Lett. 88 (2002) 011603.
[420] J.L. Flowers, H.A. Klein, H.S. Margolis, Contemporary Phys. 45 (2004) 123.
[421] P.J. Mohr, G. Plunien, G. Soff, Phys. Rep. 293 (1998) 227.
[422] V.W. Hughes, T. Kinoshita, Rev. Mod. Phys. 71 (1999) S133.
[423] P.J. Mohr, B.N. Taylor, Rev. Mod. Phys. 72 (2000) 351.
[424] T. Beier, Phys. Rep. 339 (2000) 79.
[425] V.M. Shabaev, V.A. Yerokhin, Phys. Rev. Lett. 88 (2002) 091801.
[426] T. Beier, I. Lindgren, H. Persson, S. Salomonson, P. Sunnergren, H. Häffner, N. Hermanspahn, Phys. Rev. A 62 (2000) 032510.
[427] M. Vogel, J. Alonso, S. Djekic, H.-J. Kluge, W. Quint, S. Stahl, J. Verdu, G. Werth, Nucl. Instr. and Meth. B 235 (2005) 7.
[428] H. Bettin, L. Koenders, J. Martin, A. Nicolaus, P. Becker, S. Röttger, PTB-Mitteilungen 106 (1996) 321.
[429] A. Paul, S. Röttger, A. Zimbal, U. Keyser, Hyperfine Interactions 132 (2001) 189.
[430] M.P. Bradley, F. Palmer, D. Garrison, L. Ilich, S. Rusinkiewics, D.E. Pritchard, Hyperfine Interactions 108 (1997) 144.
[431] T. Kinoshita, Phys. Rev. Lett. 75 (1995) 4728.
[432] T. Kinoshita, Rep. Prog. Phys. 59 (1996) 1459.
[433] http://physics.nist.gov/constants.
[434] E.R. Williams, G.R. Jones Jr., S. Ye, R. Liu, H. Sasaki, P.T. Olsen, W.D. Phillips, H.P. Layer, IEEE Trans. Instrum. Mess. 38 (1989) 233.
[435] M.E. Cage, R.F. Dziuba, C.T. Van Degrift, D. Yu, IEEE Trans. Instrum. Mess. 38 (1989) 263.
[436] D.E. Pritchard, M.P. Bradley, J.V. Porto, S. Rainville, J.K. Thompson, in: E. Arimondo, P. De Natale, M. Inguscio (Eds.), Atomic Physics 17, AIP Conference Proceedings, vol. 551, American Institute of Physics, New York, 2001, p. 73.
[437] P.J. Mohr, B.N. Taylor, Rev. Mod. Phys. 72 (2000) 351.
[438] Th. Udem, J. Reichert, R. Holzwarth, T.W. Hänsch, Phys. Rev. Lett. 82 (1999) 3568.
[439] D.S. Weiss, B.C. Young, S. Chu, Phys. Rev. Lett. 70 (1993) 2706.
[440] http://www.ganil.fr/eurisol/
[441] J.K. Thompson, S. Rainville, D.E. Pritchard, Nature 430 (2004) 58.